

Titre: Design of a Gas-Solid Fluidized Bed Reactor at High Temperature
Title: and High Pressure

Auteur: Borhan Abdelgawad
Author:

Date: 2013

Type: Mémoire ou thèse / Dissertation or Thesis

Référence: Abdelgawad, B. (2013). Design of a Gas-Solid Fluidized Bed Reactor at High
Citation: Temperature and High Pressure [Mémoire de maîtrise, École Polytechnique de
Montréal]. PolyPublie. <https://publications.polymtl.ca/1083/>

 **Document en libre accès dans PolyPublie**
Open Access document in PolyPublie

URL de PolyPublie: <https://publications.polymtl.ca/1083/>
PolyPublie URL:

**Directeurs de
recherche:** Jamal Chaouki
Advisors:

Programme: Génie chimique
Program:

UNIVERSITÉ DE MONTRÉAL

DESIGN OF A GAS-SOLID FLUIDIZED BED REACTOR AT HIGH
TEMPERATURE AND HIGH PRESSURE

BORHAN ABDELGAWAD

DÉPARTEMENT DE GÉNIE CHIMIQUE
ÉCOLE POLYTECHNIQUE DE MONTRÉAL

MÉMOIRE PRÉSENTÉ EN VUE DE L'OBTENTION
DU DIPLÔME DE MAÎTRISE ÈS SCIENCES APPLIQUÉES
(GÉNIE CHIMIQUE)

AVRIL 2013

UNIVERSITÉ DE MONTRÉAL

ÉCOLE POLYTECHNIQUE DE MONTRÉAL

Ce mémoire intitulé:

DESIGN OF A GAS-SOLID FLUIDIZED BED REACTOR AT HIGH TEMPERATURE AND
HIGH PRESSURE

présenté par : ABDELGAWAD Borhan

en vue de l'obtention du diplôme de : Maîtrise ès sciences appliquées

a été dûment accepté par le jury d'examen constitué de :

M.FRADETTE Louis, Ph.D, président

M.CHAOUKI Jamal, Ph.D, membre et directeur de recherche

M.DOUCET Jocelyn, Ph.D, membre

DEDICATION

To my beloved parents

ACKNOWLEDGEMENTS

Thanks be to God for my life through all tests. May your name be exalted, honoured, and glorified. I would like to express my deep appreciation and gratitude to the following people for their help and support. I have been indebted in the preparation of this thesis to my supervisor, Dr. Jamal Chaouki who gave me the opportunity to be part of this fascinating project and whose encouragement and guidance enabled me to become a better engineer. Furthermore, his ongoing care during my time of need will forever be appreciated.

The financial support provided by Total E&P, the industrial partner of this research chair and the Natural Sciences and Engineering Research Council of Canada (NSERC) is greatly appreciated. Furthermore, my sincerest gratitude goes to Dr Jean-Phillipe Laviolette who has provided me with new ideas and methods to perfect my design. I am grateful for all the support I received from Professor Chaouki's research group to whom I wish nothing but success and happiness in life. The help and support I received from Dr. Rouzbeh Jafari and Mr Yazid Belkhir along with the entire staff of Ecole Polytechnique's Chemical engineering department will forever be remembered and deeply appreciated. I would also like to express my sincerest gratitude to Dr Elizabeth Jones for her constant help and invaluable support throughout my masters.

The informal support and encouragement of my family and friends through both the good and the bad times has been indispensable, and I would like to thank all of them for being the wonderful people they are. My deepest gratitude goes to Claire Erves for all her help and support throughout, whether if it's for always making me feel like the center of attention whenever I would complain, or just for being awesome.

I would like to thank my best friend and brother Ahmed Farid for always being by my side whenever I needed him. I would also like to thank Bassel Hakoura and Omar El-Kayyali, who were always there for me whether if it was to help proof read a document, listen to my complaints or just hang out. I would like to thank Eyad El-Sadi and Youssef Ebeid for being great friends who would always take the time to check up on me whenever I disappeared to study. I would also like to thank Ahmed El-Baghdadi and Nasser El-Shawwa for always being available to help with any topic no matter how random it was. My sincerest gratitude and best wishes goes to, Ahmad Aziz, Jad Al-Rabi and Alia Bessisso for being my second family in Canada.

I am forever thankful for all the love and best wishes of my brother Mohamed and sisters Doua and Heba, which – despite their physical absence – helped me in the successful completion of my studies in Canada. I would also like to thank my uncle, Mohamed Fayek Abulela for his care and devotion during my studies as well as being a true role model. Finally, my most profound appreciation goes to my parents, Ahmed Abdelgawad and Aya Abulela who have been a constant source of support whether it be emotional, moral or of course financial – during my postgraduate years. If it were not for their sacrifices, patience and hard work this thesis would certainly not have existed. It is to them that I dedicate this work.

RÉSUMÉ

De nombreux procédés de raffinage et de pétrochimie sont réalisés dans des réacteurs agités ou dans les lits fluidisés qui impliquent des fluides polyphasiques dans des conditions extrêmes. L'utilisation de haute température et / ou haute pression lors de la conversion et la manipulation de fluides, se traduit par des conditions de traitement extrêmes pour lesquelles l'hydrodynamique demeure inconnu. En conséquence, avec seulement quelques études à haute température et très peu à haute température et haute pression, le développement de nouveaux modèles et de critères de conception lors de l'utilisation de conditions extrêmes est donc d'un intérêt immédiat pour Total, le partenaire industriel de cette chaire de recherche.

L'objectif de ce mémoire est d'examiner, ainsi que de comparer les modèles déjà publiés sur la fluidisation dans des conditions ambiantes et extrêmes, tout en mettant l'accent sur les informations nécessaires à la conception de réacteurs gaz-solide. Par conséquent, une conception détaillée d'un lit fluidisé qui permettrait un fonctionnement flexible à haute température et à haute pression sous plusieurs vitesses de gaz sera menée afin de servir pour le futur développement de nouveaux modèles hydrodynamiques.

Afin d'illustrer la nécessité de ce réacteur pilote, les effets résultant de l'utilisation de conditions d'opération extrêmes (haute température, pression et vitesse) sur la fluidisation et plus précisément la taille des bulles ont été démontrées. Ainsi, trois corrélations de taille de bulles ont été choisies: la première pour avoir été modélisée à haute pression et vitesse, la deuxième pour avoir été développée à haute température et la troisième pour avoir été une des corrélations les plus couramment citée dans les livres de conception de réacteur à lit fluidisé. Aucun de ces modèles a fourni des valeurs acceptables au-delà de sa plage désignée. En outre, l'effet de diamètre de bulles sur le transfert de masse, ainsi que sur la conversion, le taux d'entraînement et la hauteur limite de désengagement (TDH) a été étudiée tout en appliquant chacun des différents modèles de taille de bulles. Ainsi, plusieurs divergences ont été notées entre les résultats obtenus et les tendances attendues. En utilisant des représentations graphiques de l'entraînement en fonction de la hauteur au dessus du lit, TDH a été jugée indépendant de la taille des bulles. De plus, celui-ci varie avec la température, la pression et la vitesse, ce qui est contraire à plusieurs corrélations existantes. Par ailleurs, à des vitesses élevées, malgré l'obtention d'une grande valeur du TDH à la fois graphiquement et en utilisant les différents modèles existants, les changements

globaux dans le taux d'entraînement total sont négligeables. Par conséquent, dimensionner la zone de désengagement à partir de TDH tel que suggéré par la plupart des livres de conception de réacteurs à lits fluidisés, pourrait ne pas être rentable. De plus, en utilisant différents diamètres de bulles lors du calcul de la conversion du méthane dans la réaction de reformage, ce besoin de développer de nouveaux modèles a été une autre fois démontré à travers l'obtention de résultats qui diffèrent des valeurs attendues lorsque les paramètres d'opération sont changés.

Ainsi, avec ce besoin de développer de nouveaux modèles de fluidisation aux conditions extrêmes illustrées, la conception complète d'un réacteur à lit fluidisé et son procédé a été menée. Les conditions d'opération ont été choisies afin de servir en tant qu'une extrapolation adéquate à la réalité industrielle. Les dimensions du réacteur ont été choisies afin de permettre la comparaison avec un réacteur qui fonctionne à haute température existant actuellement dans notre laboratoire. En outre, ces conditions ont également été choisies tout en respectant les contraintes définies par le compresseur ainsi que les limites départementales liées à l'installation de ce réacteur au sein de l'université. Ce réacteur sera donc opéré à des températures de 25 à 1000°C et des pressions entre 1 et 20 atm, avec un diamètre de 15 cm à la base et 50 cm pour la zone de désengagement. La vitesse du gaz sera comprise entre 0,1 m/s et 2 m/s afin de couvrir le régime bouillonnant ainsi que le régime turbulent. Du sable ou autre type de catalyseur sera utilisé en tant que matière du lit. La taille de particule moyenne sera donc comprise entre 60 μm et 500 μm , de manière à inclure les particules de type Geldart A et B, avec une densité allant de 1 à 2.5g/cm³. De l'air comprimé provenant de trois différents compresseurs sera utilisé en tant que gaz de fluidisation. Afin de chauffer le réacteur aux températures requises, un système de chauffage a été conçu. Ce système comprend une conduite isolée où un appareil de chauffage électrique à haute pression capable de résister à des faibles débits sera attaché. Cet appareil de chauffage électrique sera utilisé pour préchauffer la conduite jusqu'à ce que la température d'auto-inflammation du gaz naturel est atteinte. À ce moment, le gaz naturel sera introduit avec l'air comprimé à travers des ports situés le long de la conduite. Ce système de chauffage est alors relié à la boîte à vent qui a été conçue pour permettre une conversion du méthane de plus de 99% afin d'assurer une réduction maximale de la concentration du monoxyde de carbone résultant de la combustion du gaz naturel.

De plus, pour s'assurer d'obtenir une fluidisation équitable à travers le lit, un distributeur à tuyères a été conçu afin de permettre une flexibilité d'opération sous les conditions choisies. Pour

empêcher l'entraînement des particules hors du réacteur, un cyclone ainsi qu'un filtre à haute température seront placés en série à l'intérieur de la zone de désengagement. Enfin, afin d'assurer que les vannes de régulation en aval du réacteur ne soit pas soumises à des températures supérieures à 300C, de l'eau distillée provenant d'un réservoir sous pression, sera pompée dans un purgeur vapeur à la sortie du réacteur.

Ainsi, l'atteinte de l'objectif de ce travail consistant en la conception d'un réacteur gaz-solide à lit fluidisé pour un fonctionnement souple sous des conditions ambiantes et extrêmes, a été réalisé à travers une description détaillée du procédé et une procédure d'opération.

ABSTRACT

Numerous processes of refining and petro chemistry involve multiphase fluids at extreme conditions, and are realized in agitated reactors or in fluidized beds. The use of high temperature and/or high pressure during conversion and handling of high viscosity materials and/or viscosity ratios results in extreme processing conditions for which the multiphase process hydrodynamics are completely unknown. Subsequently, with only a few studies at high temperature and almost none at high temperature and high pressure, general and reliable design criteria for the use of extreme conditions are scarce and therefore are of immediate interest to Total, the industrial partner of this research chair.

The aim of this work is to review and compare the already published models on fluidization at ambient and extreme conditions with emphasis on the information necessary for designing gas-solid reactors. Consequently, a detailed design of a fluidized bed reactor that would allow flexible operation at high temperature and high pressure at several gas velocities will be conducted in order to serve for the future development of new hydrodynamic models.

In order to illustrate the need for this laboratory scale reactor, the effect of using extreme operating conditions (high temperature, pressure and velocity) on fluidization and more specifically bubble size were demonstrated. Three bubble size correlations were chosen: the first for being respectively modeled at high pressure and velocity, the second for being modeled at high temperature and the third for being one of the most commonly used models in design books. None of these correlations provided acceptable values beyond their designated range. Furthermore, the impact of bubble diameter on mass transfer, reaction conversion, entrainment and the transport disengaging height (TDH) were studied through the application of each of these bubble size models. By doing so, several discrepancies between the obtained results and the expected trends were highlighted. Using entrainment plots, TDH was found to be independent of bubble size and vary with temperature, pressure and velocity, which is contrary to several existing correlations. Moreover, at high velocities, despite obtaining a large TDH value both graphically and by using the existing models, the overall changes in the total flux are negligible which would imply that sizing the freeboard accordingly, as suggested by most design books, might not be profitable.

By using different bubble diameters while computing the conversion of methane in the methane steam reforming reaction, the need for new models was once more demonstrated with different operating conditions providing different results from the expected trends.

With the need for new fluidization models at extreme conditions illustrated, the complete design of a fluidized bed reactor and its respective process was conducted. The operating conditions were chosen as an adequate extrapolation to industrial reality, while the reactor dimensions were chosen based on an existent reactor currently operating at high temperature in our laboratory. Furthermore, these conditions were also chosen while respecting the constraints defined by the compressor and the inherent limitations of the university experimental facility. The temperature of operation will be varied from room temperature to 1000 °C and the pressure will range from atmospheric pressure up to 20 atm. The reactor's bed diameter is 15 cm at the bottom with a freeboard diameter of 50cm. The gas velocity will range from 0.1 m/s up to 2 m/s in order to cover the bubbling and turbulent regime. The bed material will be sand or another type of catalyst with a mean particle size ranging from 60 μm up to 500 μm , so as to cover Geldart A and B particles, and a specific gravity ranging from 1 to 2.5g/cm³. The chosen fluidization medium will be compressed air that will be provided by three different compressors.

In order to heat up the reactor to the required temperatures, a heating system was designed. This heating system comprises of an insulated pipe where a high pressure electric heater capable of withstanding low flowrates is attached. This electrical heater will be used to preheat the pipe until the auto-ignition temperature of natural gas is achieved. At this point, natural gas will be fed to the pipe along with the compressed air. This heating system will be connected to the windbox which was designed to allow over 99% conversion of methane to ensure that carbon monoxide concentration resulting from the natural gas combustion is at a minimum.

In order to provide even fluidization, a bubble cap distributor was designed to allow flexibility and freedom of operation under the chosen conditions. To prevent solid entrainment out of the reactor, a cyclone and high temperature filter will be placed in series inside the freeboard. Finally, in order to ensure that the control valve downstream of the reactor would not be subjected to temperature higher than 300C, distilled water from a pressurized tank will be pumped in a steam trap at the reactor exit in order to reduce the temperature of the gas.

With a detailed process description and operating procedure provided, the objective of this work of designing a gas-solid fluidized bed reactor and its utilities for flexible operation from ambient conditions up to high temperature and high pressure, were successfully met.

TABLE OF CONTENT

DEDICATION	III
ACKNOWLEDGEMENTS	IV
RÉSUMÉ.....	VI
ABSTRACT	IX
TABLE OF CONTENT	XII
LIST OF TABLES	XV
LISTE OF FIGURES	XVII
NOMENCLATURE.....	XXI
LIST OF APPENDICES	XXVIII
CHAPTER 1 INTRODUCTION.....	1
1.1 Problem Statement and Motivation.....	1
1.2 Objectives.....	2
CHAPTER 2 LITTERATURE REVIEW	3
2.1 Fluidized Bed Principles	3
2.2 Fluidization Regimes.....	5
2.3 Effects of Particle Size and Density	7
2.4 Solid Mixing and Entrainment	8
2.5 Application of High Temperature and Pressure	9
CHAPTER 3 INFLUENCE OF USING EXTREME OPERATING CONDITIONS ON FLUIDIZED BED REACTORS	11
3.1 Influence of extreme conditions on fluidization	12
3.2 Bubble size under extreme conditions	13
3.2.1 Effect of velocity on bubble size.....	17

3.2.2	Effect of pressure on bubble size	19
3.2.3	Effect of temperature on bubble size.....	21
3.3	Influence of Extreme Operating Conditions on Entrainment and TDH.....	26
3.3.1	Entrainment modelling.....	26
3.3.2	TDH modelling and influence of extreme conditions	38
3.4	Mass Transfer in Fluidized Beds.....	42
3.4.1	Effect of velocity on mass transfer.....	44
3.4.2	Effect of pressure on mass transfer	46
3.4.3	Effect of temperature on mass transfer	48
3.5	Effect of Extreme Conditions on Reaction Conversion	50
3.5.1	Methane steam reforming kinetics	50
3.5.2	Methane steam reforming modelling	53
3.6	Conclusion.....	64
CHAPTER 4	DESIGN OF THE FLUIDIZED BED REACTOR.....	67
4.1	Operating and Design Conditions	67
4.2	Reactor Design: Techniques and Procedures	68
4.2.1	Windbox/Plenum Design	68
4.2.2	Distributor Design	70
4.2.3	Particle Separation.....	77
4.2.4	Reactor Shell and Refractory Design	81
4.2.5	Reactor Heating System	83
4.3	Process Description	85
CHAPTER 5	FINAL REACTOR DESIGN AND PROCESS DESCRIPTION.....	89
5.1	Final Reactor Dimensions	89

5.1.1	Windbox final dimensions	89
5.1.2	Distributor final dimensions.....	90
5.1.3	Cyclone and filter final dimensions	93
5.1.4	Reactor shell and refractory final dimensions.....	95
5.1.5	Heating system final dimensions.....	97
5.2	Detailed Process Description	98
5.2.1	P&ID0001: Compressor System	98
5.2.2	P&ID0002: Fluidized Bed Heater and Windbox	99
5.2.3	P&ID0003: Fluidized Bed Freeboard and Gas Sampling	101
5.2.4	P&ID0004: Water Injection System	102
5.2.5	P&ID0005: Detention Tank and Discharge Manifold	103
5.3	Operating Procedure.....	103
5.3.1	Operating Procedure.....	103
5.3.2	Reactor heating at ambient pressure ($T_{BED} \leq 800^{\circ}\text{C}$).....	105
5.3.3	REACTOR HEATING AT AMBIENT PRESSURE ($800^{\circ}\text{C} < T_{BED} \leq 1000^{\circ}\text{C}$)	105
5.3.4	INCREASING THE PRESSURE	106
5.3.5	REACTOR SHUTDOWN	106
CHAPTER 6	CONCLUSION AND RECOMMENDATIONS.....	107
6.1	Conclusion.....	107
6.2	Recommendations	109
REFERENCES	110
APPENDICES	119

LIST OF TABLES

Table 1- Applications of high temperature and pressure in industrial fluidized beds.....	10
Table 2- Applicability range of the bubble size correlations by Mori and Wen (1975), Horio and Nonaka (1987) and Cai et al (1994)	16
Table 3- Specifications of the experimental results of Yamazaki et al (1991)	17
Table 4- Specifications of the experimental results of Hoffmann and Yates (1985)	19
Table 5- Specifications of the experimental results of Sanaei et al (2012).....	22
Table 6- Choi et al (1991) correlation for entrainment rate (applicable for a velocity range from 0.3 to 7m/s, a particle diameter range of 0.005 to 1mm and a reactor diameter for 0.06 to 1m)	28
Table 7- Drag Coefficient for different Reynolds numbers	29
Table 8-Validity range of the entrainment correlation by Choi et al. (1999).....	29
Table 9-Specifications used in the simulation where the effect of the bubble size correlations by Mori and Wen (1975), Horio and Nonaka (1987) and Cai et al (1994) with respect to velocity at high temperature and pressure on the entrainment rate model by Choi et al (1999)	31
Table 10- TDH values based on the plot of the entrainment correlation of Choi et al (1999).....	39
Table 11- Common TDH correlation as reported in the handbook of fluidization and fluid-particle systems[6].....	40
Table 12- Comparison of the TDH values obtained using the entrainment model of Choi et al and the correlation of Sciazko et al	41
Table 13- Methane steam reforming reactions and kinetic models	51
Table 14- Kinetic parameters	52
Table 15- State Equations for the Dynamic Two- Phase Structure Model (DTP)	54
Table 16- Methane steam reform simulation input	55

Table 17- Comparison of the predicted bubble size using the correlations by Mori and Wen (1975), Horio and Nonaka (1987) and Cai et al (1994) with the expected trends in the literature at high temperature, pressure and velocity.	65
Table 18- Plenum Design Equations.....	69
Table 19- Natural gas combustion reactions and kinetic models.....	70
Table 20- Most common cyclone dimensions.....	79
Table 21- Circumferential and longitudinal stress equations.....	82
Table 22- Heat Flux Balance.....	83
Table 23- Methane combustion conversion with respect to pressure	89
Table 24- Stainless steel properties.....	92
Table 25- Cyclone simulation results.....	94
Table 26- Carbon steel properties	96
Table 27- Reactor wall and refractory thickness simulation results	96
Table 28- Heating system wall and refractory thickness simulation results	97

LISTE OF FIGURES

Figure 1- Fluid Bed Sections.....	4
Figure 2- Transport Disengaging Height	5
Figure 3- Fluidization regimes	6
Figure 4- Geldart Particles	7
Figure 5- Gasification process.....	10
Figure 6-Comparison of the bubble size correlations by Mori and Wen (1975), Horio and Nonaka (1987) and Cai et al (1994) with the experimental values of Yamazaki et al (1991) with respect to velocity at ambient pressure and temperature.	18
Figure 7-Comparison of the bubble size correlations by Mori and Wen (1975), Horio and Nonaka (1987) and Cai et al (1994) with the experimental values of Hoffman and Yates (1985) with respect to pressure at ambient temperature and a gas velocity of 0.12m/s.....	20
Figure 8-Comparison of the bubble size correlations by Mori and Wen (1975) and Cai et al (1994) with the experimental values of Hoffman and Yates (1985) with respect to pressure at ambient temperature and a gas velocity of 0.12m/s	20
Figure 9- Comparison of the bubble size correlations by Mori and Wen (1975), Horio and Nonaka (1987) and Cai et al (1994) with the experimental values of Sanaei et al (2012) with respect to temperature at ambient pressure and a velocity of 0.38m/s.....	23
Figure 10- Bubble size vs temperature (adapted by Sanaei et al (2012)) at ambient pressure and a velocity of 0.38m/s	23
Figure 11- Bubble size vs temperature (according to the correlation by Cai et al (1994)) at ambient pressure and a velocity of 0.38m/s at ambient pressure and a velocity of 0.38m/s .	24
Figure 12- Bubble size vs temperature (according to the correlation by Mori and Wen (1975)) at ambient pressure and a velocity of 0.38m/s	24
Figure 13- Bubble size vs temperature (according to the correlation by Horio and Nonaka (1987)) at ambient pressure and a velocity of 0.38m/s	25

Figure 14- Comparison of the entrainment rate with respect to height above the bed using the bubble size correlations by Mori and Wen (1975), Horio and Nonaka (1987) and Cai et al (1994) at ambient temperature and pressure and a superficial gas velocity of 0.3m/s	32
Figure 15- Comparison of the entrainment rate with respect to height above the bed using the bubble size correlations by Mori and Wen (1975), Horio and Nonaka (1987) and Cai et al (1994) at ambient temperature and pressure and a superficial gas velocity of 1.3m/s	32
Figure 16- Comparison of the entrainment rate with respect to height above the bed using the bubble size correlations by Mori and Wen (1975), Horio and Nonaka (1987) and Cai et al (1994) at ambient temperature, a pressure of 20atm and a superficial gas velocity of 0.3m/s	33
Figure 17- Comparison of the entrainment rate with respect to height above the bed using the bubble size correlations by Mori and Wen (1975), Horio and Nonaka (1987) and Cai et al (1994) at ambient temperature, a pressure of 20atm and a superficial gas velocity of 1.3m/s	33
Figure 18- Comparison of the entrainment rate with respect to height above the bed using the bubble size correlations by Mori and Wen (1975), Horio and Nonaka (1987) and Cai et al (1994) at ambient pressure, a temperature of 600°C and a superficial gas velocity of 0.3m/s	34
Figure 19- Comparison of the entrainment rate with respect to height above the bed using the bubble size correlations by Mori and Wen (1975), Horio and Nonaka (1987) and Cai et al (1994) at ambient pressure, a temperature of 600°C and a superficial gas velocity of 1.3m/s	34
Figure 20- Comparison of the interchange mass transfer coefficient with respect to superficial velocity using the bubble size correlations by Mori and Wen (1975) and Horio and Nonaka (1987)	45
Figure 21- Interchange mass transfer coefficient with respect to superficial velocity using the bubble size correlations by Cai et al (1999)	45

Figure 22- Comparison of the interchange mass transfer coefficient with respect to pressure using the bubble size correlations by Mori and Wen (1975), Horio and Nonaka (1987) and Cai et al (1994)	47
Figure 23- Comparison of the interchange mass transfer coefficient with respect to temperature using the bubble size correlations by Mori and Wen (1975), Horio and Nonaka (1987) and Cai et al (1994).....	49
Figure 24- Comparison of the bubble size correlations by Mori and Wen (1975), Horio and Nonaka (1987) and Cai et al (1994) with respect to pressure at $U=0.07\text{m/s}$ and $T=650\text{C}$	56
Figure 25- Comparison of the methane conversion with respect to pressure using the bubble size correlations by Mori and Wen (1975), Horio and Nonaka (1987) and Cai et al (1994) with the experimental values of Roy et al (1999) at $U=0.07\text{m/s}$ and $T=650\text{C}$	56
Figure 26- Comparison of the bubble size correlations by Mori and Wen (1975), Horio and Nonaka (1987) and Cai et al (1994) over a pressure range of (0.3 to 6MPa) at $U=0.07\text{m/s}$ and $T=650\text{C}$	57
Figure 27- Comparison of the methane conversion over a pressure range of (0.3 to 6MPa) using the bubble size correlations by Mori and Wen (1975), Horio and Nonaka (1987) and Cai et al (1994) at $U=0.07\text{m/s}$ and $T=650\text{C}$	58
Figure 28- Comparison of the bubble size correlations by Mori and Wen (1975), Horio and Nonaka (1987) and Cai et al (1994) over a pressure range of (0.3 to 6MPa) at $U=1.3\text{m/s}$ and $T=650\text{C}$	59
Figure 29- Comparison of the methane conversion over a pressure range of (0.3 to 6MPa) using the bubble size correlations by Mori and Wen (1975), Horio and Nonaka (1987) and Cai et al (1994) at $U=1.3\text{m/s}$ and $T=650\text{C}$	59
Figure 30- Comparison of the bubble size correlations by Mori and Wen (1975), Horio and Nonaka (1987) and Cai et al (1994) with respect to temperature at $U=0.07\text{m/s}$ and $P=0.55\text{MPa}$	61
Figure 31- Comparison of the bubble size correlations by Mori and Wen (1975), Horio and Nonaka (1987) and Cai et al (1994) with the experimental values of Roy et al (1999) with respect to temperature at $U=0.07\text{m/s}$ and $P=0.55\text{MPa}$	61

Figure 32- Comparison of the bubble size correlations by Mori and Wen (1975), Horio and Nonaka (1987) and Cai et al (1994) with respect to temperature at $U=1.3\text{m/s}$ and $P=0.55\text{MPa}$	62
Figure 33- Comparison of the bubble size correlations by Mori and Wen (1975), Horio and Nonaka (1987) and Cai et al (1994) with respect to temperature at $U=1.3\text{m/s}$ and $P=0.55\text{MPa}$	63
Figure 34- Schematics of bubble cap distributor	74
Figure 35- Jet configurations.....	75
Figure 36- Cyclone and filter disposition in the freeboard	77
Figure 37- Typical cyclone configuration.....	78
Figure 38- Reactor Shell Modeling.....	82
Figure 39- Heating System schematics	84
Figure 40- Process Flow Diagram.....	88
Figure 41- Final bubble cap dimensions	91
Figure 42- Final cyclone dimensions	94
Figure 43- System pressure as a function of the required Amount of Cooling Water to reduce the gas temperature from 1000 to 250C.....	102

NOMENCLATURE

AFR	Stoichiometric air-fuel ratio	-
a_i	Decay constant	-
Ar	Archimedes number	-
At	Cross sectional area of the reactor	m^2
c	Dust concentration	g/m^3
C_A	Mean concentration of specie A	$kmol/m^3$
C_{Ab}	Concentration of specie A in the bubble phase	$kmol/m^3$
C_{Ae}	Concentration of specie A in the emulsion phase	$kmol/m^3$
C_D	Discharge coefficient	-
C_d	Drag coefficient	-
C_{ph}	Plate design factor	-
D	Molecular diffusivity	m^2/s
d_b	Average bubble size	m
d_{b0}	Initial bubble diameter from Mori and Wen	m
$d_{b\infty}$	Maximum bubble diameter from Mori and Wen	m
d_{bM}	Maximum bubble diameter from Horio and Nonaka	m
D_{cyc}	Diameter of cyclone body	m
D_{cyc}	Diameter of cyclone gas outlet	m

D_{entry}	Diameter of the windbox gas inlet	m
D_{fb}	Diameter of the freeboard	m
d_{flame}	Theoretical flame dimension	m
d_h	Diameter of hole	m
D_h	Header diameter	
d_p	Particle average diameter	m
dp_{50}	Cut size for which 50% of solids of a given size are collected	m
dp_i	Diameter of a given particle i	m
D_{plenum}	Diameter of the windbox	m
D_t	Reactor diameter	m
E	Modulus of elasticity	Pa
E_{i0}	Bed surface flux	kg/(m ² .s)
$E_{i\infty}$	Elutriation flux	kg/(m ² .s)
Eu	Euler number	-
Eu_c	Euler number from Shepherd and Lapple	-
$F_{\Delta P}$	Force due to the pressure drop	N
F_d	Drag force per projection area	Pa
F_d	Froude number	-
F_g	Gravity force per projection area	Pa

f_p	Maximum allowable design stress	Pa
g	Gravitational acceleration (9.8)	m/s^2
h	Natural convection coefficient	$(W/m^2.K)$
H_b	Bed Height	M
H_{cyc}	Height of cyclone inlet	m
H_{plenum}	Height of the windbox	m
J	Momentum of fuel jet	N
K	Distributor pressure drop coefficient	-
k_1	Reaction constant	$kmol/(kgcat \cdot s \cdot kPa^{0.25})$
K_1	Equilibrium constant	kPa^2
k_2	Reaction constant	$kmol/(kgcat \cdot s \cdot kPa)$
K_2	Equilibrium constant	kPa^0
k_3	Reaction constant	$kmol/(kgcat \cdot s \cdot kPa^{0.25})$
K_3	Equilibrium constant	kPa^2
k_A	Thermal conductivity of material A	$(W/m.K)$
K_{BE}	Interphase mass exchange coefficient between bubble and emulsion	s^{-1}
K_{CO}	Adsorption coefficient	kPa^{-1}
$K_{fouling}$	Fouling factor	-
K_H	Adsorption coefficient	$kPa^{-0.5}$

K_{H_2O}	Adsorption coefficient	-
$K_{i\infty}$	Elutriation rate of a particle of size i	$\text{kg}/(\text{m}^2 \cdot \text{s})$
$L_{b_{cyc}}$	Length of cyclone cylindrical section	m
$L_{c_{cyc}}$	Length of cyclone conical section	m
L_{down}	Downwardly directed gas jet length	m
L_{flame}	Flame length	m
L_{hor}	Horizontally directed gas jet length	m
L_{mf}	Minimum fluidization height	m
L_{up}	Upwardly directed gas jet length	m
m	Constant	-
m_{gas}	Mass flowrate of the gas	kg/s
N	Number of holes	-
n	Constant	-
P	Pressure	Pa
P_A	Partial pressure of component A	kPa
Q	Volumetric flowrate of gas	m^3/s
R	Universal Gas constant (8.314)	$\text{J}/(\text{mol} \cdot \text{K})$
r	Reactor/plate radius	m
R_A	Reaction rate of specie A	$\text{kmol}/(\text{m}^3 \cdot \text{s})$

R_{emf}	Reynolds number at minimum fluidization velocity	-
Re_p	Particle Reynolds number	-
r_i	Reaction rate of reaction i	$\text{kmol}/(\text{m}^3.\text{s})$
S_{cyc}	Diameter of cyclone vortex	m
Stk_{50}	Stokes number	-
T	Temperature	K
T_∞	Ambient air temperature	K
TDH	Transport disengaging height	m
t_p	Plate minimum thickness	m
t_{shell}	Outer reactor wall metal shell thickness	m
T_w	Temperature at the reactor outer wall	K
U	Superficial gas velocity	m/s
U_b	Bubbling velocity	m/s
U_e	Emulsion Velocity	m/s
U_{fuel}	Velocity of the fuel	m/s
U_h	Gas velocity through the grid hole	m/s
U_{mf}	Minimum fluidization velocity	m/s
W	Force due to weight of the solids on the distributor	N
W_{cyc}	Width of cyclone inlet	m

x_i	Mass fraction of particles of component i in the fluidized bed	-
z	Axial height above the distributor plate	m
Z_f	Shvab-Zek'dovich variable	-

GREEK SYMBOLS

α	Parameter in methane oxidation reaction	-
δ	Bubble fraction	-
ΔP_b	Pressure drop across the bed	Pa
ΔP_{cyc}	Pressure drop across the cyclone	Pa
ΔP_d	Pressure drop across the distributor	Pa
ε	Average bed voidage	-
ε_b	Average bubble voidage	-
ε_e	Average emulsion voidage	-
ε_{mf}	Minimum fluidization voidage	-
η	Total collection efficiency	-
η_i	Collection efficiency of a particle size i	-
λ	Ligament efficiency	-
μ	Gas viscosity	kg/(m.s)
ν	Poisson's ratio	-
ρ_∞	Unperturbed gas density inside the heating system	kg/m ³

ρ_{fp}	Density of the flame product	kg/m^3
ρ_g	Density of gas	kg/m^3
ρ_p	Density of particles	kg/m^3
σ	Yield strength	Pa
Υ_M	Parameter from Horio and Nonaka	$\text{m}^{1/3}$

LIST OF APPENDICES

Appendix 1: Reactor, Cyclone and Distributor Schematics.....	119
Appendix 2: Heating System Schematic	120
Appendix 3: Piping and Instrumentation Diagrams	121
Appendix 4: Process Tables	127
Appendix 5: Equipment List	140
Appendix 6: Distributor Pressure Drop.....	141

CHAPTER 1 INTRODUCTION

1.1 Problem Statement and Motivation

In the mining and petro chemical industries, numerous conversion processes involve the use of catalysts, and are realized in fluidized bed reactors[1, 2] because of their many advantages, such as good solid mixing and good temperature control[3].

Despite being considered today as an ideal solution for many industrial applications[1], gas-solid fluidized bed reactors can vary significantly depending on the nature of the gas, the solids, and the operating conditions, which can lead to different hydrodynamic behaviours and therefore requires the use of very different flow models[2].

With feedstocks changing rapidly in the fuel and power fields due to the shortage of conventional resources; new sources, such as biomass, coal, and petcoke are emerging as future industrial solutions. However, their diversity and complex nature requires the use of extreme conditions during their handling and processing in fluidized bed reactors. In fact, most industrial gas-solid fluidized bed reactors operate at temperatures well above ambient, and some also operate at elevated pressures (pressured gasification, production of polyolefins...etc)[4]. While most design correlation are developed at ambient conditions, the effect of high temperature and high pressure have been found to cause modifications in the structure and dynamics of fluidized beds which are overlooked when only the gas properties in the equations are altered. In order to develop more appropriate hydrodynamic models, designing a bench scale fluidized bed reactor that would operate at high temperature and/or high pressure is indispensable to compensate for the lack of experimental results that exists today.

In fact, only a few laboratory scale fluidized bed reactors have been recorded to run at extreme conditions, with most of them operating at high temperature or high pressure.

Designing a reactor that operates at high temperature and high pressure is therefore of great bearing as it will contribute to the understanding of fundamental fluidization phenomena at extreme conditions by illustrating the effects of both temperature and pressure on hydrodynamics. Improvements in this field will not only have a significant impact on investments and revenues generated in the oil, petrochemical, and energy businesses; but it will also give invaluable insight on the design of fluidized bed reactors when more extreme conditions are present.

1.2 Objectives

The purpose of this thesis is to review and compare the already published models on fluidization at ambient and extreme conditions with emphasis on the information necessary for designing gas-solid reactors. Consequently, a detailed design of a fluidized bed that would allow flexible operation at high temperature and high pressure at several gas velocities will be conducted in order to serve for the future development of new hydrodynamic models. In order to accomplish this feat, the following objectives will be completed:

- 1- Study and Conduct a background study on fluidized bed technology and its application in industry as well as the different fluidization regimes.
- 2- Study and Conduct a full literature review on fluidization in order to illustrate the fundamental design variables, their respective correlations at extreme conditions and their limitations.
- 3- Design the fluidized bed reactor and its utilities, for flexible operation from ambient conditions up to high temperature and high pressure based on design books and papers.
- 4- Design a complete control process and operating procedure that would allow safe operation of this reactor.

The following chapters present the accomplishment of these objectives. At first, chapter 2 is a full literature review where the principles of fluidization and fluidized beds will be presented along with their applications. In Chapter 3, the influence of the use of extreme conditions on, bubble size, entrainment and mass transfer will be discussed. Furthermore, the impact of temperature and pressure on reaction conversion using a dynamic two-phase hydrodynamic model (DTP) will also be presented in this section. Chapter 4 is a detailed design the bench scale fluidized bed that would operate from ambient to high temperature (1000°C) and high pressure (20atm) at several gas velocities (from 0.1 to 2m/s) in order to serve for the future development of new hydrodynamic models. Chapter 5 presents the process used for the operation of the fluidized bed reactor and its utilities. Finally, in Chapter 6 the conclusion of this work as well as recommendations for future studies will be discussed. All references used can be found at the end of Chapter 6.

CHAPTER 2 LITTERATURE REVIEW

2.1 Fluidized Bed Principles

As the name would suggest, fluidized bed reactors use the principles of fluidization where gas is passed through a distributor on which granular solid materials lie (usually a catalyst) at high enough velocities to suspend the solid and cause it to behave like a fluid by subjecting it to pressure gradients. These properties result in many advantages, among which uniform particle distribution, gas solid contact and intense mixing, high conversion per unit mass of catalyst, uniform temperature gradient and continuous state operation.[5]

Before proceeding any further, it is of the upmost importance to define the different parts of a fluidized bed reactor. At the beginning, gas is passed through a grid, also known as a gas distributor, which provides stable and even fluidization across the reactor's cross-section by creating a pressure drop. A plenum chamber is usually placed under the grid in order to pre-distribute the gas uniformly before it flows through the distributor. The solids placed above the grid constitute the bed whose level, also known as the bed height, may vary based on the operating conditions of the reactor; such as gas velocity, gas properties and solid properties. The vertical space above the bed height which takes the larger volume of the whole unit is referred to by the freeboard and has the main task of preventing large amounts of the bed material from being carried out of the reactor by the gas stream.

A solid collection device such as a cyclone or filters is usually placed inside the freeboard in order to return entrained material to the bed[5]. These different sections are illustrated in Figure 1 below.

When gas flows through the bed, two distinct parts can be observed; the bubble phase and the emulsion phase. Voids, also referred to as bubbles, constitute the bubble phase and are created as a result of gas flowing through the bed. As gas velocity is increased these bubbles often lose their shape as they move upward to burst at the bed surface which induces particle ejection into the freeboard. The emulsion phase refers to the solid rich part of the bed. As particles are injected into the freeboard, their concentration will decay with height, as some will fall back into the bed, before becoming constant. The distance between the point where solids' concentration becomes

constant and the surface of the fluidized bed is referred to as the Transport Disengaging Height (TDH) [6] and is illustrated in Figure 2.

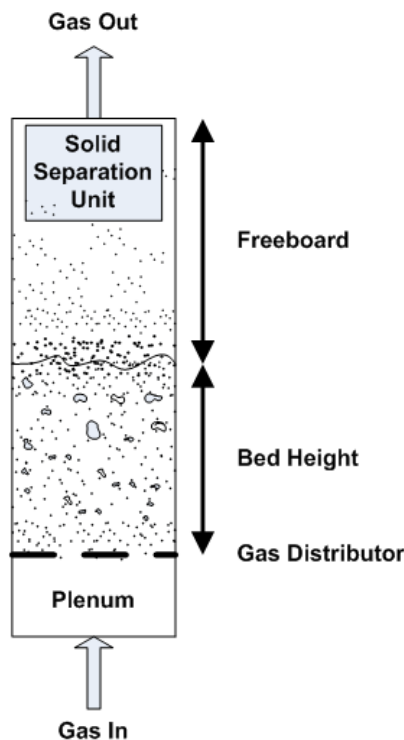


Figure 1- Fluid Bed Sections

As far as the designing of fluidized beds is concerned, the freeboard must be dimensioned to have a height of at least the TDH in order to reduce carryovers with any further height increase having little impact on entrainment. This can prove itself to be a hard task when dealing with high temperature and pressure as the determination of TDH tend to be more difficult.

In the literature, two distinct TDH values have been reported depending on the type of used particles: coarse or fine. Due to their terminal velocity being larger than the superficial gas velocity, coarse particles are ejected out of the bed by the bursting bubbles before falling back. The height they reach is referred to as the splash height or TDH(C). Fines on the other hand, have terminal velocities smaller than the gas and therefore reach more important heights which are referred to as TDH(F). In most design applications TDH(F) is simply referred to as TDH due to its higher value, and therefore this terminology will be used throughout this work.

Several research papers have been dedicated to the study and prediction of the transport disengaging height based on different influencing parameters such as the superficial gas velocity, bubble and column diameter, and solids and gas properties. Tannous et al (2008) [7] cited that the relationships to predict the TDH can be observed clearly in an extensive review outlined in three categories: graphical correlations, semi-empirical models, and empirical correlations[8-10].

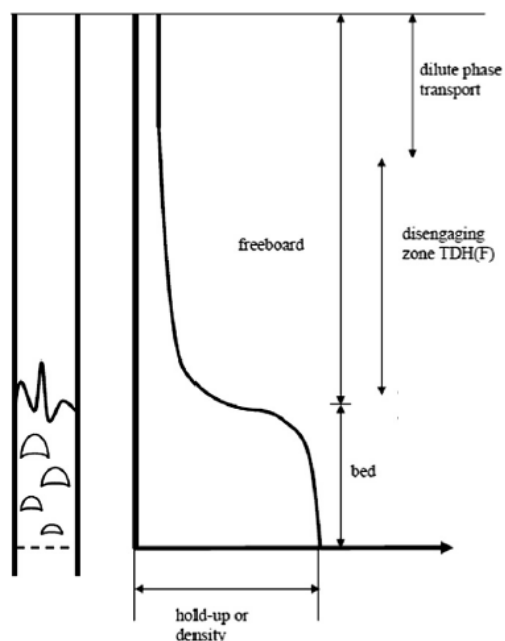


Figure 2- Transport Disengaging Height

2.2 Fluidization Regimes

Fluidization behaviour may differ based on the operating conditions of the reactor; such as gas velocity and gas and solid properties. Upon these observations, researchers have long established the existence of different fluidization regimes which are illustrated in Figure 3.

The state of fluidization begins at the minimum fluidization velocity U_{mf} . As the gas flow across the bed is increased, there exists a velocity known as the minimum fluidization velocity, U_{mf} , at which the resulting pressure drop is high enough to lift and suspend the solids by balancing the weight of the bed.

When the gas flow is further increased, the bubbling regime is reached. This regime starts when a minimum bubbling velocity, U_{mb} , is reached, where bubbles appear and a distinction between the

bubble and emulsion phase can be established. As these bubbles move upward in the bed, they tend to burst at the bed surface; ejecting particles into the freeboard.

The turbulent regime is reached when the terminal velocity of the ejected particles, U_C , is surpassed by the gas and the bed material no longer falls back as it is entrained out of the reactor. A solid particle collection device such as a cyclone or filters is usually placed at a high enough height to ensure particles recirculation and avoid depletion of the bed as the velocity is increased. Under these conditions, despite bubbles often losing their shape, beds with recognizable surfaces are referred to as turbulent fluidized beds.

The fast fluidization regime is characterized by the dominance of the gas phase as the bed level disappears due to a further increase in gas velocity. The transition velocity from the turbulent to the fast fluidization regime is referred to as the transport velocity, U_{tr} , with reactors operating under these conditions known as fast fluidization fluidized bed reactors. Finally the pneumatic transport is reached when all of the bed is depleted.

Depending on the desired product or the wanted effect, fluidized bed reactors can be operated in any of the aforementioned regimes. For instance, due to many distinct advantages, turbulent fluidized bed reactors are sometimes preferred to both bubbling and fast fluidization reactors because of their dynamic gas-solids contacting, high solids holdup, high exchange rate of the gas between the void and the emulsion phases, and relative spatial uniformity in flow properties. Industrial examples include Fischer-Tropsch synthesis, acrylonitrile production and FCC regeneration.

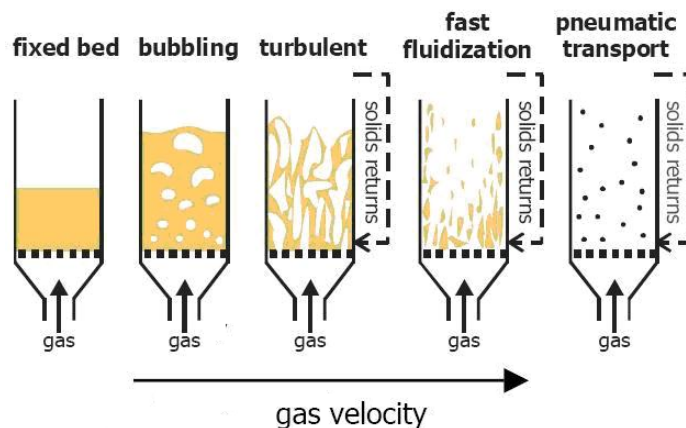


Figure 3- Fluidization regimes

2.3 Effects of Particle Size and Density

The behaviour of fluidized solids have been divided into four groups by Geldart (1973) based on the difference in density between the fluidizing gas and the used particles, $(\rho_p - \rho_g)$ and by the mean particle size d_p as illustrated on Figure 4.

Geldart C Particles: This group is characterized by cohesive or very fine particles (usually less than 20 microns). Due to their large surface area combined with low mass, interparticle forces tend to be greater than those resulting from the action of the gas which in turns renders fluidization extremely difficult. As a result, particles fail to flow in a manner that produces bubbles and the bed is unable to expand.

Geldart A Particles: In this group, particles are characterized as aeratable with a small mean particle size or/and low particle density. In fact, manufactured catalysts often belong to this group with particle sizes ranging from 20 to 100 microns. Due to the slightly cohesive structure of these particles, gas velocity must be increased beyond U_{mf} in order for bubbles to occur.

Geldart B Particles: These particles are characterized by being like sand with a mean particle diameter of about 150 microns. Due to the non cohesiveness of these particles, bubbles appear as soon as fluidization starts (ie $U_{mf} = U_{mb}$) shifting the bed's behaviour to the bubbling regime.

Geldart D Particles: These are large and/or dense particles in the order of 1 or more millimetres. When velocity is increased, a jet is formed in the bed creating a spouting motion.

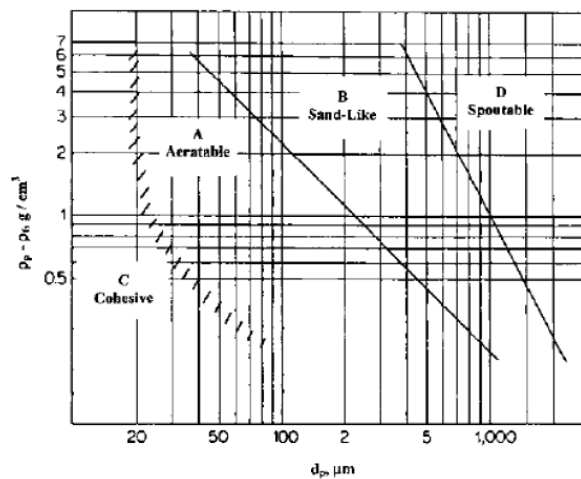


Figure 4- Geldart Particles

2.4 Solid Mixing and Entrainment

In most fluidized bed applications, the freeboard occupies the largest volume of the reactor and thus particular care must be taken when designing it. As the freeboard has the main task of preventing large amounts of the bed material from being carried out of the reactor by the gas stream, understanding solid entrainment above the bed (the flux of solids carried out of the fluidized bed by the gas) is fundamental in the sizing of this section. Furthermore, understanding the influence of the freeboard diameter, particle properties and operating conditions can play a fundamental role in the design of the solid separation unit that will be installed.

While there is a general agreement on the importance of bubbles in the projection of particle from the bed into the freeboard[11], the exact mechanism behind this phenomena remains an area of dispute.

After ejection of the particles into the freeboard, their velocity will gradually decelerate which would lead to one of two scenarios: the solids will either be entrained out of the reactor or will fall back into the bed.

The most generally used model to predict the entrainment rate was created by Large et al (1976) [12]. According to Large et al, modelling of the entrainment flux, for a given particle size i , consists of the addition of two fluxes. The first flux involved in the modelling of the total entrainment according to Large et al is that of the continuously flowing solids from the bed surface to the outlet of the reactor, also known as the elutriation flux.

The second flux involved in the modelling of the total entrainment according to Large et al is that of the solids which tend to fall back into the bed.

Furthermore, Large et al reported that the bed surface flux decreases exponentially with increasing height above the bed surface. Despite agreement between researchers on the format of the model of Large et al, developing suitable correlations to predict both the elutriation flux and the bed surface flux remains an area of dispute due to the influence of pressure and temperature on entrainment as will be presented in Chapter 3.

2.5 Application of High Temperature and Pressure

Since 1922 when fluidization was first introduced in a coal gasification process, the use of fluidized beds have significantly increased over a wide spectrum of applications due to their many advantages such as good solid mixing, high heat and mass transfer and good temperature control[13]. Despite these advantages, fewer fluidized beds are being operated today under ambient conditions due the competitive nature of the market as well as the constant need of developing more efficient solutions, which has lead to a wide interest in high temperature and pressure operation. In fact, operation under extreme conditions has been proven to be of fundamental importance in different industrial cases. For instance, in the fuel and power fields, the diversity and complex nature of new sources, such as biomass, coal, and petcoke require the use of extreme conditions during their handling and processing in fluidized bed reactors. Another good example where high temperature and pressure are used can be found in the mining industry. With the nature of ore becoming more complex and harder to refine due to the presence of carbonaceous matters or sulfides that renders gold extraction more difficult, significant pre-treatment is required to achieve feasible extraction processes. A key component to eliminate carbonaceous matters in the pre-treatment process is oxidation at high temperature and pressure. Furthermore, roasting, which is used to induce a reaction and the expelling of volatile matter without causing fusion, is commonly done in fluidized bed reactors operating at high temperature and pressure.

The use of extreme conditions can also result in higher revenues. A good testament of that is pressurized gasification.

In gasification, when pressure is increased, the material and mechanical problems associated with the gasifier are also increased not to mention that most of the combustion reactions are favored at low pressure. By looking at these restrictions, it is difficult to understand why high pressure is used or how it can generate higher revenues. In fact, when pressure is increased, one of its effects is the reduction in the required volumes which represent 30 to 40% of the fixed capital investment[14]. Moreover, an increase in pressure also results in a faster reaction rate which in turns further reduces the required equipment sizes. Another benefit of using pressurized gasification is the elimination of the costly compression steps downstream of the combustion/pyrolysis step as illustrated in Figure 5. CO₂ emissions from coal-burning power

plants have also been reported to drop when pressurized fluidized bed boilers are used since they use less fuel to produce the same amount of power.

Brown et al (1979)[15] conducted a comparative study between a high pressure and a low pressure process where ammonia is produced from coal and a high pressure and a low pressure process for the production of methanol. They concluded that the high pressure processes resulted in an increase in coal consumption not to mention a reduction in compressor power consumptions, and much more compact gas cleaning equipment.

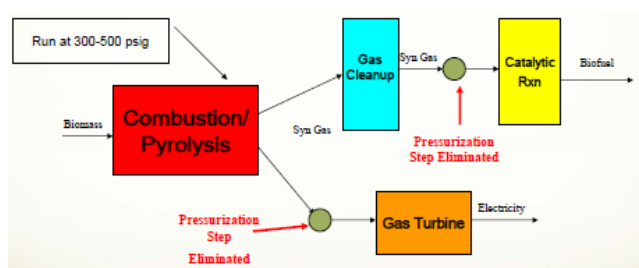


Figure 5- Gasification process

Many other examples, where extreme conditions are used, exist today in industry; some of which are illustrated in table 1 below.

Table 1- Applications of high temperature and pressure in industrial fluidized beds

Process	Pressure range (atm)	Temperature range (C)
Fischer–Tropsch [16, 17]	18-30	300-350
Ammonia synthesis [17, 18]	20-100	300-600
Methanol synthesis [17, 19]	40-100	220-280
PFBC Combined Cycle for coal combustion [17, 20]	10-16	600-1300
Coal gas desulfurization process [21]	1-25	300-900

CHAPTER 3 INFLUENCE OF USING EXTREME OPERATING CONDITIONS ON FLUIDIZED BED REACTORS

When dealing with gas-solid fluidized bed reactors at elevated temperatures and pressures, it is important to understand the influence of operating under extreme conditions in order to be able to improve upon what exists today; whether it be attaining rapid rates of chemical reaction (e.g. gasification of coal, combustion of solid fuels and fuel additives, reduction of mineral ores, synthesis of industrially useful chemicals via surface catalysis), or controlling or suppressing the resulting reactions (corrosion, gasification, or embrittlement of structural components or containment materials). Several papers and articles have been dedicated to study the effect of elevated temperature and pressure on the performance of fluidized bed reactors. In fact, operating under extreme conditions has been reported to alter fluidization behaviour and bubble size with the latter considered as one of, if not the most important variable related to reactor performance.

The purpose of the following section as the title would suggest, is to demonstrate the effect of using extreme operating conditions (high temperature, pressure and velocity) on fluidization and more specifically bubble size. Subsequently, the impact of bubble size on mass transfer, reaction conversion and the transport disengaging height (TDH) will be studied. By doing so, the aim of this section is to illustrate the limitations of some of the most common correlations found in the literature, and to demonstrate the need of developing new models at high temperature, pressure and velocity.

In section 3.1, some of the reported trends of the influence of high pressure and temperature on fluidization will be presented. In section 3.2, some of the different findings and correlations developed to estimate bubble size will be presented along with the influence of temperature, pressure and velocity on three different correlations. This section will be followed by a study of entrainment under extreme conditions and more specifically the different existing correlations to predict the transport disengaging height in section 3.3. Section 3.4 will then present a review on mass transfer in fluidized bed reactors. Finally, the methane steam reforming reaction, which was chosen for this study, will be presented in section 3.5 along with its kinetics. A detailed study using the same three bubble size correlations will then be conducted in order to illustrate the

influence of temperature, pressure and velocity on conversion. Finally, the conclusions of this chapter will be listed in section 3.6.

3.1 Influence of extreme conditions on fluidization

In process engineering, the effects of temperature and pressure have long interested researchers for many different reasons: whether it is to attain rapid rates of chemical reactions (e.g. gasification of coal, combustion of solid fuels and fuel additives, reduction of mineral ores, synthesis of industrially useful chemicals via surface catalysis), or to control or suppress the resulting reactions (corrosion, gasification, or embrittlement of structural components or containment materials), the ability to improve upon what exists is dependent upon understanding the effects related to the operating conditions[22]. Henceforth, when dealing with gas-solid fluidized bed reactors at elevated temperatures and pressures, understanding the influence of operating under these conditions on fluidization is fundamental. In fact, many research papers have been dedicated to studying the effects of pressure and temperature individually on fluidized beds.

For instance, an increase in pressure in a gaseous reaction has been reported to increase the number of collisions between reactants which in turns influences the rate constant that may change the rate of reaction and can therefore be used to improve selectivity. Pressure has also been found to have a major influence when gas-solid reactions with porous catalysts are involved, as it can alter the gas film resistance at the surface of the catalyst which in turns affects the diffusion of the reactants through the pores. The aforementioned effects have long intrigued researchers as to their influence on fluidization. For instance, at elevated pressures, many researchers concluded that fluidized bed reactors can be characterized by smaller bubbles [23, 24], a higher heat transfer rate[25], and a decrease in particle segregation[26]. Interestingly, Li et al. (2002) observed a wider range of particulate flow regime at higher pressures[4]. Lie et al. also reported a stronger effect of pressure on a bed of Geldart A particles than that of Geldart B and D[27]. Notable effects were also observed on flow patterns when subjected to high pressure. Lie et al. noted a more homogeneous structure near the turbulent regime and reported that under these conditions, the particle–fluid interactions intensified while the particle-particle interactions were suppressed allowing the gas–solid flow structure to form a more homogeneous flow. Moreover,

they also concluded that the extension in the uniform fluidization regime led to a shortening in the width of the bubbling regime[4].

Industrially, with most gas-solid fluidized beds operating within the temperature range of ambient to 1100°C, the effect of temperature has also received great interest from researchers who studied the influence it presents on different fluidization parameters, such as mean velocities and diffusivity of particles, by affecting gas density and viscosity. In fact, variations of these two parameters were until recently believed to be the only variables that determine the effect of temperature on gas-solid systems. Today however, it is believed that changes in density and viscosity of the gas are not sufficient to account for the observed deviation from classical models at high temperature [28-30]. These observations include changes in the bed's behaviour as well as in the physical properties of the particles [28, 29]. In fact, Cui et al. (2003) have observed that for FCC particles, the bed behaviour would shift significantly from Geldart A towards Geldart B [29] while Lettieri et al. (2000) showed how interparticle forces at high temperature can cause the transition of the fluidization behavior from Geldart A to Geldart C [31]. Sanaei et al. (2010) [32] explained how temperature affected emulsion surface tension which led to an increase in solid mixing and particle diffusivity when the temperature was increased from ambient to around 300°C, followed by a decrease beyond that temperature.

3.2 Bubble size under extreme conditions

Bubble size has been reported to be one of, if not the most important variable related to reactor performance. It has been proven to control the most fundamental fluidization parameters such as bubble rising velocity, gas interchange rate between phases, particle circulation rate, heat transfer, and elutriation of fine particles from the bed surface[33]. Therefore it is of the upmost importance to be able to model and understand the impact that operation under extreme conditions has on bubble size. In the literature, many papers and articles have been dedicated to the study of bubbling behaviour with some reporting the observed trends at high temperature, pressure and velocity.

High pressure has been reported to yield smaller maximum stable bubble size and reduced bubble frequency[34]. In fact, Varadi et al (1978) [35] explained that an increase in pressure induces a decrease in the apparent viscosity of the emulsion phase which in turns causes bubble splitting by division from the roof and therefore a reduction in bubble size. Interestingly, Varadi et al (1978)

[35], Row et al (1984) [36], and Cai et al (1989) [37] reported that at low gas velocities, a slight increase in bubble size can be observed in the lower pressure range (less or much less than 10 bar) followed by a decrease in the upper pressure range. With velocity clearly affecting bubble size, several sources reported its effects to differ based on the operating flow regime. Bubble size was found to increase with velocity under the bubbling regime,[38, 39] and decrease with velocity under the turbulent regime [37, 40].

With the effects of pressure and velocity agreed upon between most researchers, the effects of temperature have yielded more debates.

While some such as Tone et al. (1974) [41], Geldart and Kapoor (1976) [42], and Zhang et al. (1982) [43] reported that bubble diameter decreases with increasing temperature, others such as Chan and Knowlton (1987) [23] reported that bubble size is independent of temperature.

Sanaei et al (2012)[44], evaluated bubble diameters at high temperature and observed that bubbles can grow up to a maximum diameter by increasing the temperature up to 300 °C after which the diameter of the bubbles is decreased. They explained this observation by the effect of interparticle forces on bubble size. In fact, at temperatures below 300 an increase in the gas viscosity is dominant in comparison with gas density decrease whereas at higher temperatures the decrease in gas density is more effective. As a result, the drag force decreases after increasing initially, therefore explaining how a first increase in temperature facilitates bubble growth while further increase leads to a decrease in bubble diameter.

With these bubble size trends reported with respect to temperature, pressure and gas velocity, it is important to have a model where these observations are manifested.

Several bubble diameter correlations have been proposed in the literature with unfortunately most providing inconsistent results when high temperature, pressure and velocity are applied [33, 45]. Gogolek and Grace (1995) [46] presented an overview of different correlations to find the average bubble size at high pressure. They wrote that a reliable correlation to estimate the mean bubble size, d_b was proposed by Mori and Wen (1975) [47] for Geldart A and B powders where d_b is a function of the initial and maximum bubble size. Furthermore, this correlation has been cited in various design and fluidization books and can be considered as one of the most commonly used models to predict bubble size [1, 9, 48]:

$$d_b(z) = (d_{b\infty} - d_{b0}) \exp\left(\frac{-0.3z}{D_t}\right)$$

Where, both the initial and maximum bubble diameters d_{b0} and $d_{b\infty}$ can be predicted using the following correlations:

$$d_{b\infty} = 0.941[\pi D_t^2 (U - U_{mf})]^{0.4}$$

$$d_{b0} = 0.872[A_t (U - U_{mf})]^{0.4}$$

Cai et al (1994) [45] presented a good revue on some of the existing correlations that take into account the effects of pressure and velocity on bubble size and emphasized on the contradictory results that they offered due to several experimental factors.

In fact, Cai et al [45] observed that almost all the currently available bubble size correlations predict a monotonic increase in bubble size with gas velocity and pressure. In order to have the same trends as those observed by other researches with respect to bubble size, Cai et al developed their own correlation based on different experimental results with a wide range of velocities, pressures and particle diameters.

$$d_b = 0.38z^{0.8} P^{0.06} (U - U_{mf})^{0.42} \exp\left(-1.4 \cdot 10^{-4} P^2 - 0.25 (U - U_{mf})^2 - 0.1 P (U - U_{mf})\right)$$

Cai's correlation however was not modelled to take into account temperature due to what they considered uncertainties with respect to its effects.

Horio and Nonaka (1987) [33] developed their own bubble diameter correlation for Geldart A and B powders that takes into account the effects of temperature based on the observations of Tone et al (1974) [41].

$$d_b = \frac{D_t [-\gamma_M + (\gamma_M^2 + 4d_{bM}/D_t)^{0.5}]^2}{4}$$

Where

$$d_{bM} = 2.59g^{-0.2}[(U_0 - U_{mf})A_t]^{0.4}$$

$$\gamma_M = 2.56 \times 10^{-2} \frac{(D_t/g)^{0.5}}{U_{mf}}$$

In all of the aforementioned correlations, U_{mf} can be calculated by the correlation developed by Wen and Yu [49]. Their equation relates the particle Reynolds number at minimum fluidization velocity, Re_{mf} , to the Archimedes number, Ar .

$$Re_{mf} = \frac{d_p \cdot U_{mf} \cdot \rho_g}{\mu} = (1135.7 + 0.0408Ar)^{0.5} - 33.7$$

Where

$$Ar = d_p^3 \rho_g (\rho_p - \rho_g) g / \mu^2$$

In order to verify the efficiency of the aforementioned models with regards to extreme operating conditions, each correlation was plotted in the following sections and compared to experimental results from different sources. The applicability range of these correlations can be found in table 2 below.

Table 2- Applicability range of the bubble size correlations by Mori and Wen (1975), Horio and Nonaka (1987) and Cai et al (1994)

Correlation	D_t (m)	T (C)	$U-U_{mf}$ (m/s)	P (atm)
Mori and Wen (1975)	0.3-1.3	25	0.008-0.5	1
Horio and Nonaka (1987)	0.079-1.3	30-650	0.008-0.5	1
Cai et al (1994)	0.13-0.4	25	0.028-0.6	1-70

3.2.1 Effect of velocity on bubble size

In order to evaluate the efficiency of the chosen correlations with respect to velocity, they were plotted in Figure 6 and compared to the experimental values of Yamazaki et al (1991)[50] whose specifications are listed in table 3 below.

Table 3- Specifications of the experimental results of Yamazaki et al (1991)

Parameter	Value
D_t (m)	0.2
H (m)	0.5
d_p (μm)	64
ρ_p (kg/m^3)	850
P(atm)	1
T(C)	25
U(m/s)	0.45-1.1
Experimental method	Optical fiber probe
Parameter studied	Void rise velocity

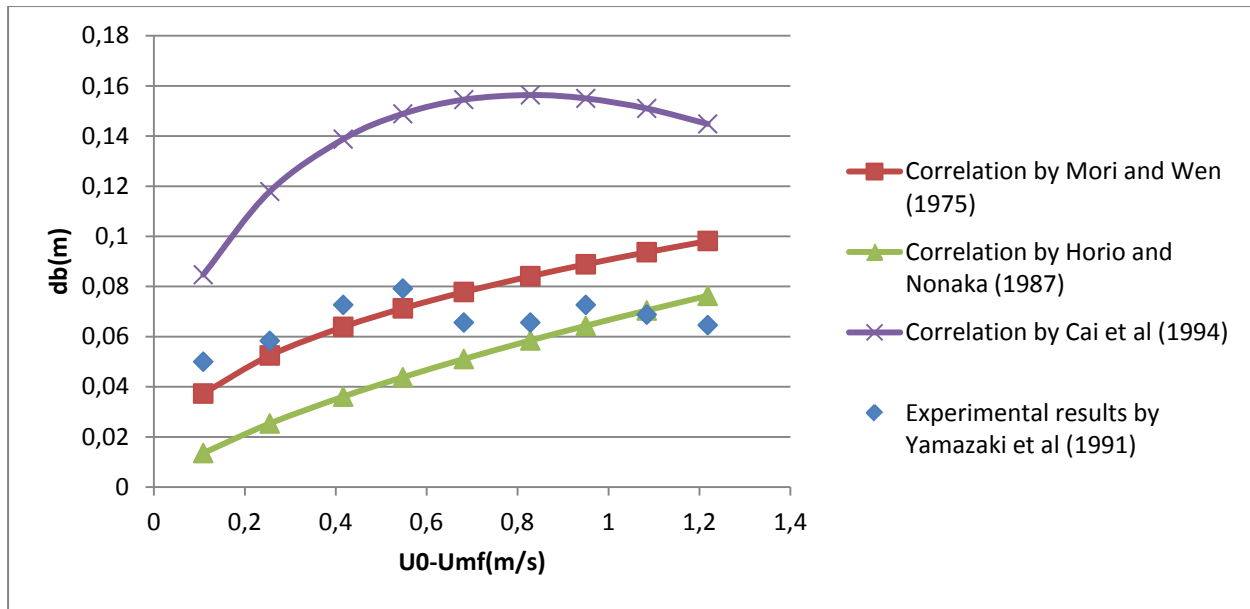


Figure 6-Comparison of the bubble size correlations by Mori and Wen (1975), Horio and Nonaka (1987) and Cai et al (1994) with the experimental values of Yamazaki et al (1991) with respect to velocity at ambient pressure and temperature.

In Figure 6, the effects of velocity on bubble size can be divided on two regions: low velocity (0.1-0.6m/s) and high velocity (>0.6m/s).

At low velocities, all three correlations predict an increase in bubble size with the model by Cai et al overestimating bubble diameter by up to twice the experimental value. At these velocities, the correlation by Mori and Wen provides the best results with a percentage error ranging between 7 and 20%. The percentage error from Horio and Nonaka is between 45 and 80%.

As velocity is increased however, Yamazaki et al show experimentally that bubble size starts to decrease. This trend is in fact consistent with the observations of Rowe et al [38], Weimer et al [39] and Sellakumar and V. Zakkay [40] who reported that the effects of velocity on bubble size differ based on the operating flow regime where the bubble diameter increases in the bubbling regime and decreases in the turbulent regime. This decrease is inconsistent with the correlation of Mori and Wen and that of Horio and Nonaka which predict an increase in bubble size over the whole velocity range.

This decrease in bubble size can be observed by the correlation of Cai et al at a higher velocity of 0.8m/s. The obtained results from this model, albeit offering the same trend as the experimental findings, still presented a very large percent error ranging from 50 to 57%.

3.2.2 Effect of pressure on bubble size

In order to assess the ability of each model to efficiently predict bubble size with respect to the applied pressure, each correlation was plotted in Figures 7 and 8 and compared to the experimental values of Hoffmann and Yates (1985)[51] whose specifications are listed in table 4 below.

Table 4- Specifications of the experimental results of Hoffmann and Yates (1985)

Parameter	Value
D_t (m)	0.17
H (m)	0.4
d_p (μm)	45
ρ_p (kg/m^3)	1417
U(m/s)	0.12
T(C)	25
P(atm)	1-81
Experimental method	X-rays imaging
Parameter studied	Bubble silhouettes

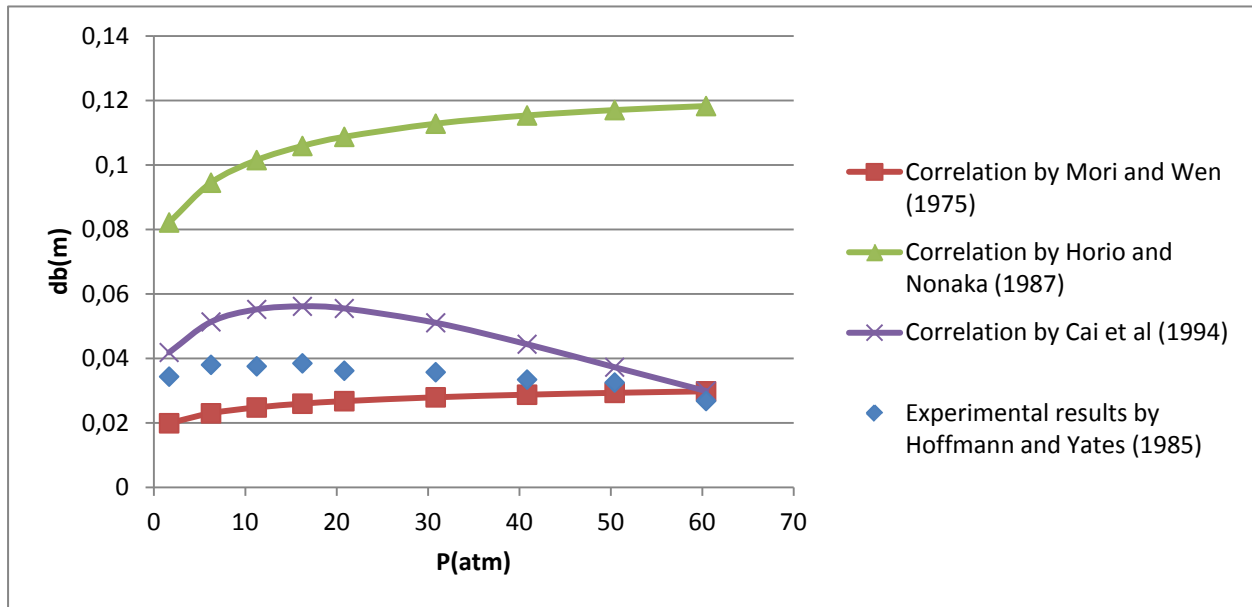


Figure 7-Comparison of the bubble size correlations by Mori and Wen (1975), Horio and Nonaka (1987) and Cai et al (1994) with the experimental values of Hoffman and Yates (1985) with respect to pressure at ambient temperature and a gas velocity of 0.12m/s

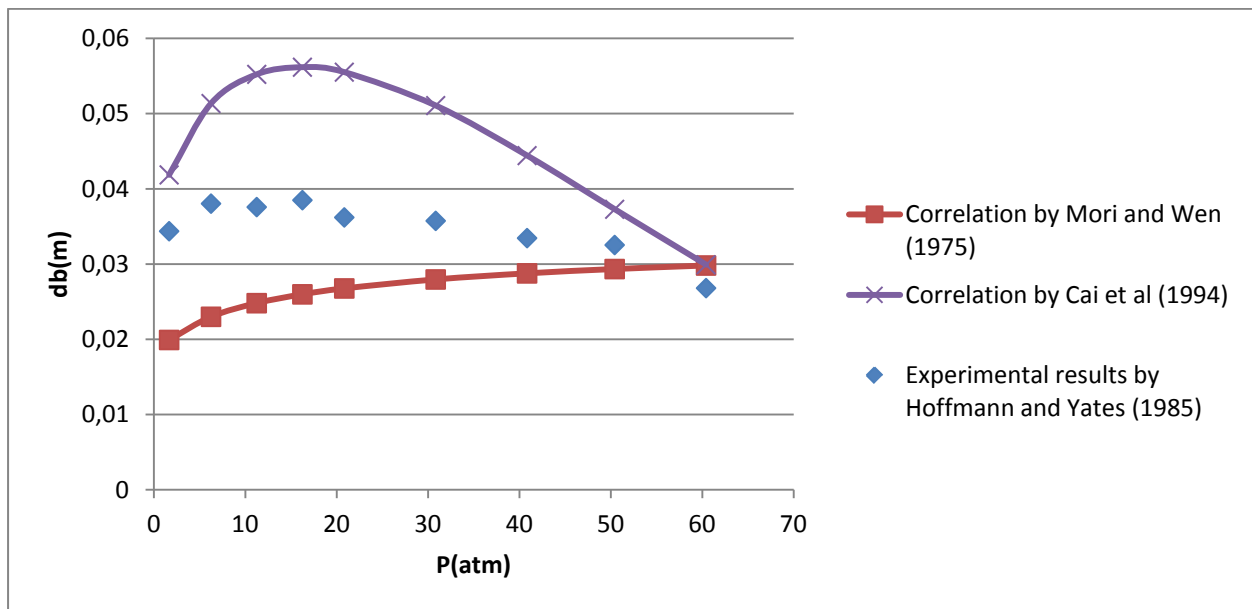


Figure 8-Comparison of the bubble size correlations by Mori and Wen (1975) and Cai et al (1994) with the experimental values of Hoffman and Yates (1985) with respect to pressure at ambient temperature and a gas velocity of 0.12m/s

At first glance, it is clear that the correlation by Horio and Nonaka greatly overestimates bubble size when compared to the experimental values of Hoffman and Yates by more than 300%.

In Figure 8, only the correlation by Mori and Wen and that of Cai et al have been plotted with the experimental values of Hoffman and Yates. The effects of pressure on bubble size can be divided into two regions: from 1 to 17atm and from 17 to 70atm.

In the first region, both correlations predict an increase in bubble size with the model by Mori and Wen providing a larger percent error ranging from 36 to 43% compared to 15 to 30% for the model by Cai et al.

When pressure is increased further, Hoffman and Yates showed that bubble size decreases. This trend has been reported by many researchers [37, 51, 52], among which Cai et al, who reported that at constant temperature and velocity, bubble size decreases with increasing pressure in both the bubbling and turbulent regimes except at very low gas velocities.

This decrease is inconsistent with the correlation of Mori and Wen and that of Horio and Nonaka which predict an increase in bubble size over the whole pressure range. Furthermore, as pressure is raised, the percent error of the obtained results from the correlation of Cai et al decreases to 10% despite yielding initially much higher percentages (30% at 17atm).

3.2.3 Effect of temperature on bubble size

In order to evaluate the influence of temperature on bubble size, the chosen correlations were plotted in Figures 9 to 13 and compared to the experimental values of Sanaei et al (2012)[44] whose specifications can be found in table 5.

Table 5- Specifications of the experimental results of Sanaei et al (2012)

Parameter	Value
D_t (m)	0.078
H (m)	0.2
d_p (μm)	250
ρ_p (kg/m^3)	2650
U (m/s)	0.38
P(atm)	1
T(C)	25-600
Experimental method	Radio-active particle tracking
Parameter studied	Time-position trajectory of particle

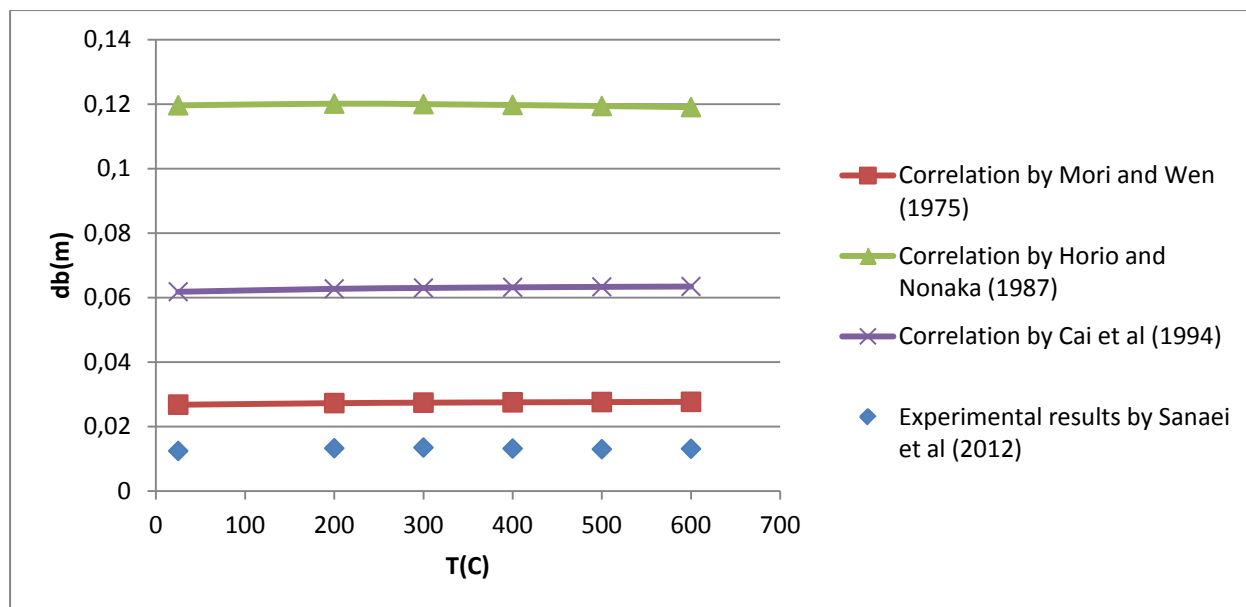


Figure 9- Comparison of the bubble size correlations by Mori and Wen (1975), Horio and Nonaka (1987) and Cai et al (1994) with the experimental values of Sanaei et al (2012) with respect to temperature at ambient pressure and a velocity of 0.38m/s

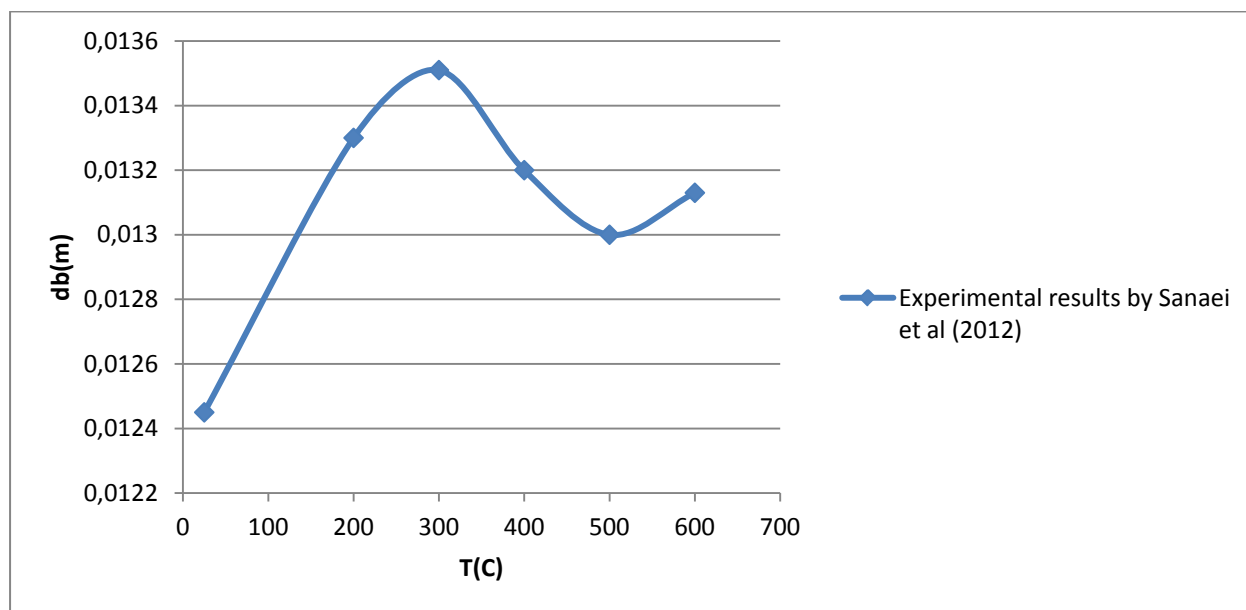


Figure 10- Bubble size vs temperature (adapted by Sanaei et al (2012)) at ambient pressure and a velocity of 0.38m/s

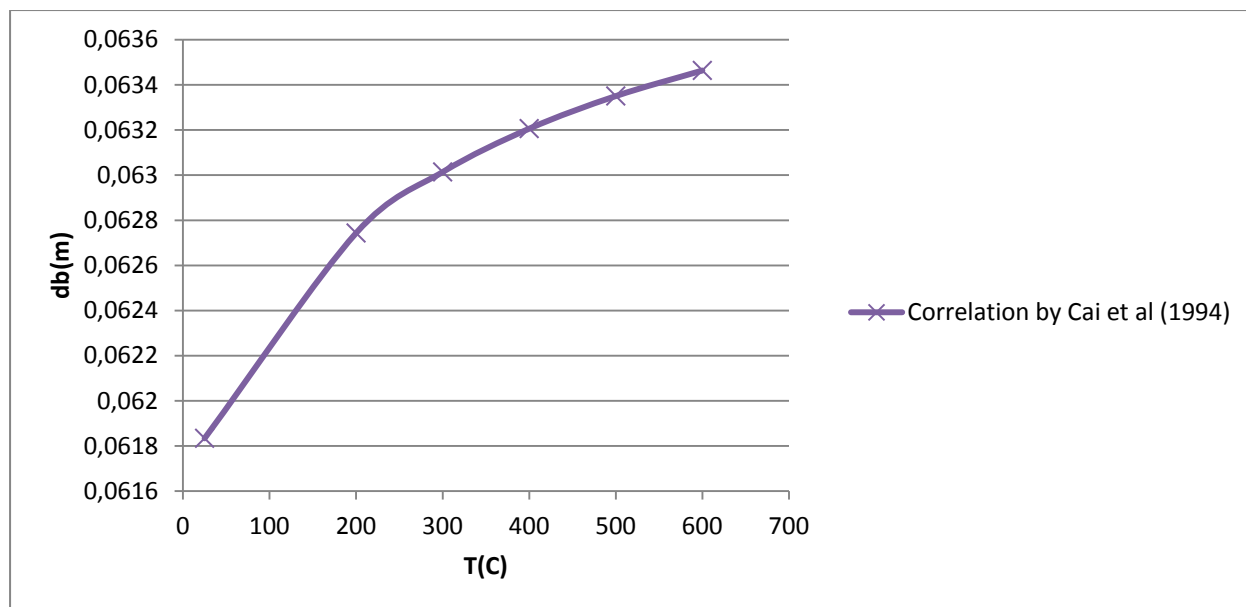


Figure 11- Bubble size vs temperature (according to the correlation by Cai et al (1994)) at ambient pressure and a velocity of 0.38m/s

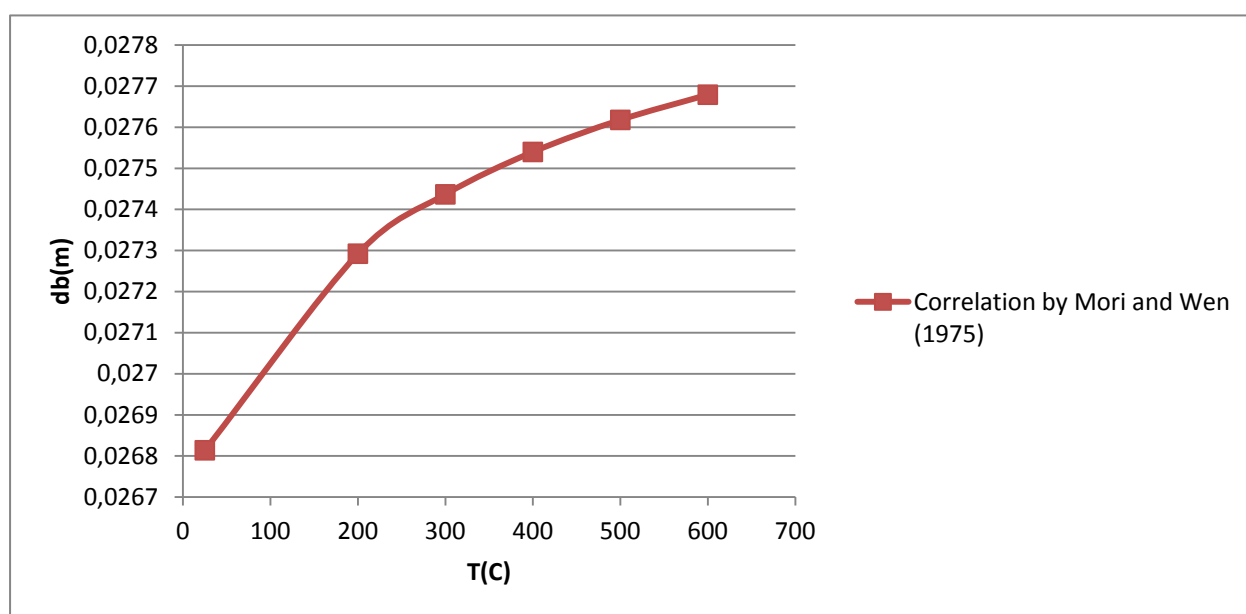


Figure 12- Bubble size vs temperature (according to the correlation by Mori and Wen (1975)) at ambient pressure and a velocity of 0.38m/s

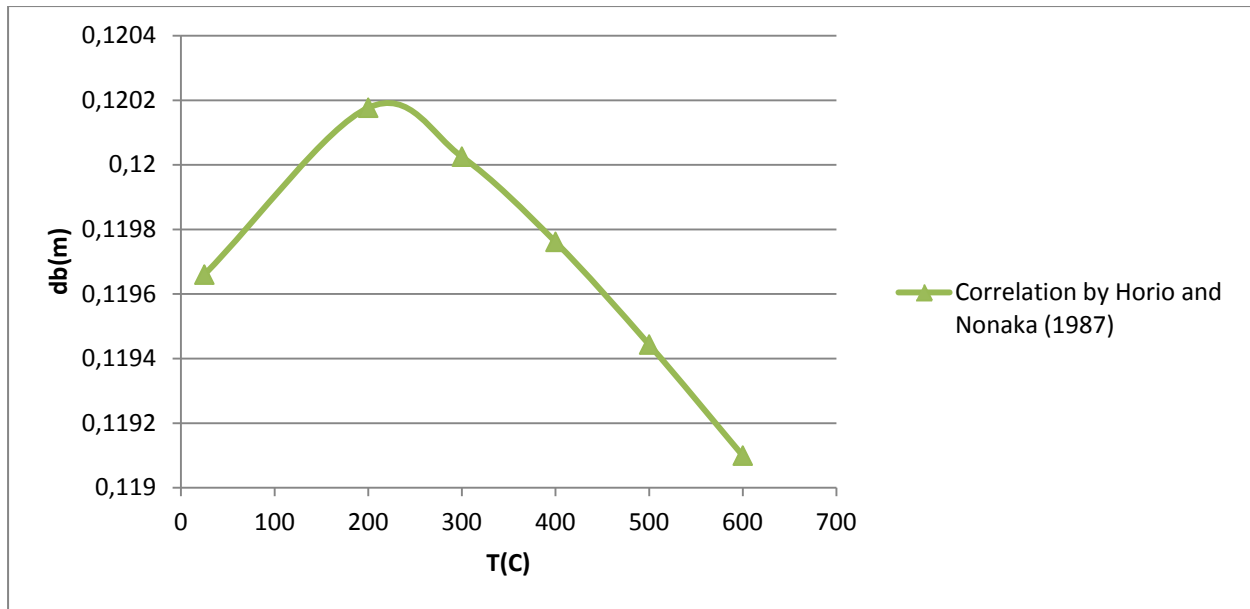


Figure 13- Bubble size vs temperature (according to the correlation by Horio and Nonaka (1987)) at ambient pressure and a velocity of 0.38m/s

All three correlations overpredict bubble size with respect to temperature. Furthermore the correlation by Mori and Wen and that by Cai et al seem to predict a monotonic increase in bubble size with respect to temperature which does not correspond to the experimental results where bubbles grow up to a maximum diameter of 1.35cm at 300 °C after which their diameter decreases. This trend is observed in the correlation by Horio and Nonaka which however overestimates bubble size by almost 800%. It is clear that more work needs to be done on bubble size models with respect to temperature since the closest obtained values were those by the correlation of Mori and Wen which overestimates bubble size by 50%.

Finally, it is interesting to note that despite these opposite trends, the magnitude of the change in bubble size due to the effect of temperature seems to be very small when compared to the changes obtained from varying pressure or velocity. For instance, a change of 3.2%, 0.9% and 2.6% between the largest and the smallest bubble was recorded respectively while varying the temperature for the correlations of Mori and Wen(1975), Horio and Nonaka (1987) and Cai et al(1994), compared to 180%, 530% and 91% with respect to velocity and 50%, 44% and 88% with respect to pressure.

3.3 Influence of Extreme Operating Conditions on Entrainment and TDH

As explained in section 2.4, when bubbles reach the bed surface, particles are ejected into the freeboard where their concentration decays before becoming constant at the transport disengagement height, TDH [6]. This height plays an important role in fluidized bed design since it must equal that of the freeboard to reduce carryovers, with any further increase not affecting entrainment. Unfortunately, there is no commonly accepted method for the calculation of the TDH [6], but only several empirical correlations which were developed under ambient conditions. Furthermore, with very little studies showing the effects of temperature, pressure and velocity on TDH, finding experimental results can be a real challenge. Nevertheless, the effects of operating under extreme conditions have received a lot of interest in entrainment modelling. Therefore, with the appropriate entrainment plot, one may graphically estimate TDH.

In the next section, different entrainment models will be plotted versus height with the consequent effect of temperature, pressure and velocity studied. Moreover, the impact of using different bubble size correlations on entrainment will also be presented along with a graphical estimation of TDH. Finally, the obtained values and trends will be compared to some of the existing TDH correlations.

3.3.1 Entrainment modelling

Several papers have recorded the effects of temperature on entrainment. Choi et al. (1998)[53] studied the effects of temperature on the entrainment rate for a fluidized bed and observed that the plot of the entrainment rate vs. temperature yielded a positive parabolic curve. Wouters and Geldart(1998) [54], while reporting a similar trend for a plot of elutriation rate constant vs temperature, did not find a minimum when they plotted entrainment rate vs. temperature.

The effect of pressure on entrainment has also been studied by several authors. Chan and Knowlton (1984) [55] studied the effect of pressure (up to 31bar) on sand fluidization and observed a significant increase in TDH and entrainment with pressure and velocity. These findings were confirmed by Pemberton and Davidson (1984) [56] who explained the observed entrainment increase by the fact that entrainment is inversely proportional to bubble size which decreases at high pressures.[57]

As seen in Chapter 2, Large et al (1976) [12] developed the most generally used model to predict entrainment rate, E_{ih} :

$$E_{ih} = E_{i\infty} + E_{i0}'.$$

Where $E_{i\infty}$ is the elutriation flux and E_{i0}' , the solid entrainment flux at the surface of the bed.

Despite agreement between researchers on the format of this model, several correlations exist in order to predict the elutriation flux and the solid entrainment flux at the surface of the bed because of the influence of pressure and temperature on entrainment.

Elutriation flux, $E_{i\infty}$

Zenz and Weil (1958) [58] defined the elutriation flux, $E_{i\infty}$, as the product of the mass fraction x_i of the particles in the bed and the elutriation rate constant $K_{i\infty}$. This simply signifies that, for all particle size classes, a mass flux at least equal to $E_{i\infty}$ is ejected from the bed into the freeboard. A very good review of the different correlations to find $E_{i\infty}$ and $K_{i\infty}$ can be found in the handbook of fluidization and fluid-particle systems[6]. These correlations, with the exception of Choi et al (1999) [59], whose correlation is presented in table 6 below, were developed under ambient conditions as a function of velocity, bed diameter and particle size and therefore might not be applicable when high temperature and pressure are involved.

Bed surface flux, E_{i0}

This flux is calculated based on the solid entrainment flux at the surface of the bed, E_{i0}' .

Multiple equations have been developed to calculate E_{i0}' with respect to bubble size, frequency and velocity. Many of these correlations can again be found in the handbook of fluidization and fluid-particle systems [6], with the correlation by Choi et al (1999) [59] (presented in table 6) being the only one suitable for high temperature and high pressure systems.

Furthermore, as mentioned earlier in Chapter 2, Large et al reported that the bed surface flux decreases exponentially with increasing height, z , above the bed surface as a function of a constant, referred to as the decay constant, a_i , such as:

$$E_{i0} = E_{i0}' \exp(-a_i z).$$

The total entrainment flux model by Large et al can therefore be expressed as:

$$E_{ih} = E_{i\infty} + E_{i0} \exp(-a_i z).$$

There is disagreement however between researchers on the magnitude and dependencies of the decay constant, a . In fact, different values can be found in the literature for fluidized beds under ambient conditions ranging from 0.5 to 6.4m⁻¹ [46, 60, 61]. The only available correlation predicting the decay constant was again developed by Choi et al and can also be found in table 6.

Table 6- Choi et al (1991) correlation for entrainment rate (applicable for a velocity range from 0.3 to 7m/s, a particle diameter range of 0.005 to 1mm and a reactor diameter for 0.06 to 1m)

Variable	Correlation
Elutriation flux	
Elutriation rate	$K_{i\infty} = \frac{\mu}{d_p} A_r^{0.5} \exp\left(6.92 - 2.11 F_g^{0.303} - \frac{13.1}{F_d^{0.902}}\right)$
Gravity force per projection area	$F_g = g \cdot d_p (\rho_p - \rho_g)$
Drag force per projection area	$F_d = C_d \frac{\rho_g \cdot U^2}{2}$
Elutriation flux	$E_{i\infty} = x_i K_{i\infty}$
Bed Surface Flux	
Original bed surface flux	$E_{i0}' = 9.6 A_t (U - U_{mf})^{2.5} d_b \left(\frac{298}{T}\right)^{3.5}$
Decay constant	$a = \frac{1}{d_p} \exp\left(-11.2 + 210 \frac{d_p}{D_t - d_p}\right) \left(\frac{d_p \rho_g (U - U_{mf})}{\mu}\right)^{-0.492} \left(\frac{d_p g \rho_p}{\rho_g (U - U_{mf})^2}\right)^{0.725} \left(\frac{\rho_p - \rho_g}{\rho_g}\right)^{0.731} C_d^{-1.47}$
Bed Surface Flux	$E_{i0} = E_{i0}' \exp(-a_i z)$

In Choi's correlation, C_d is the drag coefficient and can be have different values for different particle Reynolds numbers, Re_p . These values were presented by Choi et al (1999) [59] and are listed in table 7 below:

Table 7- Drag Coefficient for different Reynolds numbers

Range	Correlation
$Re_p \leq 5.8$	$C_d = 24/Re_p$
$5.8 < Re_p \leq 540$	$C_d = 10/Re_p^{0.5}$
$540 < Re_p$	$C_d = 0.43$

Choi et al's correlation has been confirmed to be valid in predicting the particle entrainment rate at the freeboard gas exit for the experimental range listed in table 8.

Table 8-Validity range of the entrainment correlation by Choi et al. (1999)

Variable	Range
Particle diameter	21-710 μm
Particle density	2400-6158 kg/m^3
Gas velocity	0.15-2.8 m/s
Temperature	12-600 $^{\circ}\text{C}$
Pressure	1-31 atm
Column diameter	0.1-0.91 m
Column height	1.97-9.1 m

In order to study the effects of extreme conditions on entrainment, the correlation of Choi et al has been plotted versus height for several temperatures, pressures and velocities within the stated range in table 8. The purpose of this simulation is to verify whether all the aforementioned effects of operating under extreme conditions are represented through the correlation of Choi et al. Furthermore, with the original bed surface flux a function of bubble size, the three studied correlations in the previous section will be used in this study, with their respective impacts on entrainment analyzed. Finally, the height at which entrainment stabilizes will be taken as the TDH. The used variables in this simulation can be found in table 9 below. Six plots were conducted in total. In figure 14 and 15, entrainment was plotted versus height at ambient temperature and pressure and superficial gas velocities of 0.3m/s and 1.3m/s respectively in order to cover both the bubbling and turbulent regimes. In figure 16 and 17, entrainment was plotted versus height at ambient temperature, a pressure of 20atm and superficial gas velocities of 0.3m/s and 1.3m/s respectively in order to study the effect of pressure under both regimes. At last, in figure 18 and 19, entrainment was plotted versus height at ambient pressure, a temperature of 600C and superficial gas velocities of 0.3m/s and 1.3m/s respectively in order to study the effect of temperature under both regimes. Unfortunately, due to the limited access to experimental results under these conditions, only the results of the simulation will be shown.

Table 9-Specifications used in the simulation where the effect of the bubble size correlations by Mori and Wen (1975), Horio and Nonaka (1987) and Cai et al (1994) with respect to velocity at high temperature and pressure on the entrainment rate model by Choi et al (1999)

Variable	Range
Particle diameter	250 μ m
Particle density	2560 kg/m ³
Gas velocity	0.3-1.3 m/s
Temperature	25-600 °C
Pressure	1-20 atm
Column diameter	0.2 m
Minimum bed height	1 m

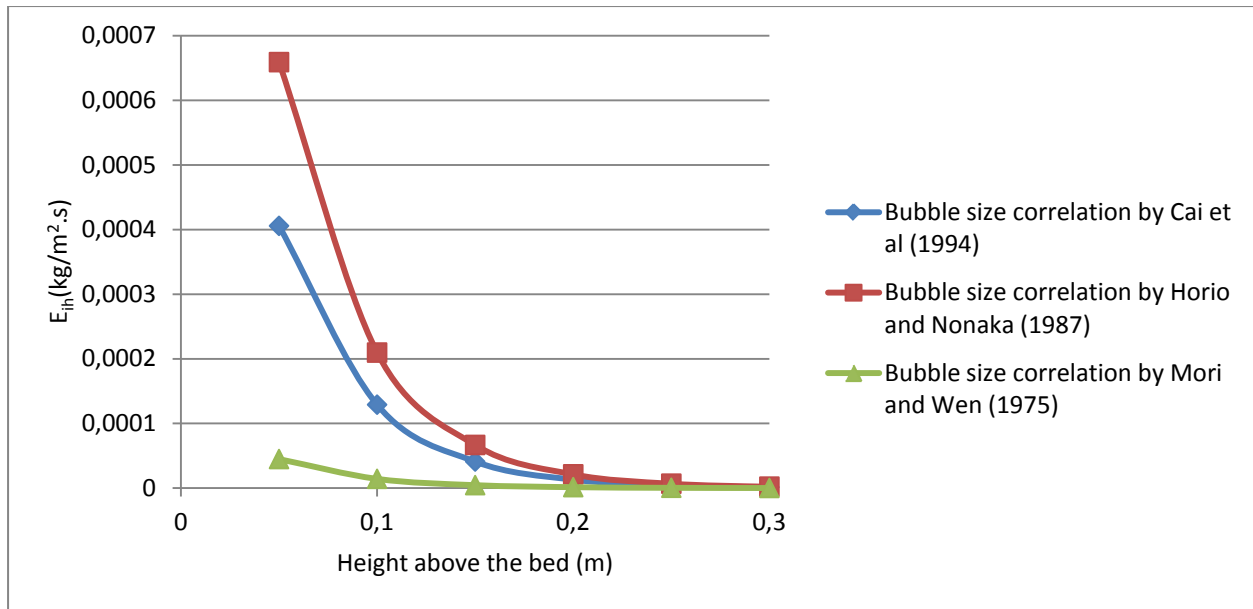


Figure 14- Comparison of the entrainment rate with respect to height above the bed using the bubble size correlations by Mori and Wen (1975), Horio and Nonaka (1987) and Cai et al (1994) at ambient temperature and pressure and a superficial gas velocity of 0.3m/s

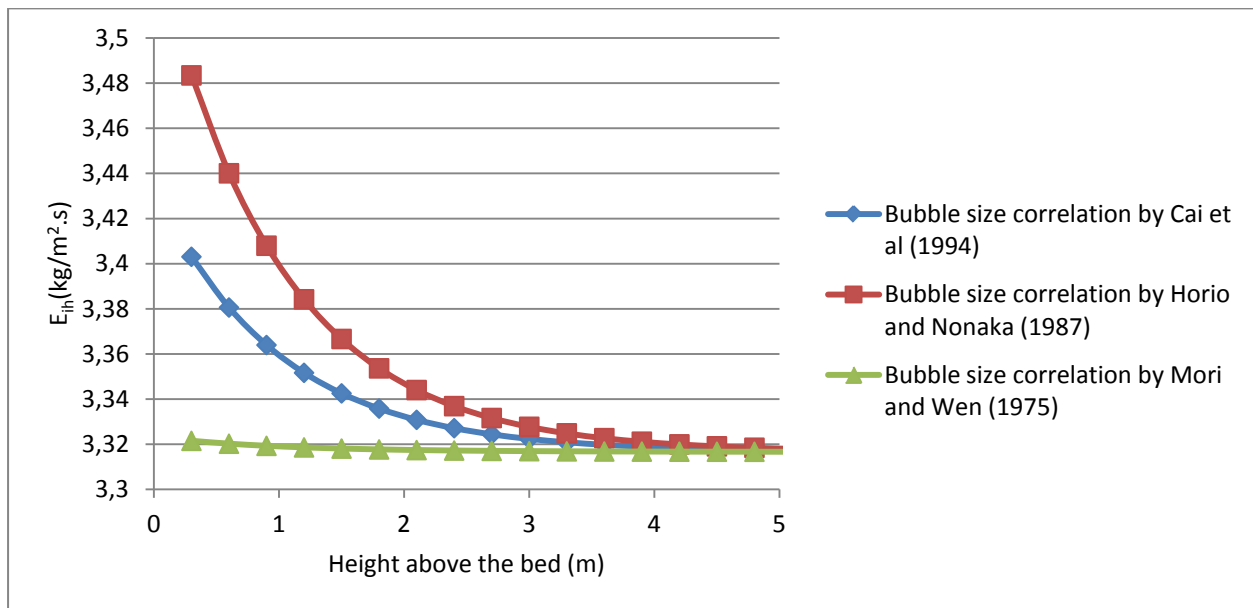


Figure 15- Comparison of the entrainment rate with respect to height above the bed using the bubble size correlations by Mori and Wen (1975), Horio and Nonaka (1987) and Cai et al (1994) at ambient temperature and pressure and a superficial gas velocity of 1.3m/s

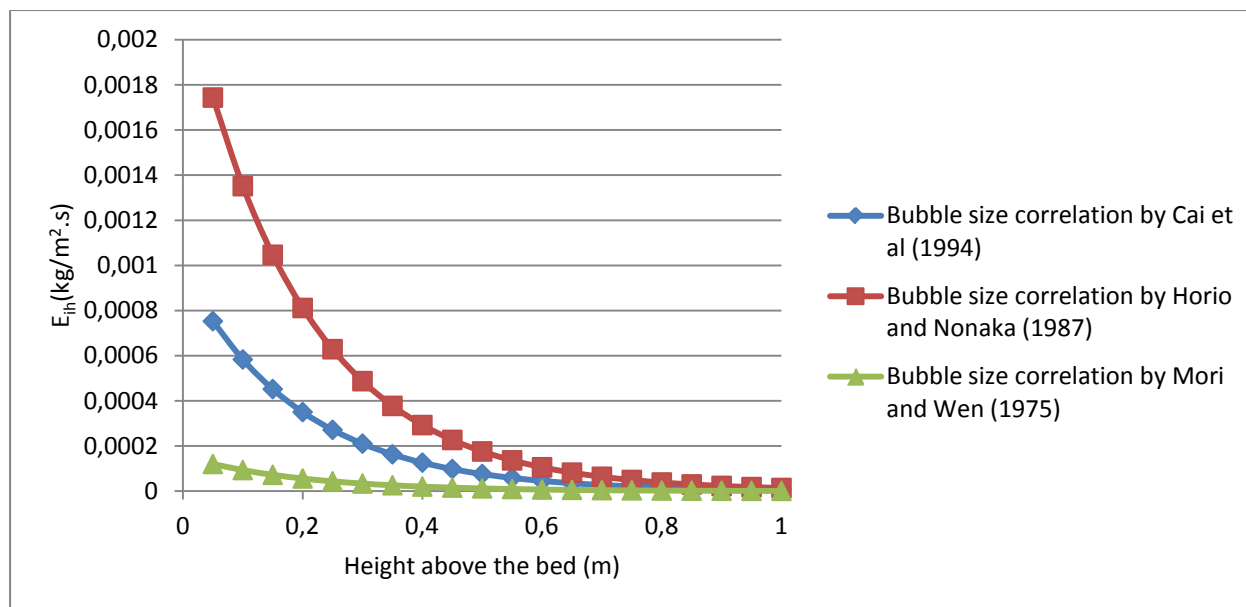


Figure 16- Comparison of the entrainment rate with respect to height above the bed using the bubble size correlations by Mori and Wen (1975), Horio and Nonaka (1987) and Cai et al (1994) at ambient temperature, a pressure of 20atm and a superficial gas velocity of 0.3m/s

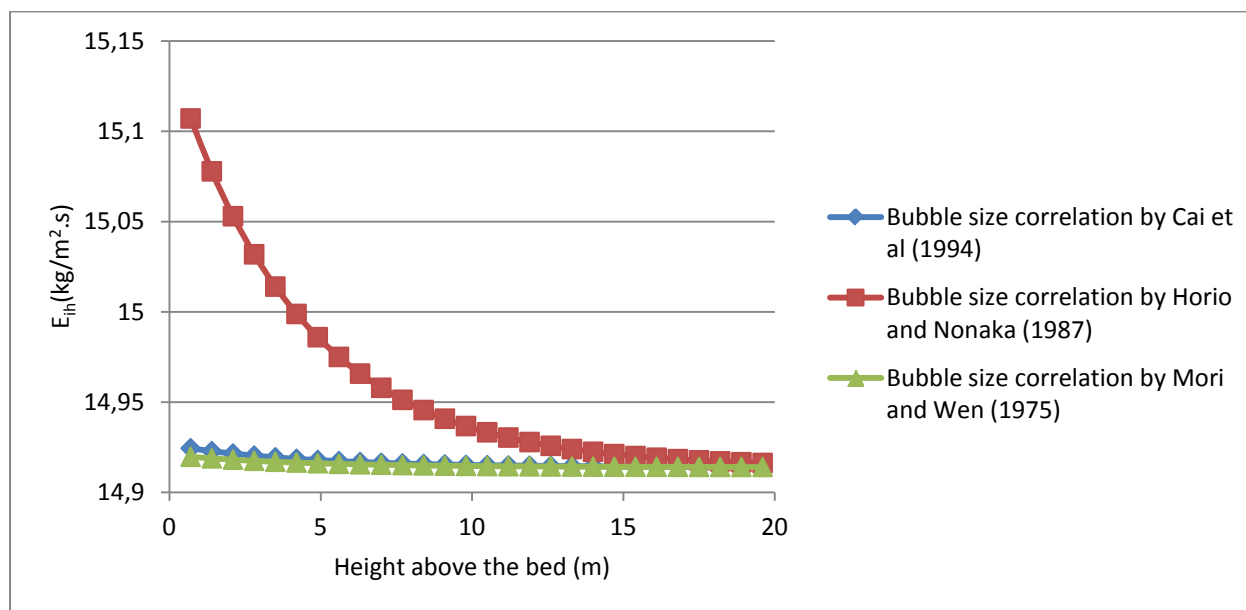


Figure 17- Comparison of the entrainment rate with respect to height above the bed using the bubble size correlations by Mori and Wen (1975), Horio and Nonaka (1987) and Cai et al (1994) at ambient temperature, a pressure of 20atm and a superficial gas velocity of 1.3m/s

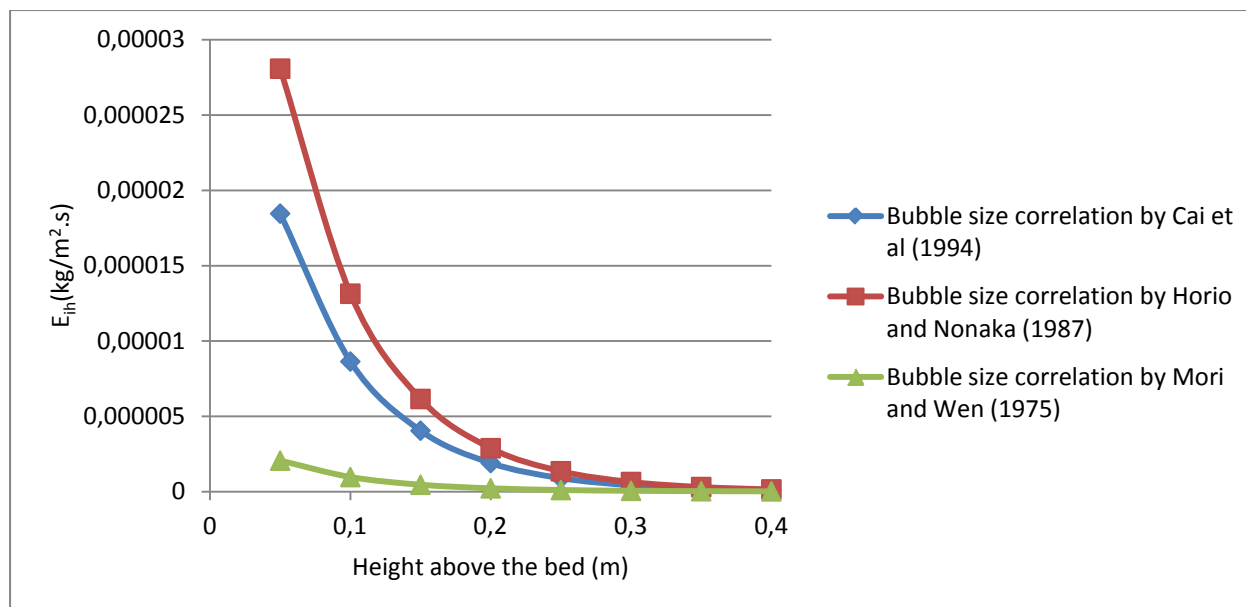


Figure 18- Comparison of the entrainment rate with respect to height above the bed using the bubble size correlations by Mori and Wen (1975), Horio and Nonaka (1987) and Cai et al (1994) at ambient pressure, a temperature of 600°C and a superficial gas velocity of 0.3m/s

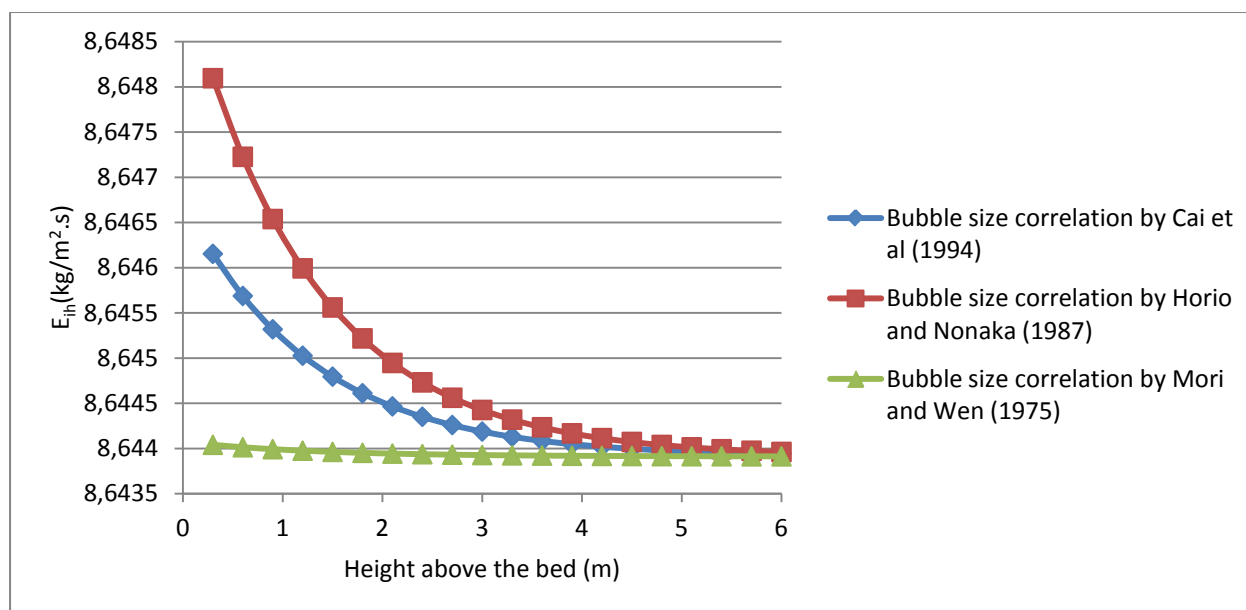


Figure 19- Comparison of the entrainment rate with respect to height above the bed using the bubble size correlations by Mori and Wen (1975), Horio and Nonaka (1987) and Cai et al (1994) at ambient pressure, a temperature of 600°C and a superficial gas velocity of 1.3m/s

3.3.1.1 Effect of velocity on entrainment

Similarly to the observations of Chan and Knowlton (1984) [55], when comparing Figure 14 and Figure 15, the total entrainment rate was correctly modeled by Choi et al to increase with velocity regardless of the used bubble size correlation. Bubble size however, seems to affect the magnitude of the total entrainment rate depending on the gas superficial velocity. For instance, at the bed surface when a gas velocity of 1.3m/s is used, the bubble size correlation by Horio and Nonaka predicted an entrainment rate 5% larger than the one obtained from the model of Mori and Wen. However, in case of a smaller superficial velocity of 0.3m/s, applying the correlation by Horio and Nonaka results in an entrainment rate 13 times larger than when the bubble size model of Mori and Wen is used.

This observation is due to the effect of velocity on the drag coefficient. In fact, at low velocities most particles fall back into the bed with the total entrainment rate mainly depending on the original bed surface flux. Since the latter is directly related to bubble size, using different correlations would therefore lead to different entrainment rate values. As velocity is increased however, the drag coefficient increases independently of bubble size until the elutriation rate reaches a maximal value that is solely a function of the solid and gas properties. As a result, fewer particles tend to fall back into the bed as the original bed surface flux becomes negligible. One may therefore conclude that the impact of bubble size on entrainment decreases as velocity is increased.

By using these plots to determine the value of the TDH, several observations can also be made. Despite using different bubble size correlations, all three curves converged at the same value for a given velocity which might suggest that TDH is independent of bubble diameter. When velocity was varied, TDH was found to increase. This observation is in agreement with Chan and Knowlton (1984) [55] and Pemberton and Davidson (1984) [56] who reported TDH to linearly increase with velocity. Zenz and Othmer (1960)[62] provided a diagram of TDH versus velocity for different bed diameters based on industrial values which clearly illustrates the increase in TDH with respect to velocity. This diagram is usually used as a first guess for industrial fluidized bed reactors. Finally, at high velocities, despite observing a decrease in entrainment with respect to height until a constant value is reached, the overall changes in the total flux are negligible with a difference of less than 5%. Therefore, despite graphically obtaining a TDH value of 4m, sizing

the freeboard accordingly might not be beneficial. A more specific definition of TDH with respect to entrainment is therefore needed.

3.3.1.2 Effect of pressure on entrainment

When comparing Figures 16 and 17 with Figures 14 and 15 in the previous section, it is clear that entrainment increases with pressure for every used bubble size correlation. The magnitude however seems to be greatly affected by the superficial gas velocity. For instance, at a low velocity of 0.3m/s, the total entrainment rate is 2.6 times larger when the pressure is increased from ambient to 20 atm. On the other hand, for a higher velocity of 1.3m/s, the entrainment rate increases by up to 4.3 times. This trend agrees with Chan and Knowlton (1984) [55] who reported a significant increase in entrainment with pressure. Furthermore, they observed that the dependence of entrainment on gas velocity increased with pressure. This can be explained by the effect of pressure on gas density which when raised increases the elutriation flux and the bed surface flux by increasing the gravity force per projection area and the Archimedes number.

When Figures 16 and 17 are compared in order to study the effect of using different bubble size correlations, several observations can be made. The bubble size by Horio and Nonaka seems to yield the highest rate while the correlation of Mori and Wen results in the lowest. Similarly to the previous study on the effect of velocity, the impact of bubble size on entrainment decreased as velocity was increased. At high velocities, the additional effect of pressure resulted in a smaller difference of 1.2% between the obtained entrainment rates using the model of Mori and Wen and Horio and Nonaka when compared to the observed difference at ambient conditions. Interestingly, at low velocities, the opposite is observed as a larger difference of 17.6% is obtained between the used models at high pressure when compared to the results at ambient conditions. This could again be explained by the fact that at low velocities the total entrainment rate depends mainly on the original bed surface flux which is directly related to bubble size. As presented in section 3.2.2, when pressure is increased, the correlation by Horio and Nonaka resulted in the largest bubble diameter while that of Mori and Wen resulted in the smallest, therefore explaining the smaller difference at ambient conditions. One can therefore conclude that in the bubbling regime, using different bubble size correlations can result in large differences in entrainment rate. At higher velocities, the latter increases with pressure but offers no

significant differences when different bubble size correlations are used due to the dominance of the elutriation rate compared to the bed surface flux.

By using these plots to determine the value of the TDH, similar observations to that with respect to velocity can be made. Despite using different bubble size correlations, all three curves converged at the same value for a given pressure which would suggest once more that TDH is independent of bubble diameter. When pressure was increased, TDH was also found to follow the same trend. This observation is in agreement with Chan and Knowlton (1984) [55] and Pemberton and Davidson (1984) [56] who stated that TDH increased with pressure due to the resulting elevation in gas density and thus decrease in single particle terminal velocity. Finally, at high pressure and velocity, despite observing a decrease in entrainment with respect to height until a constant value is reached, the overall changes in the total flux are negligible with a difference of less than 2%. Therefore, with a graphically obtained TDH value of 15m, sizing the freeboard accordingly might not be profitable. One might conclude once more that a more specific definition of TDH with respect to entrainment is needed.

3.3.1.3 Effect of temperature on entrainment

Similarly to the previous study on the effects of pressure, Figures 18 and 19 were compared with Figures 14 and 15 in order to study the impacts of temperature on entrainment. By doing so, it is clear that based on the correlation of Choi et al for a given bubble size model, the total entrainment rate seems to decrease with temperature at low velocity by up to 26 times. This can be explained once more by the dominance of the bed surface flux at low velocities, which decreases with temperature and is greatly affected by bubble size as seen in the previous sections. At a higher velocity of 1.3m/s, the opposite is however observed with the total entrainment rate increasing by 2.5 times for a given bubble size correlation. In fact, Choi et al investigated the qualitative effect of temperature on the particle entrainment rate at the freeboard gas exit of a gas fluidized bed at high velocities (1.2 to 1.8m/s). According to their results, the particle entrainment rate increased with temperature, after an initial decrease. Their justification for this observation resides in the decrease in gas density and increase in gas viscosity with temperature. The opposite trend was however observed by Wouters and Geldart (1998)[63] who, using small particles (7 to 48 μm), reported a decrease of the total entrainment rate with an increase in temperature up to 400 °C. In their paper, Choi et al (2007)[64] explained that their correlation did

not take into account interparticle forces which caused the decrease in entrainment for the case of Wouters and Geldart (1998) due to the small particle size used.

Furthermore, similarly to the previous studies on the effect of bubble size on entrainment at high velocities, the correlations by Mori and Wen, Cai et al and Horio and Nonaka, offered little to no significant difference (less than 1%) when temperature was raised.

Once more, one may conclude that in the bubbling regime, using different bubble size correlations can result in large differences in entrainment rate. At higher velocities, entrainment increases with temperature but offers no significant differences when different bubble size correlations are used due to the dominance of the elutriation rate compared to the bed surface flux. This is however not the case for small particles (less than 48 μm) where entrainment decreases with temperature due to the influence of interparticle forces. With the correlation of Choi not taking into account the latter, more work needs to be done on developing an entrainment model that would account for the smaller particles and fines.

When these plots are used to determine the value of the TDH, more observations could be reported with respect to temperature. Despite using different bubble size correlations, all three curves converged once again at the same value for a given temperature, suggesting that TDH is not a function of bubble diameter. When temperature was raised however, a slight increase in TDH was observed. Finally, at high temperature and velocity, despite observing a decrease in entrainment with respect to height until a constant value is reached, the overall changes in the total flux are negligible with a difference of less than 1%. Therefore, with a graphically obtained TDH value of 5m, sizing the freeboard accordingly might once again not be profitable.

3.3.2 TDH modelling and influence of extreme conditions

As stated in chapter 2, in most fluidized bed applications, the freeboard occupies the largest volume of the reactor and therefore its design can be crucial since it has the main task of preventing large amounts of the bed material from being carried out by the gas stream. With any further height increase having little impact on entrainment, most design books have required the freeboard to have a height of at least the TDH in order to reduce carryovers [1, 9, 48].

Unfortunately, there is no commonly accepted method for the calculation of the TDH [6], but only several empirical correlations which were developed under ambient conditions. Therefore,

the entrainment plots presented in the previous section were used in order to graphically estimate TDH and study the resulting impact of operating under extreme conditions. The respective results are presented in table 10 below, based on the solid properties stated in table 9. With the expected trends with regards to temperature pressure and velocity reported in the last section, the purpose of this study is to observe and highlight any discrepancies between the existing TDH correlations and the obtained results from the entrainment plots of Choi et al. Some of the most common TDH correlations that are used in design books can be found in table 11 below.

Table 10- TDH values based on the plot of the entrainment correlation of Choi et al (1999)

Pressure (atm)	Temperature (°C)	Velocity (m/s)	Estimated TDH (m)
1	25	0.3	0.25
1	25	1.3	4
1	600	0.3	0.3
1	600	1.3	5
20	25	0.3	0.8
20	25	1.3	15

Table 11- Common TDH correlation as reported in the handbook of fluidization and fluid-particle systems[6]

Author	Correlation
Correlations not based on bubble size	
Fournol et al (1973) [65]	$TDH = 1000 \frac{U^2}{g}$
Chan and Knowlton (1984) [55]	$TDH = 0.85U^{1.2}(7.33 - 1.2\log_{10}U)$
Sciazko et al (1991) [66]	$TDH = \frac{1500H_b Re_p}{A_r}$
Correlations based on bubble size	
Horio et al (1980) [67]	$TDH = 4.47d_b^{0.5}$
Fung and Hamdullahpur (1993) [68]	$TDH = 13.8d_b$
Smolders and Baeyens (1997) [69]	$TDH = 6[(U - U_{mf})d_b]^{0.6}$

Despite the entrainment model of Choi et al resulting in TDH values that are independent of bubble size, three of the correlations in table 11 are directly based on the average bubble diameter: These are the models by Horio et al (1980), Fung and Hamdullahpur (1993) and Smolders and Baeyens (1997). In their case, TDH is expected to follow the same trend as bubble size with respect to temperature, pressure and velocity. This is in fact contradictory to the expected TDH trend since the latter was reported to linearly increase with velocity and pressure. Furthermore, the correlations by Fournol et al (1973) and Chan and Knowlton (1984) are only a function of velocity and therefore will not exhibit any changes in the TDH when temperature and pressure are varied.

With only the correlation by Sciazko et al (1993) based on velocity, pressure and temperature through the bed height and the particle Reynolds number, a comparison of its results with the obtained TDH values from the entrainment correlation of Choi et al can be found in Table 12 below.

Table 12- Comparison of the TDH values obtained using the entrainment model of Choi et al and the correlation of Sciazko et al

Pressure (atm)	Temperature (°C)	Velocity (m/s)	TDH (m) from the entrainment correlation of Choi et al	TDH (m) from the correlation of Sciazko et al (1991)	% error
1	25	0.3	0.25	6.7	2580
1	25	1.3	4	42	950
1	600	0.3	0.3	14	4567
1	600	1.3	5	88.7	1674
20	25	0.3	0.8	6.8	750
20	25	1.3	15	42	180

With the correlation of Sciazko et al (1991) greatly overestimating TDH when compared to the obtained results from the entrainment model of Choi et al, one may conclude that none of the correlations presented in table 11 can accurately estimate TDH. Moreover, all of these correlations will provide a very large TDH values at high velocities despite entrainment decreasing by as little as (0.05%). As far as design purposes are concerned, a new TDH model must be developed with respect to temperature and pressure.

3.4 Mass Transfer in Fluidized Beds

As explained earlier, when gas flows through the bed, two distinct parts can be observed; the bubble phase and the emulsion phase. As opposed to gas-liquid systems, an interchange of gas occurs between the bubble and dense phase; a phenomena that many have tempted to describe. In fact, this inter-phase mass transfer have been reported to influence the reaction rate per unit bed volume as well as process efficiency by reducing the bypassing of unreacted gas in the bubble phase to the freeboard [70].

In the literature, mass exchange has been measured experimentally by varying tracer concentration with time and analyzing the results for two cases: single bubbles and freely bubbling beds.

In case of single bubbles, they are introduced in a fluidized bed with a known concentration of a non-reactive tracer. By measuring the concentration, a differential mass balance can be performed relating the concentration of the tracer in the bubble and emulsion phase, and the vertical location [71, 72].

In case of freely bubbling beds, the tracer is introduced as a step-input or pulse with its concentration measured above the point of injection. An issue however that has been highlighted when using this method is the absence of a universally acceptable hydrodynamic model since a suitable one has to be used to analyse the measured response.

Several researchers using the freely bubbling beds and the single bubble methods have developed expressions for the estimation of the interphase mass exchange coefficient [1, 73]. Sit and Grace (1981) [73] reviewed some of the available expressions and classified them into three groups of models: 1- Diffusion controlled models, 2- Additive convective and diffusive transfer models, 3- Interaction models.

In diffusion controlled models, diffusion across the cloud boundary is assumed to be solely controlling the interphase mass transfer. These models were reported to consistently underestimate the overall mass transfer by an order of magnitude.

In additive convective and diffusive transfer models, two mechanisms are reported to control mass transfer: 1- diffusion, and 2- convection or bubble “throughflow”. These two mechanisms

are each evaluated and then summed. Sit and Grace reported that these models seemed to correctly evaluate mass transfer coefficient with respect to experimental values.

In interaction models, diffusion, and convection are also assumed to control mass transfer. In this case, the main difference lies in the assumption that both diffusive and convective mass transfer interact and therefore the overall mass transfer coefficient can be less than the sum of the two effects in isolation. This method, despite yielding great results for some cases, seems to lack consistency over the whole range of particle size examined.

The most commonly used additive convective and diffusive transfer model was developed by Davidson and Harrison (1963) [74] who obtained an expression for mass interchange coefficient per unit bubble volume.

$$K_{BE} = 4.5 \left(\frac{U_{mf}}{d_b} \right) + 5.85 \left(\frac{D^{0.5} g^{0.25}}{d_b^{1.25}} \right)$$

Where K_{BE} is the interchange coefficient, U_{mf} is the minimum fluidization velocity, d_b is the bubble diameter and D is the molecular diffusivity of the gas. The diffusive transfer is illustrated by the second term on the right hand side of the equation, while the convective transfer is represented by the first term.

In a review article, Sit and Grace (1978) reported that this model underpredicts mass transfer coefficient values and subsequently presented later their own correlation for single spherical three-dimensional bubbles:

$$K_{BE} = \frac{2U_{mf}}{d_b} + 6.77 \left(\frac{D \cdot \epsilon_{mf} \cdot U_b}{d_b^3} \right)^{1/2}$$

Where U_b is the bubble velocity, ϵ_{mf} is the voidage at minimum fluidization and U_{mf} is the minimum fluidization velocity.

Thus, it is clear that the overall transfer coefficient K_{BE} is directly related to bubble diameter in both models. In the following section, the three bubble size correlation studied thus far will be again used to illustrate the effect of pressure, temperature and velocity on the overall mass transfer coefficient. The model of Clift and Grace (1985)[75] will be used in order to compute the bubble velocity:

$$U_b = \left\{ \begin{array}{ll} 0.711\sqrt{g \cdot d_b} & \text{for } d_b \leq 0.125D_t \\ 0.803\sqrt{g \cdot d_b} \exp\left(-\frac{d_b}{D_t}\right) & \text{for } 0.125D_t < d_b \leq 0.6D_t \\ 0.35\sqrt{g \cdot D_t} & \text{for } d_b > 0.6D_t \end{array} \right\}$$

3.4.1 Effect of velocity on mass transfer

The effect of velocity has been well documented with researchers agreeing that mass transfer increases with velocity [76-79]. Unfortunately, very few articles have been dedicated to studying the effect of velocity on the mass transfer interchange coefficient, K_{BE} . Kunni and Levenspiel (1991) [1] explained that the product of the mass transfer coefficient of a single particle, k_g , and the surface area of solid per volume of solid, a' , is inversely proportional to the overall interchange transfer coefficient, K_{BE} , by the bubble fraction, δ , which they reported to increase with velocity. It is therefore possible to conclude that the overall interchange transfer coefficient K_{BE} , might decrease with velocity. With this in mind, the purpose of this section is to illustrate the impact of using different bubble size correlation on the estimated overall mass transfer coefficient for the correlation of Sit and Grace (1978). In order to conduct this study, the interchange mass transfer coefficient was plotted in Figures 20 and 21 for every bubble size correlation based on the specifications used in table 3. The molecular diffusivity of CO₂ ($2 \times 10^{-5} \text{ m}^2/\text{s}$)[81] was used in this simulation.

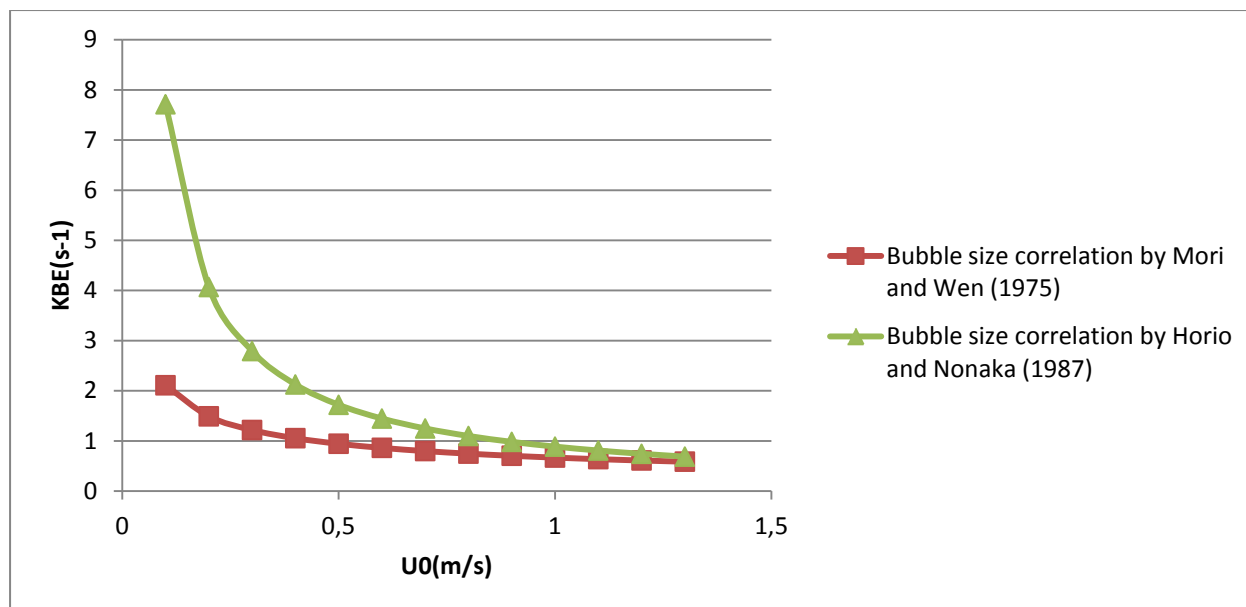


Figure 20- Comparison of the interchange mass transfer coefficient with respect to superficial velocity using the bubble size correlations by Mori and Wen (1975) and Horio and Nonaka (1987)

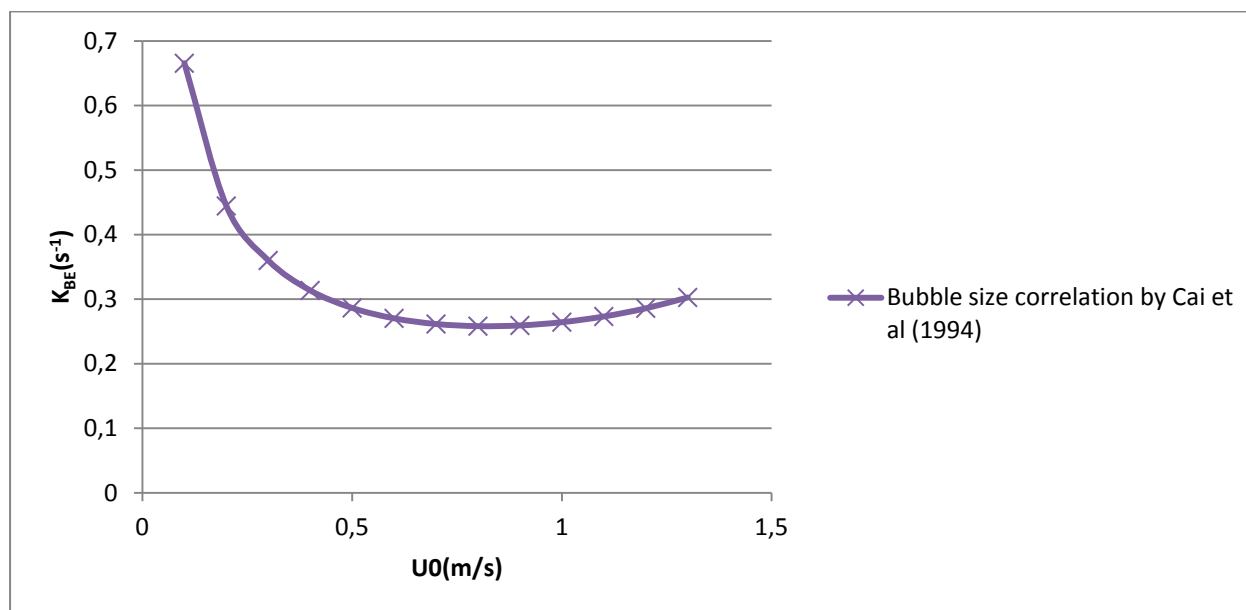


Figure 21- Interchange mass transfer coefficient with respect to superficial velocity using the bubble size correlations by Cai et al (1999)

It is clear from Figures 20 and 21 that using different bubble size correlations lead to different trends in the total mass transfer interchange coefficient with respect to velocity. At low velocities (0-0.6m/s), all three bubble size models predicted a decrease in the total interchange coefficient, which agrees with the observations of most researchers [76-79]. As we recall, under these velocities, all correlations predicted an increase in bubble size which would explain this observed decrease in K_{BE} . Furthermore, bubble size seems to affect the magnitude of the interchange coefficient depending on the gas superficial velocity. For instance, at a velocity of 0.1m/s, the bubble size correlation of Horio and Nonaka (1987) predicted a bubble diameter 6 times smaller than that predicted by Cai et al (1994). Subsequently, due to the inverse relation between d_b and K_{BE} , using the model of Horio and Nonaka (1987) resulted in an interchange coefficient 11 times larger than when the correlation of Cai et al (1994) was used.

Interestingly, when velocity is increased further, the correlation of Cai et al (1994) predicted an increase in the total interchange coefficient. In fact, as we recall, when the turbulent regime is reached, smaller bubbles are formed, resulting in an increase in K_{BE} . This increase was not observed by the correlations of Horio and Nonaka (1987) and Mori and Wen (1975) who predicted a monotone increase in bubble size. Moreover, despite greatly affecting the magnitude of the interchange coefficient at low velocities, bubble size seems to have a less pronounced effect at higher velocities. This can be observed as all three bubble size models seem to converge.

3.4.2 Effect of pressure on mass transfer

Similarly to velocity, the effect of pressure has been studied by several researchers. Sechenov et al (1966) [82] has reported that the mass transfer coefficient, k_g , decreases when pressure is increased. A similar conclusion was made by Zhang et al (2013)[83] who also reported a decrease in mass transfer when pressure is increased which they explained to be the result of a sharp decrease in the diffusion coefficient as well as a larger ratio of convective mass transfer because of smaller bubbles and larger average bed voidage. Unfortunately, no studies have been dedicated to the effect of pressure or bubble size on K_{BE} with the only available experimental data with respect to pressure on the mass transfer coefficient, k_g [82, 83]. It is therefore the objective of this section to study the impact of using different bubble size models at different pressures on the estimated overall interchange transfer coefficient for the correlation of Sit and

Grace (1978). The resulting plots are presented in Figure 22 below and are based on the specifications in table 4.

In regards to the effect of pressure on the diffusion coefficient, Zhang et al (2013)[83] demonstrated that it followed a decreasing trend. In fact, Sechenov et al (1966) [82] reported that the diffusion coefficient D decreases in inverse proportion to the pressure increase. Cussler (1997)[84] correlated the change in the molecular diffusion as:

$$D = D_0 \frac{P_0}{P}$$

Where D and D_0 are the diffusion coefficient at P and P_0 respectively

The molecular diffusivity of CO_2 [81] was again used in this simulation.

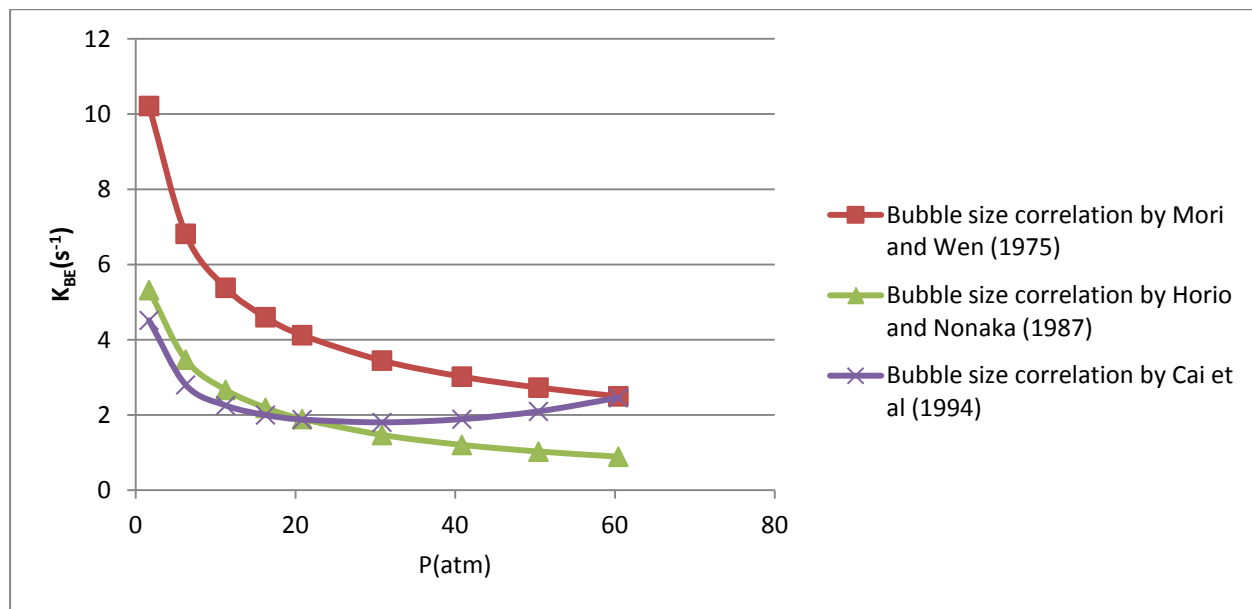


Figure 22- Comparison of the interchange mass transfer coefficient with respect to pressure using the bubble size correlations by Mori and Wen (1975), Horio and Nonaka (1987) and Cai et al (1994)

Similarly to the conducted study on the effects of velocity, using different bubble size correlations seems to result in different trends in the total mass transfer interchange coefficient with respect to pressure. Both bubble size correlations by Mori and Wen (1975) and Horio and Nonaka (1987) predict a decrease in K_{BE} with respect to pressure. In fact, as pressure increases, the minimum fluidization velocity[85] and the diffusivity coefficient decrease. The effect of the latter in addition to the predicted increase in bubble size from both correlations, explain the observed decreasing trend in K_{BE} . In the case of the correlation by Cai et al (1994), an initial decrease can be seen, followed by an increase in the total mass interchange coefficient. This observation is directly related to the predicted bubble size trend. As we recall, the correlation of Cai et al predicts an increase followed by a decrease in bubble size as pressure increases. This shift in behaviour explains the observed mass interchange coefficient trend by being inversely proportional to bubble size at high pressures.

Interestingly, at lower pressures despite accounting for the observed trend, bubble size does not seem to be inversely proportional to K_{BE} . For instance, while the correlation of Horio and Nonaka (1987) predicts the largest bubble size at ambient pressure, the expected mass interchange coefficient is not the lowest. This can be explained by the dependence of the bubbling velocity on bubble size at lower bubble diameters. As the latter is increased however, the bubble velocity is predicted to reach a constant value as illustrated by the used correlation of Clift and Grace (1985)[75].

3.4.3 Effect of temperature on mass transfer

Similarly to velocity and pressure, the effect of temperature on mass interchange has been studied by several researchers[70, 86]. Wu et al reported that K_{EB} decreases as temperature is increased over a range of ambient to 500C.

Once again, the impact of using different bubble size correlation on the estimated overall mass transfer coefficient for the correlation of Sit and Grace (1978) was presented and compared with the expected trends with respect to temperature. The interchange mass transfer coefficient was plotted in Figure 23 for every bubble size correlation based on the specifications used in table 5.

According to the Stokes-Einstein law, the diffusion coefficient is a function of temperature and can be approximated in the following manner:

$$D = D_0 \frac{T}{T_0} \frac{\mu_{T_0}}{\mu_T}$$

Where μ_{T_0} and μ_T are the viscosities at T_0 and T respectively

The molecular diffusivity of CO₂ [81] was again used in this simulation.

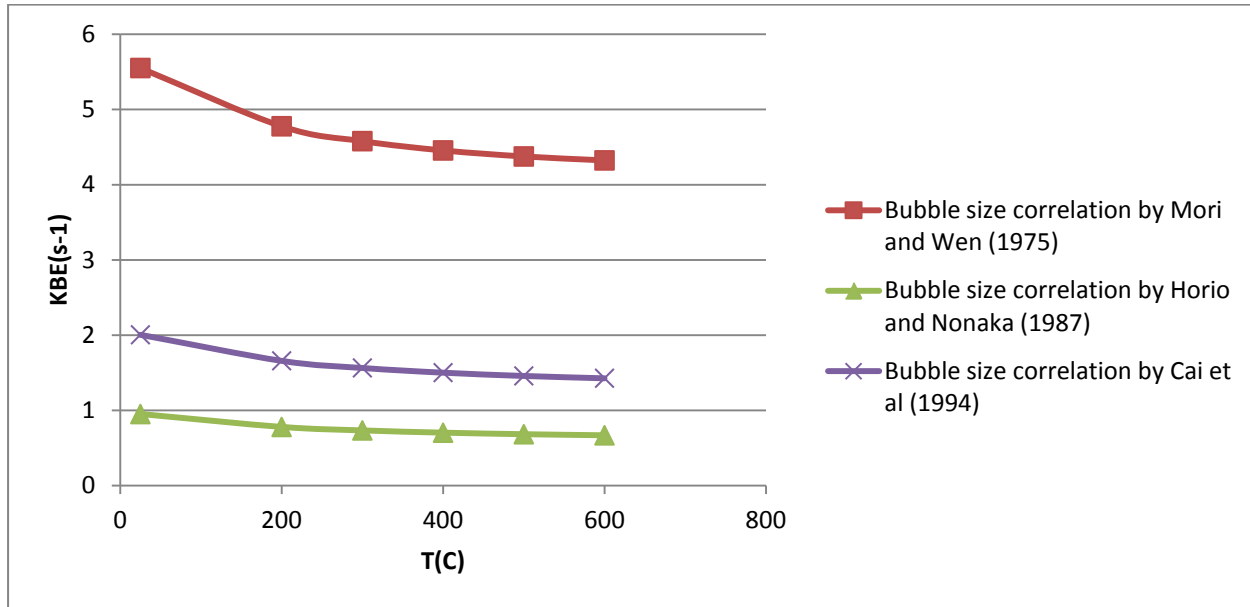


Figure 23- Comparison of the interchange mass transfer coefficient with respect to temperature using the bubble size correlations by Mori and Wen (1975), Horio and Nonaka (1987) and Cai et al (1994)

Contrary to the conducted studies on the effects of velocity and pressure, using different bubble size correlations seems to result in the same decreasing trend in the mass transfer interchange coefficient with respect to temperature. Despite the correlations of Mori and Wen (1975) and Cai et al (1994) predicting an increase in bubble size while the correlation of Horio and Nonaka resulted in a decrease, K_{BE} seems unaffected by these trends. In fact as we recall, the magnitude of the change in bubble size due to the effect of temperature was very small when compared to the changes obtained from varying pressure or velocity. Due to this observation, the increase in U_{mf} and the decrease in D are the major contributors to the observed changes in K_{BE} with respect to temperature. Moreover, Wu et al (2003)[70] explained that this competing effect is the reason for the observed small change in K_{BE} when temperature is varied.

3.5 Effect of Extreme Conditions on Reaction Conversion

With the effects of temperature, pressure and velocity on bubble size, entrainment and mass transfer presented in the previous sections, developing an understanding of reaction conversion is fundamental for most engineering processes. Similarly to the previous studies, the purpose of the following section is to demonstrate the effect of using extreme operating conditions on reaction conversion, and the consequent impact of using different bubble size correlations.

3.5.1 Methane steam reforming kinetics

Oil consumption has become more and more important over the past 50 years with a projected 33% increase by 2020 [87]. In fact, at this rate of usage, researchers predict most known oil and fossil fuel reserves to be depleted by 2038. Furthermore, additional environmental concerns related to oil consumption have risen over the years with the energy industry contributing to about 22 billion tons of carbon dioxide (CO₂) and other greenhouse gases into the earth's atmosphere each year [87]. An alternative solution to fossil fuels is hydrogen which when reacted with oxygen releases energy [88]. Hydrogen production methods such as steam reforming, has therefore attracted a lot of attention. Methane reforming constitutes today the predominant hydrogen production method (95% in the USA) [89] because of its low cost compared to all hydrogen production pathways [90]. Methane steam reforming is a series of reactions that take place at high temperatures (700 – 1100 °C) in the presence of a metal-based catalyst (nickel) [91].

Our interest in this reaction process has come from its industrial application at elevated temperatures and pressures. In fact, it was reported that while high temperature increases conversion, high pressure tends to have the opposite effect [92]. Good understanding of the effect of pressure and temperature in this case can prove to be crucial. Furthermore, with fluidized bed reformers receiving a lot of interest because of their high rate of heat transfer, methane conversion and hydrogen yield [92-94], this process is of great relevance to this work.

Methane steam reforming has been thoroughly studied [92-94] in the literature and consists majorly of 2 highly endothermic reforming reactions (1) and (2) and a moderately exothermic reaction: the water gas shift reaction (3) [88], producing CO, CO₂ and H₂. Furthermore, methane can also undergo oxidation to produce CO, CO₂ and H₂O according to reaction (4). These

reactions are presented in table 13 below. Hough and Hughes (2000) [91] presented a widely used kinetic model for reactions (1) to (3) over a Ni/a-Al₂O catalyst, while Yermakova et al (1993) [95] studied and modelled reaction (4). These models along with their respective reactions are summarized in table 13 and the kinetic parameters are presented in table 14.

Table 13- Methane steam reforming reactions and kinetic models

#	Reaction	Kinetic Model
1	$CH_4 + H_2O \leftrightarrow CO + 3H_2$	$r_1 = \frac{k_1(P_{CH_4}P_{H_2O}^{0.5}/P_{H_2}^{1.25})\left(1 - (P_{CO}P_{H_2}^3/K_1P_{CH_4}P_{H_2O})\right)}{DEN^2}$
2	$CH_4 + 2H_2O \leftrightarrow CO_2 + 4H_2$	$r_2 = \frac{k_2(P_{CO}P_{H_2O}^{0.5}/P_{H_2}^{0.5})\left(1 - (P_{CO_2}P_{H_2}/K_2P_{CO}P_{H_2O})\right)}{DEN^2}$
3	$CO + H_2O \leftrightarrow CO_2 + H_2$	$r_3 = \frac{k_3(P_{CH_4}P_{H_2O}/P_{H_2}^{1.75})\left(1 - (P_{CO_2}P_{H_2}/K_3P_{CH_4}P_{H_2O}^2)\right)}{DEN^2}$
4	$CH_4 + \left(2 - \frac{\alpha}{2}\right)O_2 \leftrightarrow \alpha CO + (1 - \alpha)CO_2 + 2H_2O$	$r_4 = K_4Y_{CH_4}^mY_{O_2}^n$

Table 14- Kinetic parameters

Kinetic Parameters	Units
$DEN = 1 + K_{CO}P_{CO} + K_{H_2}P_{H_2}^{0.5} + K_{H_2O}\left(\frac{P_{H_2O}}{P_{H_2}}\right)$	-
$K_1 = 1.198.10^{17}\exp\left(\frac{-26830}{T}\right)$	kPa^2
$K_2 = 1.767.10^{-2}\exp\left(\frac{4400}{T}\right)$	kPa^0
$K_3 = 2.117.10^{15}\exp\left(\frac{-22430}{T}\right)$	kPa^2
$k_1 = 5.922.10^8\exp\left(\frac{-Ea_1}{R.T}\right)$	$kg\ cat.s.kPa^{0.25}$
$Ea_1 = 209.2$	kJ/mol
$k_2 = 6.028.10^{-4}\exp\left(\frac{-Ea_2}{R.T}\right)$	$kg\ cat.s.kPa$
$Ea_2 = 15.4$	kJ/mol
$k_3 = 1.093.10^3\exp\left(\frac{-Ea_3}{R.T}\right)$	$kg\ cat.s.kPa^{0.25}$
$Ea_3 = 109.4$	kJ/mol
$K_{CO} = 5.127.10^{-13}\exp\left(\frac{-\Delta H_{CO}}{R.T}\right)$	kPa^{-1}
$\Delta H_{CO} = -140$	kJ/mol
$K_{H_2} = 5.68.10^{-10}\exp\left(\frac{-\Delta H_{H_2}}{R.T}\right)$	$kPa^{-0.5}$

$\Delta H_{H_2} = -93.4$	kJ/mol
$K_{H_2O} = 9.251 \exp \left(\frac{-\Delta H_{H_2O}}{R.T} \right)$	kPa
$\Delta H_{H_2O} = 15.9$	kJ/mol

3.5.2 Methane steam reforming modelling

In order to study the influence of using extreme operating conditions on reaction conversion in fluidized bed reactors, a suitable hydrodynamic model that would allow flexibility in the operating conditions must be chosen. Different models have been developed for fluidized reactor, most of which are only applicable for one fluidization regime. Based on the work of Mostoufi and Cui (2001) [96] a dynamic two-phase (DTP) model was chosen as it was proven to cover both the bubbling and the turbulent regime. This model considers the reaction to occur in both the bubble and emulsion phase which does not remain at the minimum fluidization conditions. This model also considers that as the superficial gas velocity varies; the phase fractions as well as the mean voidage of the bubble and emulsion phase changes. Mostoufi and Cui (2001) evaluated the aforementioned hydrodynamic parameters based on correlations given by Cui et al [97] that are applicable for both Geldart A and B particles.

In this work, the fluidized bed steam reformer is simulated using the DTP model. The state equations for this model are listed in table 15.

Table 15- State Equations for the Dynamic Two- Phase Structure Model (DTP)

Mole balance for species A in the emulsion phase	$\frac{dC_{Ae}}{dz} = \frac{R_{Ae}(1 - \varepsilon_e)\rho_s(1 - \delta) + K_{BE}\delta(C_{Ab} - C_{Ae})}{U_e(1 - \delta)}$
Mole balance for species A in the bubble phase	$\frac{dC_{Ab}}{dz} = \frac{R_{Ab}(1 - \varepsilon_b)\rho_s - K_{BE}(C_{Ab} - C_{Ae})}{U_b}$
Mean concentration of species A	$C_A = \frac{U_e(1 - \delta)}{U} C_{Ae} + \frac{U_b\delta}{U} C_{Ab}$
Average emulsion voidage [97]	$\varepsilon_e = \varepsilon_{mf} + 0.00061 \exp\left(\frac{U - U_{mf}}{0.262}\right)$
Average bubble voidage [97]	$\varepsilon_b = 0.784 - 0.139 \exp\left(\frac{U - U_{mf}}{0.272}\right)$
Bubble fraction [97]	$\delta = 1 - \exp\left(-\frac{U - U_{mf}}{0.62}\right)$
Emulsion velocity	$U_e = \frac{U - \delta U_b}{1 - \delta}$
Average bed voidage	$\varepsilon = (1 - \delta)\varepsilon_e + \delta\varepsilon_b$

The experimental methane reforming reactor of Roy et al (1999) [92] was used in this study along with the gas composition and the bed properties. A commercial steam methane reforming catalyst (United Catalyst Inc., C11-9-02) was assumed in this work. All of these values can be found in table 16 below.

Table 16- Methane steam reform simulation input

Variable	Value
$D_t(\text{m})$	0.0972
$H_b(\text{m})$	0.35
$dp(\mu\text{m})$	180
$\rho_p (\text{kg/m}^3)$	1100
$D_{\text{CH}_4} (\text{m}^2/\text{s})$	2.064×10^{-5}
$D_{\text{H}_2\text{O}} (\text{m}^2/\text{s})$	2.178×10^{-5}
$D_{\text{CO}} (\text{m}^2/\text{s})$	1.92×10^{-5}
$D_{\text{H}_2} (\text{m}^2/\text{s})$	6.34×10^{-5}
$D_{\text{O}_2} (\text{m}^2/\text{s})$	1.53×10^{-5}
$D_{\text{CO}_2} (\text{m}^2/\text{s})$	1.381×10^{-5}

3.5.2.1 Effect of pressure on conversion

Roy et al (1999) [92] studied the effect of pressure on the steam methane reform reactions and concluded that conversion decreased with pressure over a range of 0.35 to 0.6MPa. Using the DTP model and the values in table 16, conversion was plotted versus pressure for each of the three bubble size correlations presented earlier, and compared to the experimental finding of Roy et al (1999) [92]. Furthermore, in order to provide an explanation for the observed trends, a plot of bubble size versus pressure was also conducted for each of the three bubble size correlations.

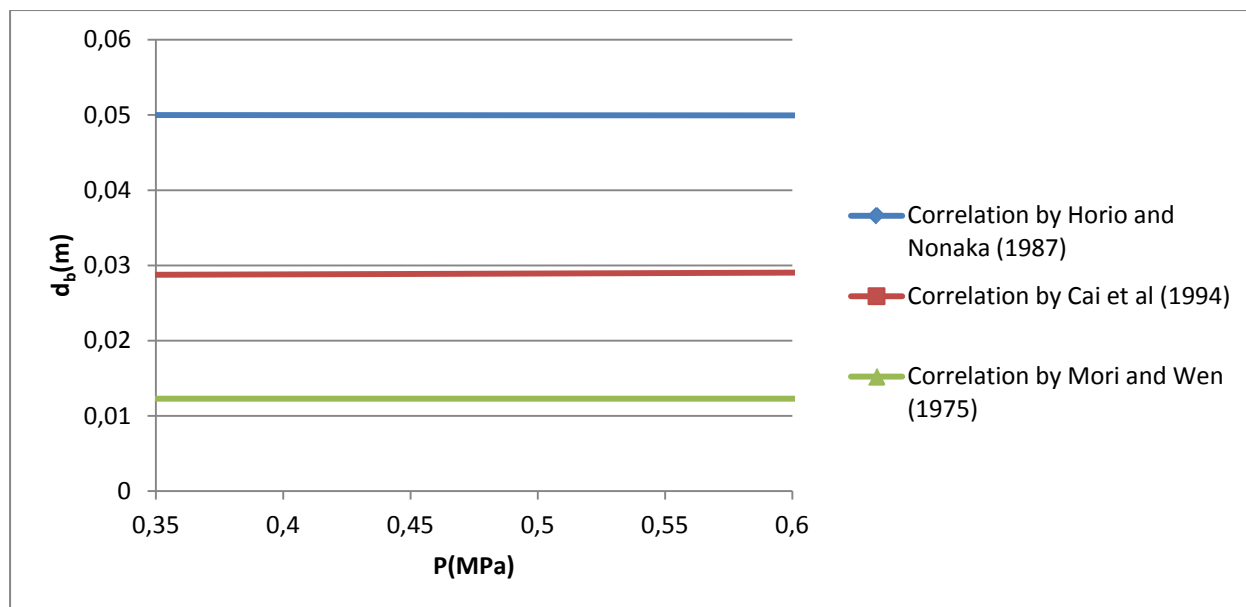


Figure 24- Comparison of the bubble size correlations by Mori and Wen (1975), Horio and Nonaka (1987) and Cai et al (1994) with respect to pressure at $U=0.07\text{m/s}$ and $T=650\text{C}$

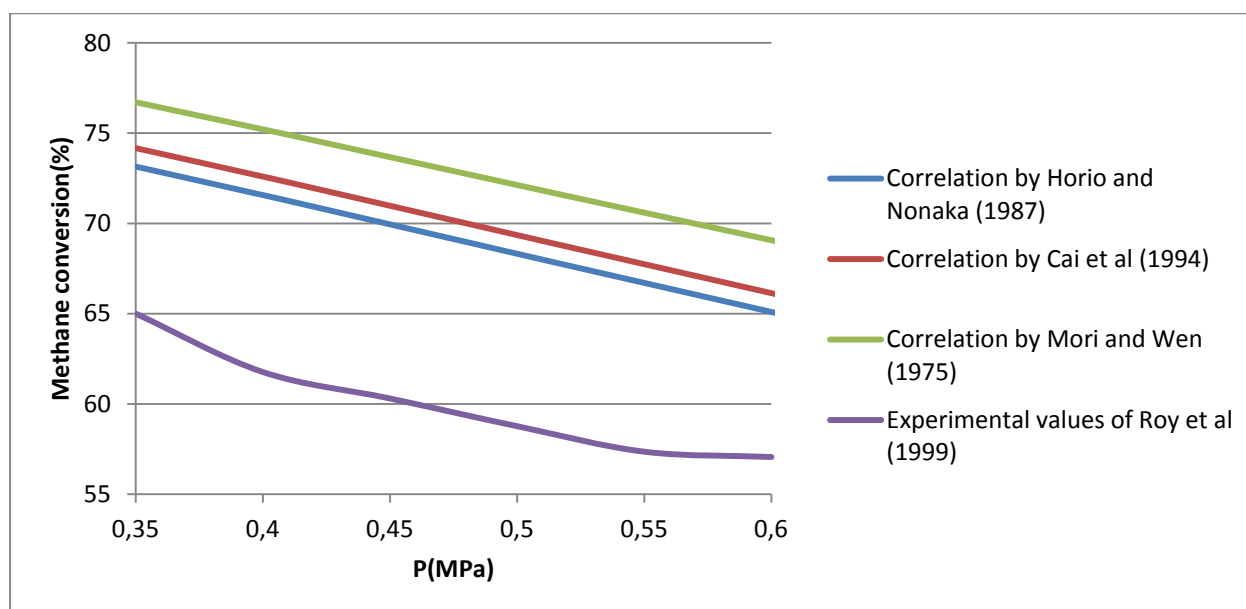


Figure 25- Comparison of the methane conversion with respect to pressure using the bubble size correlations by Mori and Wen (1975), Horio and Nonaka (1987) and Cai et al (1994) with the experimental values of Roy et al (1999) at $U=0.07\text{m/s}$ and $T=650\text{C}$

From Figure 25, it is clear that despite following the same decreasing trend with respect to pressure, all correlations overpredict conversion by at least 12%. One can also observe that the curves obtained using different bubble sizes seem to be parallel. This could be explained by the bubble size plots obtained in Figure 24, which predict no change in bubble diameter with respect to pressure. In fact, it is clear that the given pressure range is too narrow to observe the trends discussed in section 3.22, such as the decrease in bubble size by the correlation of Cai et al (1994). It is also evident that bubble diameter is inversely proportional to the conversion of methane, since the correlation of Horio and Nonaka (1987) which predicted the largest bubbles, resulted in the smallest conversion. The opposite could also be reported for the correlation of Mori and Wen which predicted the smallest bubbles and the largest conversion.

In order to test this theory, conversion was plotted versus pressure in Figure 27 over a wider range (0.3 to 6MPa) to allow changes in bubble diameter.

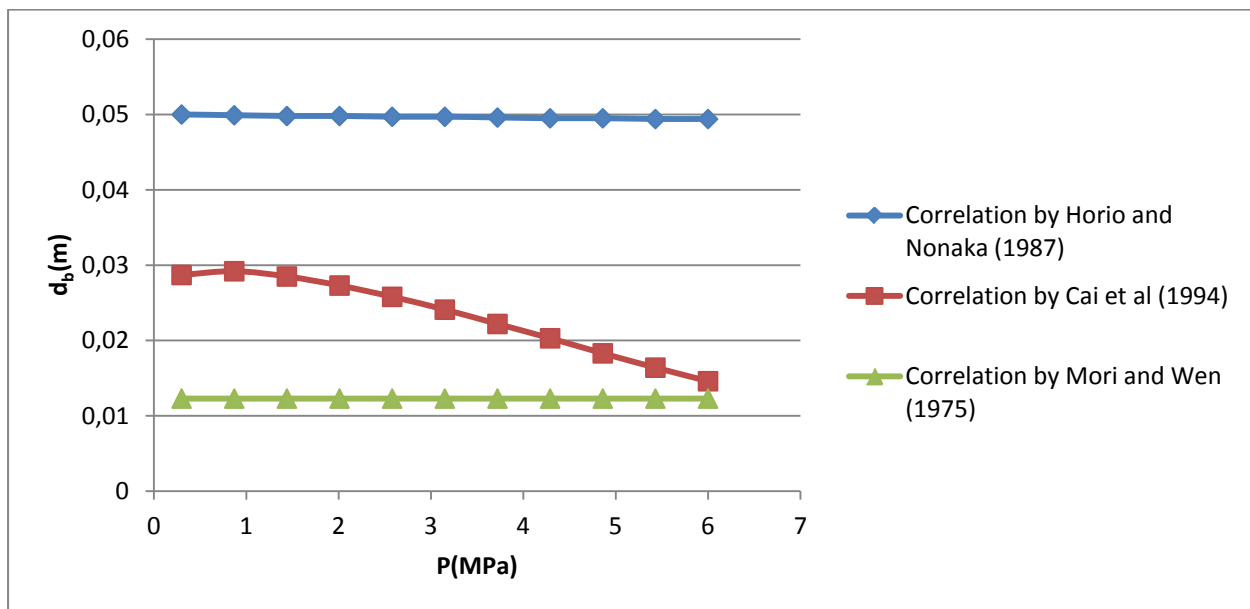


Figure 26- Comparison of the bubble size correlations by Mori and Wen (1975), Horio and Nonaka (1987) and Cai et al (1994) over a pressure range of (0.3 to 6MPa) at $U=0.07\text{m/s}$ and $T=650\text{C}$

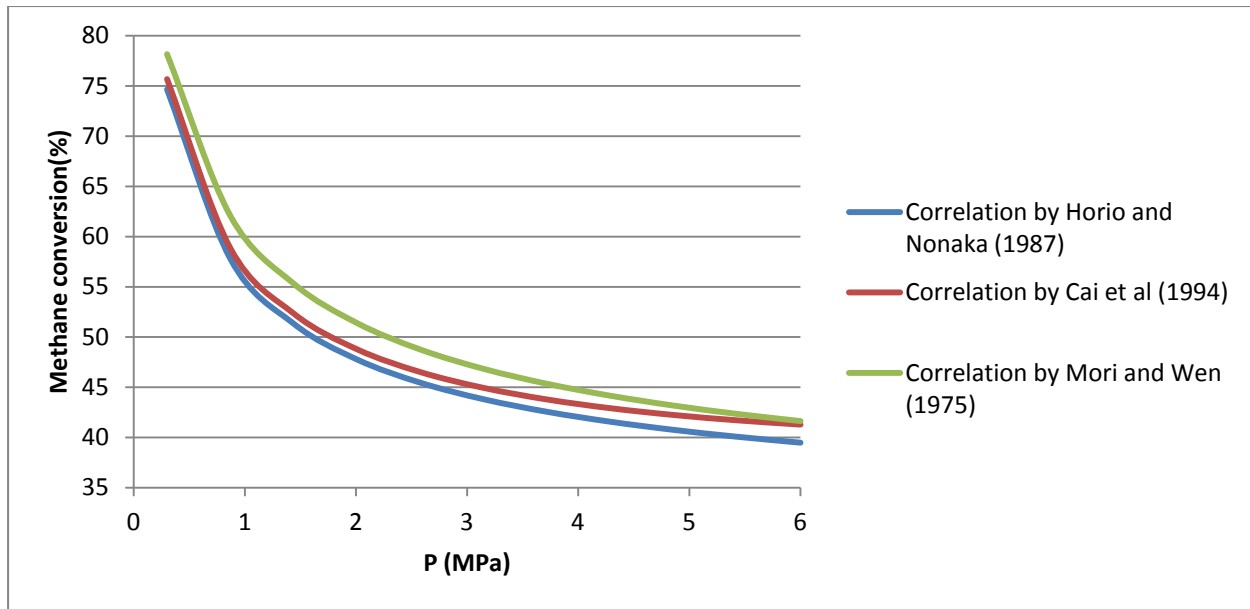


Figure 27- Comparison of the methane conversion over a pressure range of (0.3 to 6MPa) using the bubble size correlations by Mori and Wen (1975), Horio and Nonaka (1987) and Cai et al (1994) at $U=0.07\text{m/s}$ and $T=650\text{C}$

In Figure 26, when bubble diameter was plotted over a wider pressure range the same reported trends in section 3.2.2 were observed. Interestingly, one can note that as bubble size decreased according to the correlation of Cai et al (1994), its respective conversion plot increased. Furthermore, as the estimated bubble diameter by the correlation of Cai et al approached that by Mori and Wen, their respective conversion plots also converged. It seems therefore once more that conversion is inversely related to bubble size with respect to pressure.

Finally, with the experiment of Roy et al (1999) conducted under the bubbling regime in order to achieve a high conversion, the DTP model was used to study the impact of pressure under the turbulent regime. Using the values in table 16, conversion was plotted versus pressure for each of the three bubble size correlations at a superficial velocity of 1.3m/s .

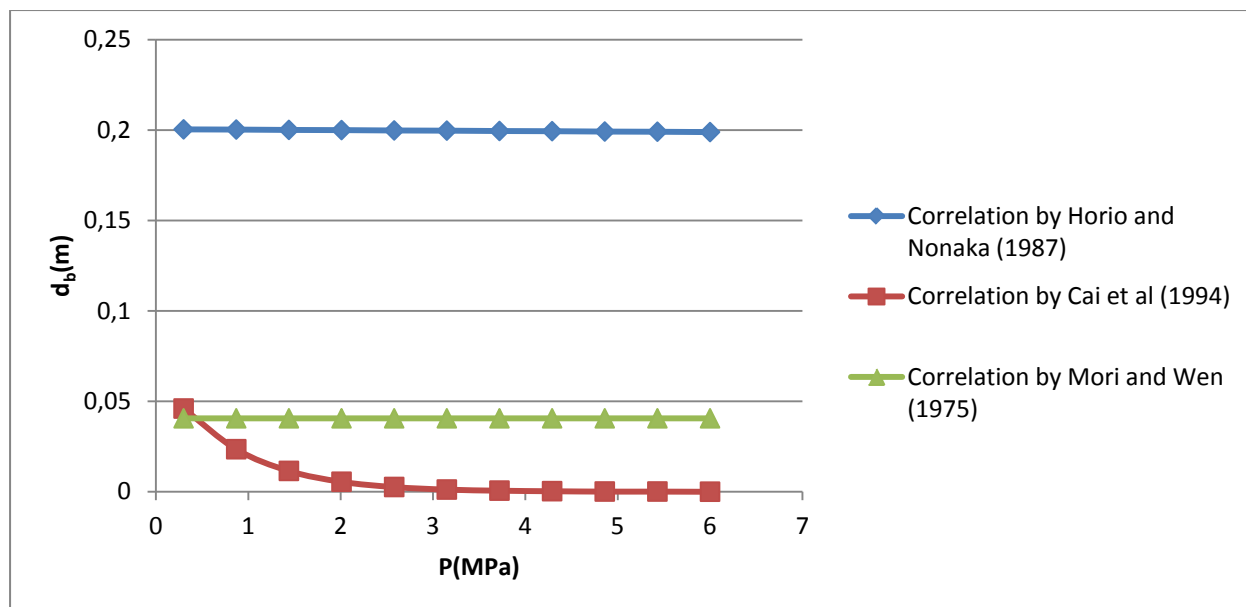


Figure 28- Comparison of the bubble size correlations by Mori and Wen (1975), Horio and Nonaka (1987) and Cai et al (1994) over a pressure range of (0.3 to 6MPa) at $U=1.3\text{m/s}$ and $T=650\text{C}$

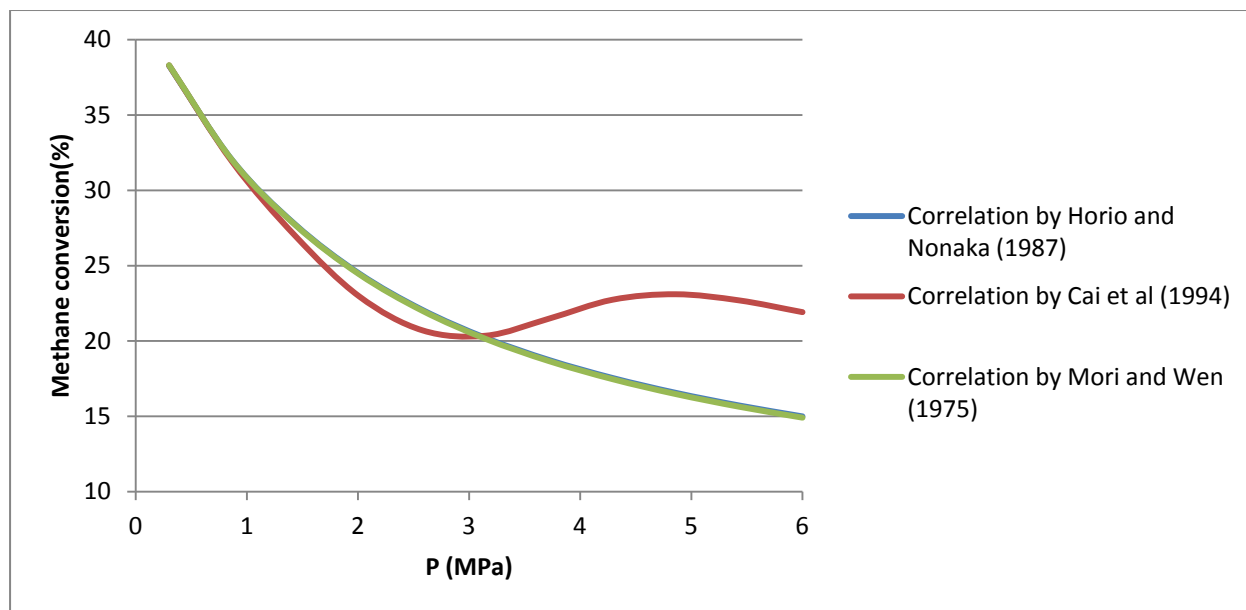


Figure 29- Comparison of the methane conversion over a pressure range of (0.3 to 6MPa) using the bubble size correlations by Mori and Wen (1975), Horio and Nonaka (1987) and Cai et al (1994) at $U=1.3\text{m/s}$ and $T=650\text{C}$

Under the turbulent regime, bubble size doesn't seem to affect conversion based on the obtained results from the correlation of Mori and Wen (1975) and Horio and Nonaka (1987). A completely different trend is however observed by the model of Cai et al (1994). This correlation predicted an initial decrease in bubble size over the pressure range of 0.3 to 2.8MPa, followed by an increase over the pressure range of 2.8 to 5MPa then a decrease. This fluctuation with respect to pressure, suggests that the relation between bubble size and conversion is not as simply predicted earlier. Furthermore, despite the correlation by Cai et al being developed under high pressure and velocity, its combination with the DTP model resulted in curious results. It is therefore evident that additional work must be performed to study the effects of pressure on conversion under the turbulent regime.

3.5.2.2 Effect of temperature on conversion

Similarly to pressure, Roy et al (1999) [92] studied the effect of temperature on the steam methane reform reactions and concluded that conversion increased with temperature over a range of 575 to 675C. Using the DTP model and the values in table 16, conversion was plotted versus temperature for each of the three bubble size correlations, and compared to the experimental finding of Roy et al (1999) [92]. Furthermore, in order to provide an explanation for the observed trends, a plot of bubble diameter versus temperature was also plotted for each bubble size model used.

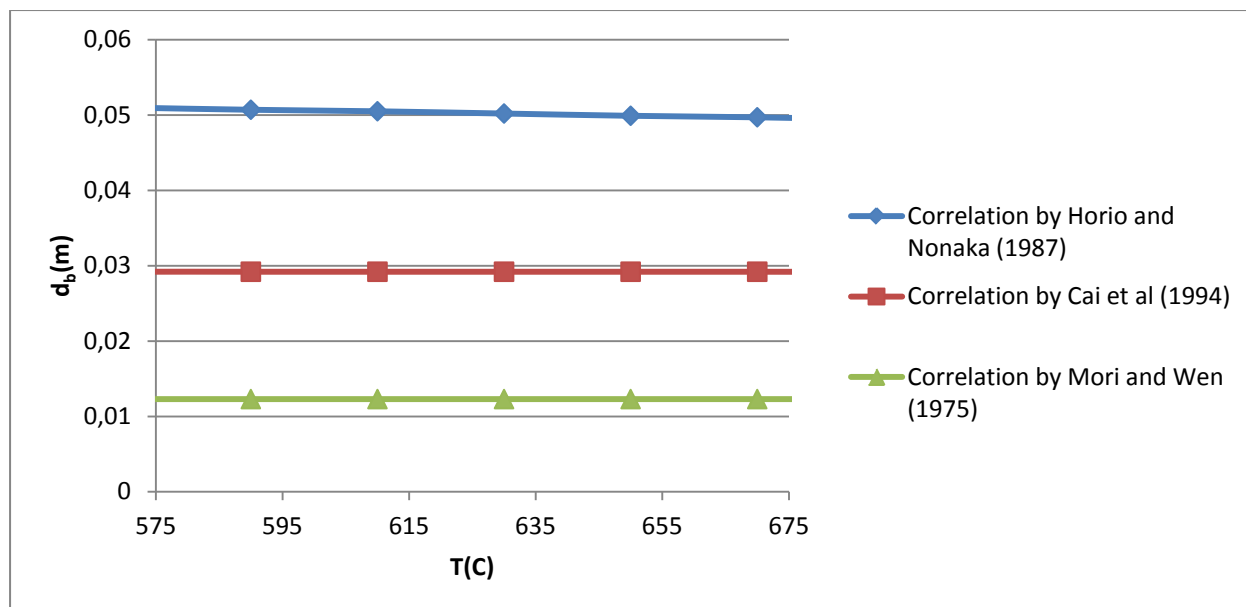


Figure 30- Comparison of the bubble size correlations by Mori and Wen (1975), Horio and Nonaka (1987) and Cai et al (1994) with respect to temperature at $U=0.07\text{m/s}$ and $P=0.55\text{MPa}$

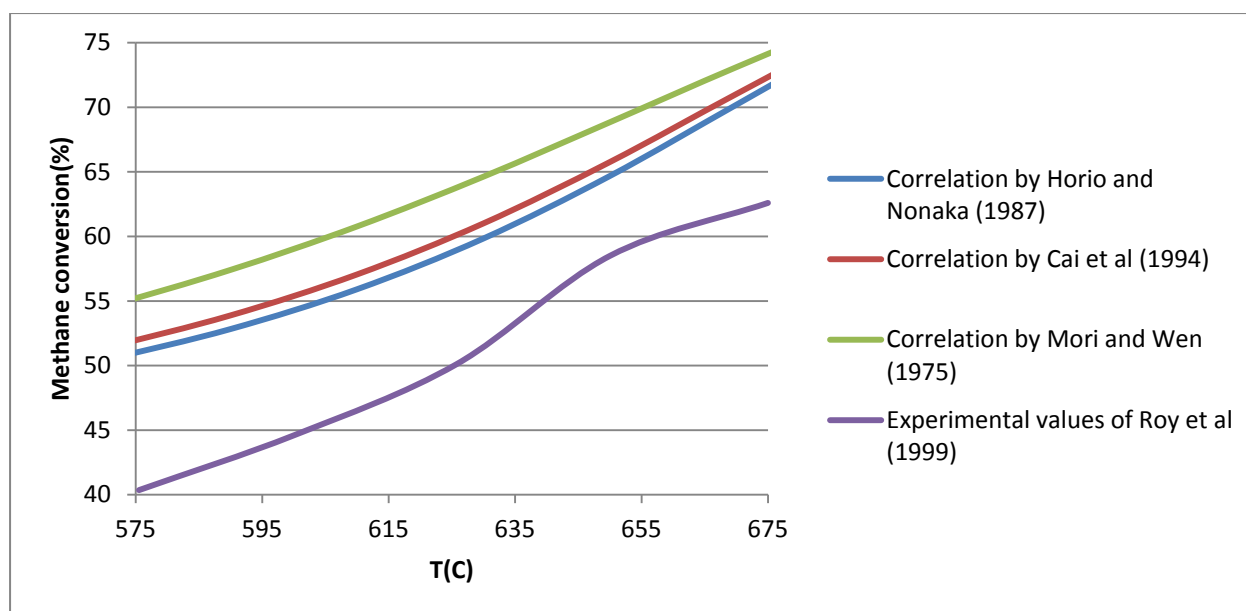


Figure 31- Comparison of the bubble size correlations by Mori and Wen (1975), Horio and Nonaka (1987) and Cai et al (1994) with the experimental values of Roy et al (1999) with respect to temperature at $U=0.07\text{m/s}$ and $P=0.55\text{MPa}$

From Figure 31, it is clear that despite following the same increasing trend with respect to temperature, all correlations overpredict conversion by at least 25%. One can also observe that the curves obtained using different bubble sizes seem to be parallel. This could be explained by the bubble size plots obtained in Figure 30, which predict no change in bubble diameter with respect to temperature. Similarly to the observation made with respect to pressure, it seems that bubble diameter is inversely proportional to the conversion of methane, since the correlation of Horio and Nonaka (1987) which predicted the largest bubbles, resulted in the smallest conversion. The opposite could also be reported for the correlation of Mori and Wen which predicted the smallest bubbles and the largest conversion.

Finally, with the experiment of Roy et al (1999) conducted under the bubbling regime in order to achieve a high conversion, the DTP model was used to study the impact of temperature under the turbulent regime. Using the values in table 16, conversion was plotted versus temperature for each of the three bubble size correlations at a superficial velocity of 1.3m/s.

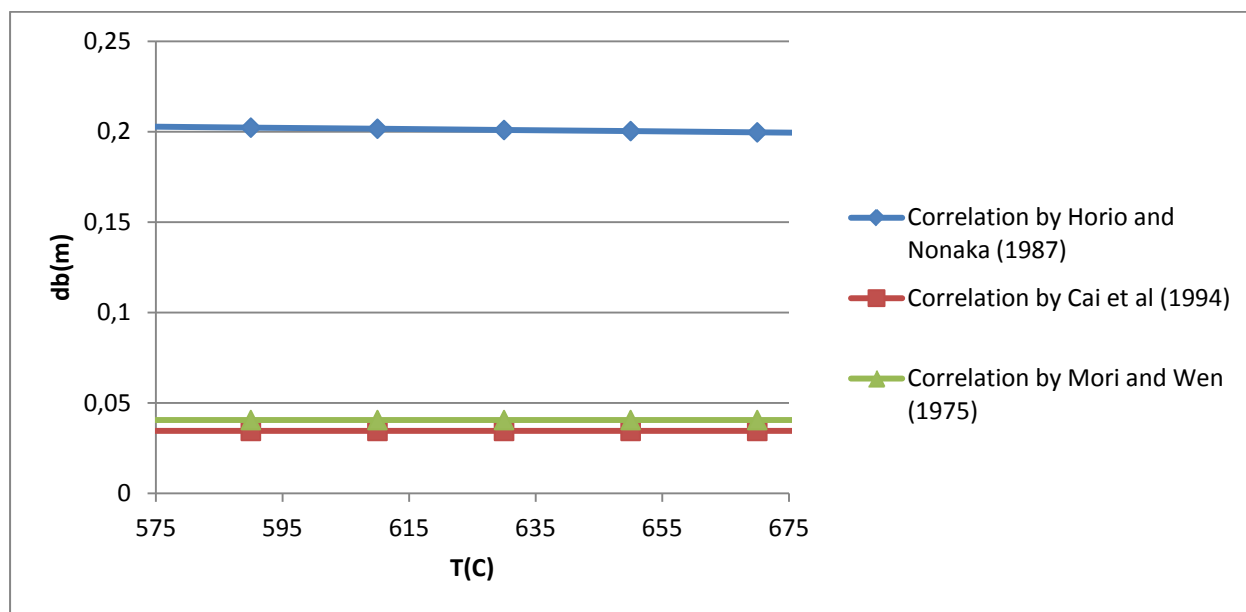


Figure 32- Comparison of the bubble size correlations by Mori and Wen (1975), Horio and Nonaka (1987) and Cai et al (1994) with respect to temperature at $U=1.3\text{m/s}$ and $P=0.55\text{MPa}$

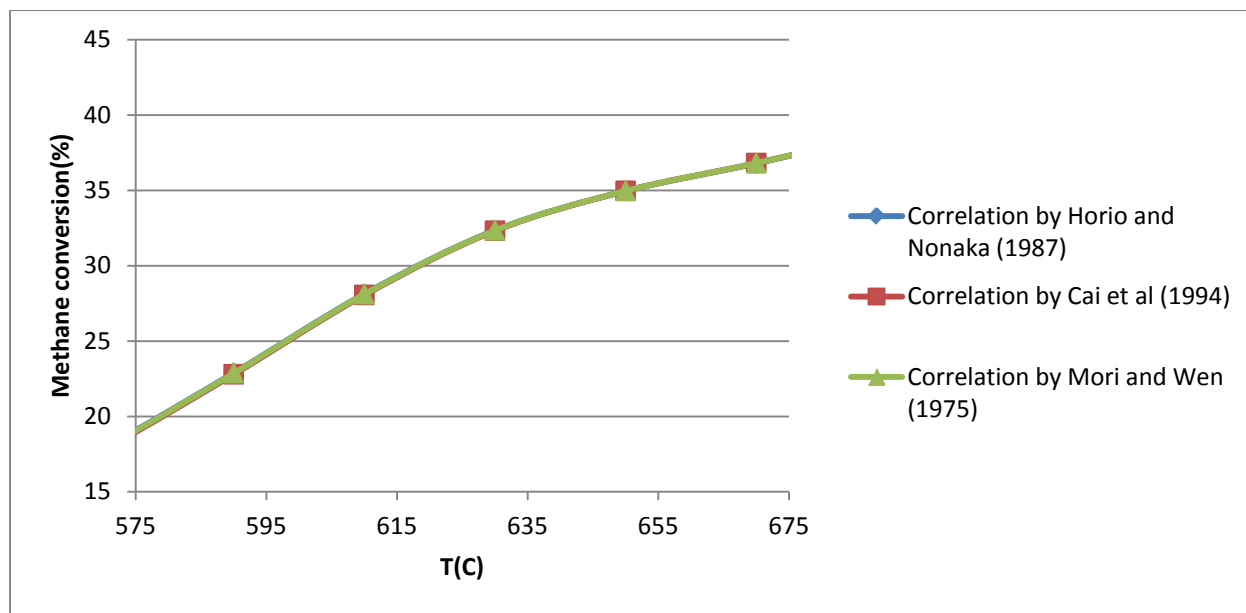


Figure 33- Comparison of the bubble size correlations by Mori and Wen (1975), Horio and Nonaka (1987) and Cai et al (1994) with respect to temperature at $U=1.3\text{m/s}$ and $P=0.55\text{MPa}$

Under the turbulent regime, bubble size doesn't seem to affect conversion based on the obtained results from the correlation of Mori and Wen (1975) and Horio and Nonaka (1987) and Cai et al (1994). Despite yielding a higher bubble size, the correlation of Horio and Nonaka still leads to the same methane conversion as that predicted by the model of Cai et al (1994) and Mori and Wen (1975).

3.6 Conclusion

The purpose of this chapter was to demonstrate the effect of using extreme operating conditions (high temperature, pressure and velocity) on fluidization and more specifically bubble size.

Three bubble size correlations were chosen in this section: Cai et al (1994) for being modeled at high pressure and velocity, Horio and Nonaka(1987) for being developed under high temperature and Mori and Wen (1975) for being one of the most commonly used correlations in design books. Each of these correlations was compared to the reported trends in the literature with the results presented in table 17 below.

Table 17- Comparison of the predicted bubble size using the correlations by Mori and Wen (1975), Horio and Nonaka (1987) and Cai et al (1994) with the expected trends in the literature at high temperature, pressure and velocity.

	d_b trend from the literature	D_b by Mori and Wen (1975)	d_b by Hori and Nonaka (1987)	d_b by Cai et al (1994)
P	d_b decreases with increasing pressure in both the bubbling and turbulent regimes. At very low gas velocities a slight initial increase in bubble size can be observed.	d_b increases over the whole pressure range.	d_b increases over the whole pressure range.	Followed the expected trend with a percent error between 30 at low pressures and 10% at higher pressures.
T	d_b increases up to a maximum then decreases.	d_b increases over the whole temperature range.	Followed the expected trend but overestimated bubble size by almost 800%	d_b increases over the whole temperature range.
U	d_b increases in the bubbling regime and decreases in the turbulent regime.	d_b increases over the whole velocity range.	d_b increases over the whole velocity range.	Followed the expected trend but overestimated bubble size by up to twice the experimental value.

Subsequently, the impact of bubble size on mass transfer, reaction conversion and the transport disengaging height (TDH) were studied through the application of each of the aforementioned models. By doing so, the limitations of some of these correlations were highlighted, and the need of developing new models and a better understanding of fluidization under high temperature, pressure and velocity was demonstrated.

The total entrainment rate was found to increase with velocity and pressure regardless of the used bubble size correlation which only affected its magnitude. The impact of bubble size on entrainment however was found to decrease as velocity increased. As for the effect of temperature, the total entrainment rate decreased with temperature at low velocities and increased at higher velocities.

Using entrainment plots, TDH was found to be independent of the used bubble size correlation and vary with temperature, pressure and velocity. Furthermore, by comparing the graphically estimated TDH values to some of the most common correlations, it was concluded that while many did not exhibit the expected dependencies, none provided acceptable values. Moreover, at high velocities, despite obtaining a large TDH value both graphically and by using the existing models, the overall changes in the total flux are negligible which suggests that sizing the freeboard accordingly might not be profitable.

The need for further studies at extreme conditions was further illustrated through the use of the different bubble size correlations while computing the mass transfer interchange coefficient. This led to different results that sometimes opposed the expected trends from the literature.

Finally, reviewing the effects of pressure and temperature on the conversion of methane in methane steam reforming with respect to each of the bubble size correlations emphasized the need of additional studies. From this simulation, it was observed once more that depending on the operating conditions and the used bubble size correlation, the obtained results could greatly differ from the expected trends.

It is therefore safe to conclude that more work needs to be done on fluidization under high temperature, pressure and velocity, making the design of a reactor capable of operating under extreme conditions of great bearing.

CHAPTER 4 DESIGN OF THE FLUIDIZED BED REACTOR

In this chapter, the complete and detailed design of the fluidized bed reactor will be presented. In section 4.1, the operating and design conditions will be presented. Section 4.2 will give a detailed description of the techniques and procedures used in the design while identifying the different reactor parts. Finally, section 4.3 will present a general description of the proposed process control of this reactor.

4.1 Operating and Design Conditions

As mentioned earlier, the main objective of this work is to design of a fluidized bed reactor that would allow flexible operation at high temperature and high pressure at several gas velocities in order to serve for the future development of new hydrodynamic models. To do so, a set of operating conditions as well as dimensions have been chosen prior to starting the design procedure. The operating conditions were chosen as an adequate extrapolation to industrial reality, while the reactor dimensions were chosen based on an existent reactor currently operating at high temperature in our laboratory while respecting the constraints defined by the compressor and the inherent limitations of the university experimental facility. The reactor's operating conditions and dimensions are therefore as follows:

The temperature will be varied from room temperature to 1000 °C and the pressure will range from atmospheric pressure up to 20 atm. The reactor's bed diameter is 15 cm at the bottom with a freeboard diameter of 50cm. The gas velocity will range from 0.1 m/s up to 2 m/s in order to cover the bubbling and turbulent regime. The bed material will be sand or another type of catalyst with a mean particle size ranging from 60 μm up to 500 μm , so as to cover Geldart A and B particles, and a specific gravity ranging from 1 to 2.5g/cm³. The chosen fluidization medium will be compressed air which may or may not be mixed with other gases.

4.2 Reactor Design: Techniques and Procedures

4.2.1 Windbox/Plenum Design

4.2.1.1 Gas distribution

If we start describing the different parts of a fluidized bed reactor by following the path of the gas, the first section that we will encounter is the plenum chamber or the wind box located under the distributor plate.

The purpose of this section is to pre-distribute the gas uniformly before it passes the distributor plate [98]. Based on the location of the gas entry into the wind box, certain design may be preferred over others [99]. Litz (1972) [100] developed correlations for horizontal and vertical gas entries. He assumed that a high velocity gas stream entering the plenum horizontally expands as a conical-free jet until it dissipates itself, hits the opposite wall, or have its upper edge strike the bottom of the distributor plate which can cause maldistribution. In case of vertical entry through a nozzle centered in the bottom, the high velocity gas stream would also expand as a conical-free jet until it dissipates itself, have its diameter coincide with the vessel diameter or hit a central portion of the plate causing maldistribution. In order to ensure uniform distribution of the gas, the gas entry point must be separated from the distributor plate by a distance H_{plenum} based on the criteria presented in table 18.

Table 18- Plenum Design Equations

Gas Entry	Condition	Equation
Horizontal	$D_{\text{entry}} > D_{\text{plenum}}/100$	$H_{\text{plenum}} = 0.2D_{\text{plenum}} + 0.5D_{\text{entry}}$
	$D_{\text{entry}} < D_{\text{plenum}}/100$	$H_{\text{plenum}} = 18D_{\text{entry}}$
Vertical	$D_{\text{entry}} > D_{\text{plenum}}/36$	$H_{\text{plenum}} = 3(D_{\text{plenum}} - D_{\text{entry}})$
	$D_{\text{entry}} < D_{\text{plenum}}/36$	$H_{\text{plenum}} = 100D_{\text{entry}}$

Litz used the assumption that gas enters the plenum chamber with a half angle of about 10 deg. The importance of plenum design has long been debated. While many believes that plenum design might not be critical if the bed-pressure-drop-to-grid-pressure-drop ratio is high enough [99], others such as Kage et al (1991) [101] believes that it plays a critical role as it can be used to predict bubble formation and eruption.

4.2.1.2 Natural gas combustion

As will be discussed in section 4.2.5, the windbox will also be used to burn natural gas at high pressure and therefore its volume must ensure total combustion in order to reduce CO emissions. Knowledge of the kinetics of natural gas combustion is therefore very important.

Many different kinetic models can be found in the literature. For simplicity purposes, the global two-step reaction model by Dryer and Glassman [102] was used:

Table 19- Natural gas combustion reactions and kinetic models

#	Reaction	Kinetic Model	Kinetic Parameter
1	$CH_4 + \frac{3}{2}O_2 \rightarrow CO + 2H_2O$	$r_1 = k_{CH_4} C_{CH_4}^{0.7} C_{O_2}^{0.8}$	$k_{CH_4} = 235 \exp\left(-\frac{198000}{R}\left(\frac{1}{T} - \frac{1}{973}\right)\right)$
2	$CO + \frac{1}{2}O_2 \rightarrow CO_2$	$r_2 = k_{CO} C_{CO} C_{O_2}^{0.25} C_{CO_2}^{0.5}$	$k_{CO} = 371000 \exp\left(-\frac{171000}{R}\left(\frac{1}{T} - \frac{1}{973}\right)\right)$

4.2.2 Distributor Design

Once the gas is pre-distributed uniformly in the wind box, it passes the distributor plate.

In a fluidized bed reactor, the gas distributor or grid, serves many purposes and its design is often a key component for hydrodynamic studies. While having to provide stable and even fluidization across the reactor's cross-section, the distributor must also minimize attrition of the solids and prevent them from falling into the wind box beneath. The distributor must also be capable of supporting the bed's weight during shutdown and start-up [99]. Multiple research papers have been published on distributors, however very few have addressed its design at high temperature and high pressure. Before getting into the specific design criteria related to high temperature and high pressure, it is important to define some of the fundamental properties of gas distributors.

Many different distributor models exist today with some used more than others depending on the reactor's operating variables. Nonetheless, all distributors can be divided into three types based on the direction of the gas entry: upwardly, laterally, or downwardly.

The most common type of distributor is the perforated plate which has an upwardly-directed flow [103]. Although used in many applications because of its simple fabrication, low price and easy design, the perforated plate was proven on many occasions to allow bed weepage to the wind box. While laterally and downwardly directed flow distributors, such as bubble cap or spargers, have been used to reduce weepage, their higher price has always been a major disadvantage [5].

Currently in our laboratory, a high temperature fluidized bed reactor is being operated efficiently with a bubble cap distributor and therefore for comparison purposes, and due to the advantages

that it has over perforated plates, the design of a bubble cap distributor will be presented in the following section along with a detailed design procedure.

4.2.2.1 Distributor pressure drop

Many variables have to be considered when designing a distributor plate. The first and upmost important variable is the pressure drop across the distributor, commonly known as ΔP_d . As explained earlier, fluidization occurs when a pressure drop is high enough to lift and suspend the solids by balancing the weight of the bed. This pressure drop must also be sufficient in order to provide equal distribution of gas flow through all pores and prevent temporary orifice blockage. One can therefore understand that a minimum pressure drop must exist across the distributor in order for the aforementioned conditions to be met. In most design books [5, 103], the pressure drop across the distributor is expressed as follows:

$$\Delta P_d \geq K \Delta P_b$$

Where K is the grid pressure drop coefficient and ΔP_b is the pressure drop across the bed which is a function of the minimum bed height, L_{mf} , the solid density, ρ_p , and the minimum bed voidage, ϵ_{mf} , defined as:

$$\Delta P_b = g \times \rho_p \times L_{mf}(1 - \epsilon_{mf})$$

At minimum fluidization, the bed voidage, ϵ_{mf} , corresponds to the loosest packing of a packed bed, which is cubic for uniform spheres and can be estimated as 0.476 [103]. Kunii and Levenspiel [1] summarized the effect of pressure and temperature on fluidization behavior observed by several researchers for beds of porous carbon powder, coal, char and uniformly sized glass beads: ϵ_{mf} was observed to increase slightly (1-4%) with a rise in operating pressure (up to 80 bar) and with temperature for fine particles (up to 8% for temperatures up to 500 °C). ϵ_{mf} seemed however unaffected by T for coarse particles. One can therefore conclude that in our operating conditions, ϵ_{mf} can be safely considered constant with a value of 0.476.

Many researchers have tried to identify the value of K and have concluded that it depends on different factors such as the distributor type, the reactor diameter, the minimum bed height, etc.

The most common value of K that can be found in the literature [103] is that of Zenz (1969) who recommends the ratio of distributor to bed pressure drop be 0.3 for bubbling fluidized beds with upwardly and laterally directed flow and 0.1 for downwardly directed flow [104].

Quershi and Creasy[105] on the other hand reported that for pilot scale reactors, such as the one in question, K tends to be a lot smaller. Using values obtained from prototypes and pilot scale plants, they found that in order for all holes to be operational, the pressure drop should obey the following rule for Geldart B:

$$\frac{\Delta P_d}{\Delta P_b} \geq 0.01 + 0.2 \left[1 - \exp \left(\frac{-0.5 D_t}{L_{mf}} \right) \right]$$

With the value of K now known, it is important to be able to relate the pressure drop across the distributor to some of the fundamental design variables such as the number of holes, holes' diameter, operating conditions, etc... in order to be able to design the most flexible distributor for our operating range.

In order to relate the number of holes with the pressure drop across the distributor, the first variable to consider is the gas velocity, U_h , across one hole:

$$U_h = C_D \sqrt{\frac{2 \Delta P_{grid}}{\rho_g}}$$

C_D is the discharge coefficient which can be found graphically to be about 0.6 for a shape edged orifice. However, since grids are not shaped-edged, C_D has a higher value of about 0.8 [99].

The second variable to consider is the volumetric flow rate of the gas, Q , which can be expressed as a function of the number of holes, N , holes' diameter, d_h , and the gas velocity U_h as follow:

$$Q = N \frac{\pi d_h^2}{4} U_h$$

By combining this relation with the definition of the gas velocity across one hole, we can obtain a relation for the pressure drop across the distributor with respect to the operating variables.

$$\Delta P_d = \left[\frac{4Q}{N \pi d_h^2 C_D} \right]^2 \left(\frac{\rho_g}{2} \right)$$

Since temperature, pressure and gas velocity will be varied depending on the intended experiment, it is fundamental to know how each of the variables in this equation is affected by the operating conditions.

While Q is directly proportional to the velocity, the gas density, ρ_g , is proportional to the pressure and inversely proportional to the temperature. One can therefore conclude that the pressure drop across the distributor, ΔP_d , is proportional to the pressure, the square of the velocity, and inversely proportional to the temperature.

Using this equation, the value of d_h or N can be found by fixing the other. However, in order to do so, it is important to be aware of any existing restrictions on the number of holes and hole diameter.

Concerns regarding hole diameters differ based on the nature of the used distributor. For bubble cap distributors, in order to ensure that the pressure drop across the header is at an acceptable level, the following criteria should be met [103]:

$$\left(\frac{D_h^2}{N_h d_h^2} \right)^2 > 5$$

Where D_h is the diameter of the header.

4.2.2.2 Bubble cap distributor dimensioning and spacing

Very limited information exists on the exact equations used in the sizing of bubble cap distributors, with most researchers basing their design on previous existing models. Sandersson (2002) [106] wrote in his thesis that for comparison of results, distributors must be geometrically similar. The schematics of the bubble cap distributor currently used in our laboratory can be found in Figure 34 below.

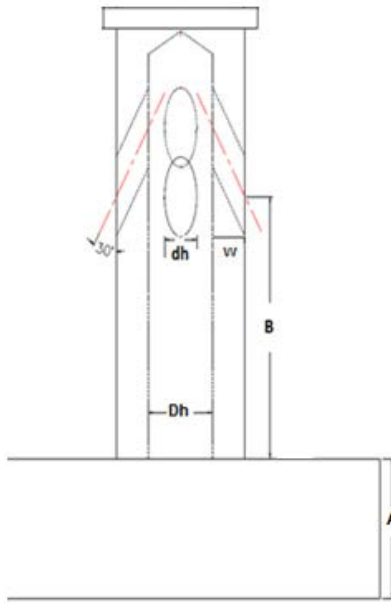


Figure 34- Schematics of bubble cap distributor

Despite the remark of Sandersson, multiple variables such as the plate thickness, the distance between the bubble caps and the wall, and the holes of the distributor cannot be designed simply by geometric similarities and require different design techniques due to their dependency on temperature, pressure and velocity. Therefore, in order to design our new bubble cap distributor, a procedure must be developed for each of these variables in addition to that of d_h and D_h discussed earlier.

4.2.2.2.1 Bubble cap spacing

The manner in which the gas flows through the distributor can have a significant impact on its design. Gas flowing from the holes is usually in the form of a continuous jet. The jet length is important in order to determine how far to keep internals and minimize erosion. Karri (1991) [103, 107] noted that the jet penetrations for various orientations at both ambient and extreme conditions can be approximated by:

$$L_{up} \sim 2 L_{hor} \sim 3 L_{down}$$

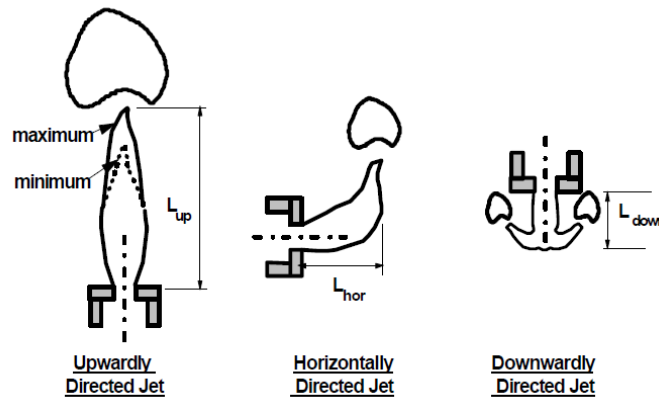


Figure 35- Jet configurations

Many different correlations have been developed over the years for different orientations and operating conditions. In his thesis, Sauriol (2011) [108], cited many of the different jet correlations along with their respective conditions. One correlation that is of great interest to this design is that by Blake et al (1990) [109] for upwardly directed jets which seems to be applicable for high temperature (20-700 °C), high pressure (1, 3, 4-51 atm) and for Geldart A, B and D particles.

$$\frac{L_{up}}{d_h} = 110 \left(\frac{U_h^2}{g d_h} \right)^{0.304} \left(\frac{\rho_g}{\rho_p} \right)^{0.513} \left(\frac{\rho_s U_h d_p}{\mu} \right)^{-0.189}$$

Being that this correlation is for upwardly directed jets, a combination with the relation of Kari (1991) described earlier, can provide results for all jet configurations.

Consequently, knowing the holes diameter and height can lead to the determination of the required spacing between each cap and the wall to minimize erosion by using simple geometry.

4.2.2.2.2 Plate thickness, A

The plate should be able to carry the weight of the solids during start-up and shutdown, and handle the maximum pressure drop during operation. The thickness calculations will be performed based on which ever of these two applied forces is higher.

The force due to the weight of the solids, W, can be calculated by:

$$W = \rho_p L_{mf} A_t (1 - \varepsilon_{mf}) g$$

The force due to the pressure drop, $F_{\Delta P}$, can be calculated by:

$$F_{\Delta P} = \Delta P_d A_t$$

Several methods exist in order to determine the minimum required plate thickness to support this load, two of which are presented below.

The first method was developed for perforated plates used in shell and tube heat exchangers [110]:

$$t_p = C_{ph} D_t \sqrt{\frac{\Delta P_d}{\lambda f_p}}$$

Where λ is the ligament efficiency which represents the material between the holes that holds them together: $\lambda = (L_h - d_h) / L_h$

f_p is the maximum allowable design stress for the plate which can be approximated by (1/3.5) times the yield strength [111].

C_{ph} is the design factor which depends on the edge support of the grid (clamped, supported, etc.) and can be approximated to 0.4 for clamped plates [111].

The second method used was developed for circular supported plates [110].

$$\sigma = \frac{3 \Delta P_d r^2 (3 + \nu)}{8 t_p^2}$$

Where r is the plate radius, ν is Poisson's ratio, and σ , the applied stress on the plate. This equation can be applied with the yield strength of the plate material in order to determine the minimum required thickness to avoid any permanent deformation.

For safety purposes, the largest thickness obtained, using both methods, will be chosen in the design.

4.2.3 Particle Separation

Once the gas is uniformly injected into the reactor by the distributor plate, fluidization starts. As mentioned earlier, bursting of bubbles at the surface of the bed ejects particles into the freeboard to various heights. In order to prevent the bed from being depleted, a solid collection device is usually placed inside the freeboard so that entrained material can be returned to the bed. Two types of gas-particle separation units are often recommended in the literature; these are cyclones and filters [112]. Cyclones have been globally renowned because of their simple structure, low cost and ease of operation despite their low efficiencies for small particles [113]. Filters, despite remaining a new concept in fluidized beds [114], has emerged as a promising technology for the separation of small particles. Therefore, in order to allow flexibility of our reactor, an internal cyclone and filter will be placed in series in the freeboard as illustrated in Figure 36.

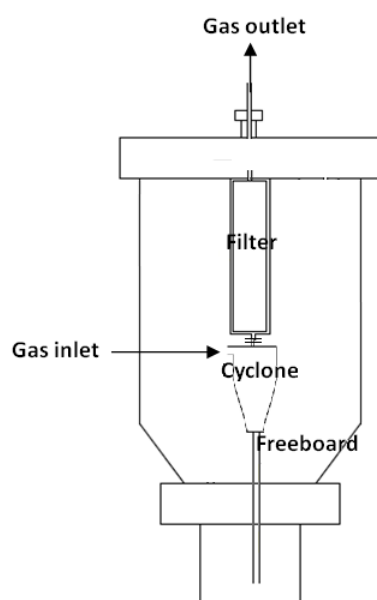


Figure 36- Cyclone and filter disposition in the freeboard

A review on both cyclone and filters is presented below, along with their design procedure. However, before presenting these design procedures, it is important to introduce another variable, the dust concentration, c (g/m^3), which is fundamental in the design of both cyclone and filter.

4.2.3.1 Dust loading

As we recall in Chapter 3, E_i is the entrainment rate which can be calculated based on several parameters, among which the diameter of the reactor. In order to reduce the amount of entrained solids out of the reactor, in addition of having a particle separation device, a common practice is to increase the diameter of the freeboard [115, 116]. As observed by Smolders and Baeyens (1997) [69], increasing the freeboard diameter reduces the gas velocity by a factor $(D_t/D_{fb})^2$. This reduction in velocity leads to a significant reduction of the entrainment flux.

Using the relation by Smolders and Baeyens (1997), it is possible to obtain an equation that relates the dust load, c , the entrainment rate, E_i , the reactor diameter, D_t , and the freeboard diameter, D_{fb} , as follows:

$$c = \frac{E_i \rho_g}{U} \left(\frac{D_t}{D_{fb}} \right)^2$$

4.2.3.2 Cyclones

A gas cyclone is a gas-particle separation device where the gas-solid stream is introduced tangentially into a cylindrical body, therefore creating a vortex which in turns pushes any particle denser than the carrier gas towards the walls of the cyclone while the gas exits at the top. A typical cyclone separator can be viewed in Figure 37.

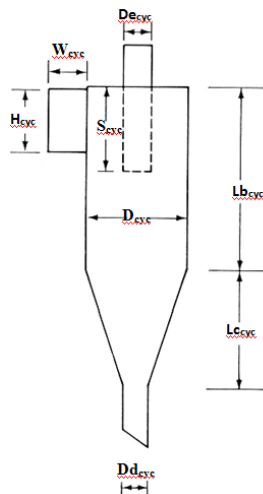


Figure 37- Typical cyclone configuration

Several cyclone models have been reported in the literature [117, 118] with the most common listed in table 20.

Table 20- Most common cyclone dimensions

		High Efficiency		Conventional		High Throughput	
Model number		(1)	(2)	(3)	(4)	(5)	(6)
Body Diameter	D_{cyc}/D_{cyc}	1	1	1	1	1	1
Height of Inlet	H_{cyc}/D_{cyc}	0.5	0.44	0.5	0.5	0.75	0.8
Width of Inlet	W_{cyc}/D_{cyc}	0.2	0.21	0.25	0.25	0.375	0.35
Diameter of Gas Outlet	$D_{e_{cyc}}/D_{cyc}$	0.5	0.4	0.5	0.5	0.75	0.75
Length of Vortex Finder	S_{cyc}/D_{cyc}	0.5	0.5	0.625	0.6	0.6	0.875
Length of Body	$L_{b_{cyc}}/D_{cyc}$	1.5	0.4	2	1.75	1.5	1.7
Length of Cone	$L_{c_{cyc}}/D_{cyc}$	2.5	2.5	2	2	2.5	2
Diameter of Dust Outlet	$D_{d_{cyc}}/D_{cyc}$	0.375	0.4	0.25	0.4	0.375	0.4

As can be clearly seen, all cyclone dimensions are directly related to the cyclone body diameter, D_{cyc} . In order to determine this diameter so as to design the most efficient cyclone, several key parameters must be calculated.

The pressure drop across the cyclone is often regarded as one of the most important performance parameters as it is directly related to the separation efficiency.

Generally, the pressure drop is defined as the difference of static pressure between the inlet and the outlet of the cyclone and is usually related to the square of the gas flowrate by a dimensionless group referred to as the Euler number, Eu .

$$\Delta P_{cyc} = 8\rho_g Eu \left(\frac{Q}{\pi D_{cyc}^2} \right)^2$$

The Euler number, also known as the resistance coefficient, represents the ratio of pressure to inertial forces acting on the gas flow and is constant for a given cyclone geometry or design. Eu

is usually measured experimentally with clean air; however, in case of the lack of test data, different correlations exist in the literature.

Leith and Mehta [119] reviewed several theoretical expressions and concluded that the correlation by Shepherd and Lapple [120] (given below) was the best available due to its simplicity and high accuracy.

$$Eu = \pi^2 \left(\frac{D_{cyc}}{L_{cyc}} \right) \left(\frac{D_{cyc}}{H_{cyc}} \right) \left(\frac{D_{cyc}}{De_{cyc}} \right)^2$$

Interestingly, Eu tends to decrease when significant amounts of solids are present. In order to account for this effect, several researchers have tempted to develop correlations relating Eu with the dust concentration, c (g/m^3) [121, 122]. According to Romeo et al [121], the best available method to account for dust loading was developed by Baskakov et al (1990) [122] and is presented below.

$$Eu = Eu_c \left(\frac{1}{3.1c^{0.7}} + 0.67c \right)$$

Eu_c refers to the Euler number calculated previously using the correlation by Shepherd and Lapple.

Furthermore, Romeo et al observed that Eu dropped after time due to fouling by a factor, $K_{fouling}$, from 0.7 to 0.9, and concluded that Eu can be expressed as:

$$Eu = Eu_c \left(\frac{1}{3.1c^{0.7}} + 0.67c \right) K_{fouling}$$

The second key parameter needed in order to determine the cyclone body diameter D_{cyc} , is the cyclone efficiency, η .

$$\eta_i = \frac{x_i}{1 + (dp_{50}/dp_i)}$$

Where x_i is the particle size fraction, which can be obtained from the particle size distribution.

dp_{50} , which represents the cut size for which 50 percent of solids of a given size are collected [118], is related to a dimensionless group referred to as the Stokes number, Stk_{50} as follows:

$$Stk_{50} = \frac{4dp_{50}^2 \rho_p Q}{18\mu\pi D_{cyc}^3}$$

The Stokes number, Stk_{50} , is defined as the ratio of the centrifugal (less buoyancy) to the drag force, both acting on a particle of size dp_{50} . Finally, a direct relation exists between Eu and Stk_{50} [9] as follows:

$$Eu = \sqrt{\frac{1}{Stk_{50}}}$$

4.2.3.3 Filters

Following the cyclone, a filter will be placed in series. The most important parameter in gas-solid filters is the pore size which is directly proportional to filter efficiency. Coagulation of particles and filter cake, have also been reported to affect filter efficiency [114].

It is however important to note that due to the high temperature nature of our reactor, very few information have been reported in the literature regarding gas-solid filters at elevated temperatures.

A gas filter manufacturing company was therefore contacted in order to provide invaluable insight on the different available filters. The specification of the chosen filter can be found in section 5.1.3.

4.2.4 Reactor Shell and Refractory Design

The thickness of the reactor metal shell will be computed based on the restrictions by the American Society of Mechanical Engineers (ASME) which dictates that for cylindrical vessels and piping under high pressure [123], the minimum allowable thickness should be taken as the greater value between the one obtained under circumferential stress and the one calculated for longitudinal stress. The equation to compute both methods are listed below in table 21.

Table 21- Circumferential and longitudinal stress equations

Stress Type	Equation
Circumferential	$t_{shell} = \frac{P \cdot r}{\sigma \cdot E - 0.6P}$
Longitudinal	$t_{shell} = \frac{P \cdot r}{2\sigma \cdot E + 0.4P}$

It is however important to note that certain rules apply in order to use this method. At high pressure, the American Society of Mechanical Engineers restricts shell surface temperatures to specific values depending on the nature of the metal. Special care must therefore be taken when choosing the appropriate refractory in order to ensure that this limit is not exceeded.

Straight forward heat flux balances (table 22) are used in order to determine the required thickness of the different refractory, by modelling the reactor as a cylinder with multiple layers (Figure 38).

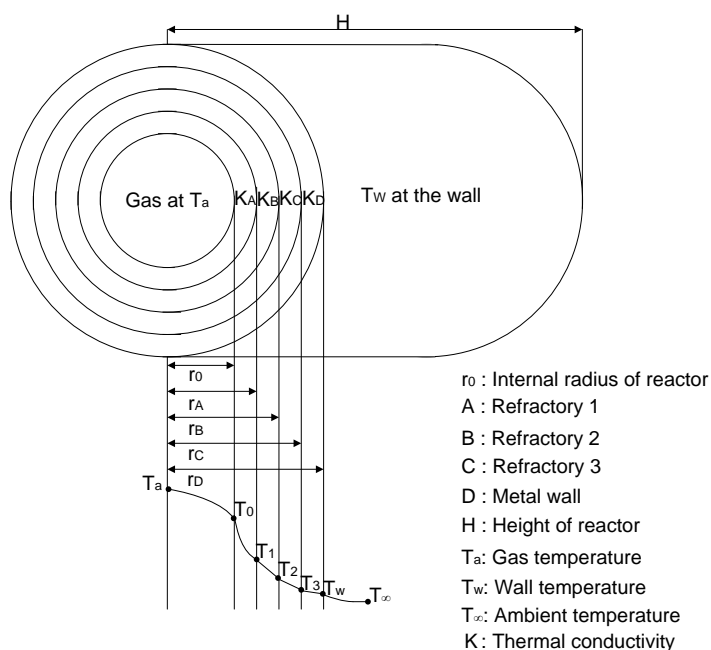


Figure 38- Reactor Shell Modeling

Table 22- Heat Flux Balance

Layer	Heat flux balance
Refractory 1	$T_0 - T_1 = \frac{r_0 q_0 \ln \left(\frac{r_A}{r_0} \right)}{k_A} = r_0 q_0 R_A$
Refractory 2	$T_1 - T_2 = \frac{r_0 q_0 \ln \left(\frac{r_B}{r_A} \right)}{k_B} = r_0 q_0 R_B$
Refractory 3	$T_2 - T_3 = \frac{r_0 q_0 \ln \left(\frac{r_C}{r_B} \right)}{k_C} = r_0 q_0 R_C$
Carbon steel	$T_3 - T_4 = \frac{r_0 q_0 \ln \left(\frac{r_D}{r_C} \right)}{k_D} = r_0 q_0 R_D$
Metal Wall	$T_w - T_\infty = \frac{q_0 r_0}{h r_D} = r_0 q_0 R_\infty$ <p>h is the natural convection coefficient</p>

4.2.5 Reactor Heating System

In order to achieve the required operating temperatures, a suitable heating system must be used. Currently in our laboratories, a high temperature fluidized bed reactor is being operated using a natural gas burner. In order to achieve higher temperatures inside the reactor, natural gas or propane is directly burned inside the bed. Unfortunately, due to large expenses related with high pressure burners, this system can not be applied to a reactor at elevated pressures. Furthermore, with electrical heaters also proving to be very expensive when covering the full gas velocity range in question, a cheaper heating method had to be improvised.

Combining both of the aforementioned technologies, a high pressure heating system was designed and will be connected to the windbox. This heating system, shown in Figure 39, comprises of an insulated pipe where a high pressure electric heater capable of withstanding low flowrates is attached. This electrical heater will be used to preheat the pipe until the auto-ignition temperature of natural gas is achieved. At this point, natural gas will be fed to the pipe along with compressed air. The amount of natural gas will be varied automatically until the desired temperature is achieved inside the windbox. Several injection ports will be located on the pipe to allow flexible temperature control and ensure that the design temperature is not exceeded in the pipe.

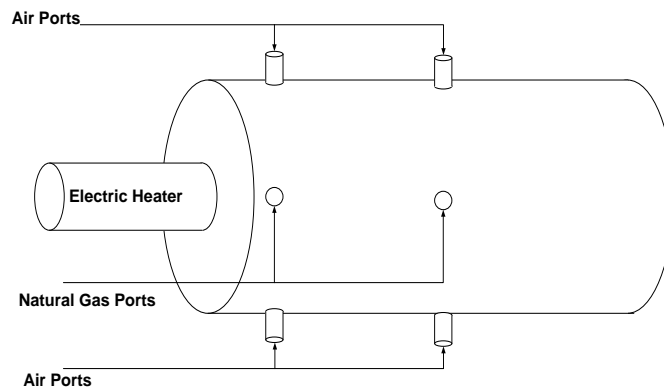


Figure 39- Heating System schematics

In order to design such a system, knowledge of the flame length can be crucial. In fact, in any burner system design, the flame's ability to burn persistently at a given position is characteristic of its stability [124]. The heating pipe must therefore be designed to have at least the same length as the flame. Blake et al (1999) [125] found a relation between the flame length, L_{flame} , and a variable called the theoretical flame dimension, d_{flame} .

Blake et al (1999) modelled the theoretical flame dimension, d_{flame} , as a function of the mass flowrate of the gas, m_{gas} , the density of the flame product, ρ_{fp} , the momentum of the fuel jet, J , and the Shvab-Zek'dovich variable, Z_f .

$$d_{flame} = \frac{2m_{gas}}{Z_f(\pi\rho_{fp}J)^{0.5}}$$

Where J is the fuel jet momentum, defined as the product of the mass flowrate of the gas, m_{gas} , and the velocity of the fuel, U_{fuel}

The Shvab-Zek'dovich variable, Z_f , is directly related to the stoichiometric air-fuel ratio, AFR such as:

$$Z_f = \frac{1}{1 + AFR}$$

Blake et al (1999) related the flame length, L_{flame} , and the theoretical flame dimension, d_{flame} , by the Froude number, Fd such as

$$Fd = \frac{4J}{\pi\rho_{\infty}d_{flame}^3}$$

Where ρ_{∞} is the unperturbed density of the gas

$$L_{flame} = \begin{cases} 6d_{flame} \times Fd^{\frac{1}{5}} & \text{for } Fd < 10 \\ 11Fd & \text{for } Fd \geq 10 \end{cases}$$

4.3 Process Description

Due to its elevated pressure and temperature, extra precautions must be taken when operating the reactor and therefore an understanding of the operating process is fundamental. With the design of the fluidized bed reactor and its heating system presented in the previous section, the next step is their integration in the process.

Compressed air will be provided by one to two compressors capable of pressurizing the reactor and compensate for the pressure drop created by the distributor plate. The compressors will feed a tank that will be used to deliver a constant pressure of 30 bars, via pressure regulator, V-101. In order to obtain the desired gas flowrate inside reactor, a valve V-140 will be adjusted by several transmitters. By using a valve downstream of the reactor, V-120, the pressure of the gas will be controlled.

Solid particles will be inserted inside the reactor prior to operation in order to achieve the desired static bed height. In case of operation under atmospheric conditions and a superficial gas velocity of 0.1 m/s, the solids could also be injected in the freeboard region.

As mentioned in the previous section, in order to heat up the fluidized bed reactor, a heating system was developed and will be connected to the windbox. This heating system comprises of an insulated pipe where a high pressure electric heater capable of withstanding low flowrates is attached. This electrical heater will be used to preheat the pipe until the auto-ignition temperature of natural gas is achieved. At this point, natural gas from a pressurized cylinder (~2260 psia that will be controlled with a pressure regulator) will be fed to the insulated cylinder along with the compressed air from the compressors. The amount of natural gas will be varied automatically until the desired temperature is achieved inside the windbox.

In order to reach a fluidized bed temperature of 1000°C, natural gas from a second pressurized cylinder will be injected directly inside the bed of solids. This natural gas injection will only be performed in case the detected bed temperature is equal or above 800°C as specified by the National Fire Protection Association (NFPA 85) [126]. The mass flow rate of the injected natural gas inside the bed will therefore be controlled via two temperature measurements inside the fluidized bed as well as oxygen measurement from a gas analyzer located downstream of the reactor.

In order to prevent or minimize particle elutriation out of the reactor, a cyclone and a high pressure filter will be used in series inside the freeboard. The cyclone will remove most particles (~95 - 99%) and its efficiency will increase with increasing gas flow rate. On the other hand, the high-temperature filter will remove most of the smaller particles and fines. If clogging of the filters occurs, the fluidized bed reactor system will be shutdown (compressors, heating system, etc) and a manual backwash will be performed to clean the filters.

The exhaust gas will be purged via the existing gas manifold inside the lab, which operates at a slightly sub-atmospheric pressure with a fan and discharges onto the roof of the building.

Under high temperature and high pressure operation, water atomizing nozzles will be used to cool down the gas at the reactor outlet. Water injection will occur in a steam trap upstream of the valve controlling the reactor pressure. Downstream of this valve, the temperature will quickly drop to acceptable levels prior to reaching the fan.

Finally, in order to separate this quantity of water from the air, a detention or flash tank will be placed downstream of the reactor, where by lowering the gas pressure to atmospheric, condensation will occur. The gas outflow of the tank will be connected to the existing manifold that discharges to the atmosphere. An overview of the process can be seen in the process flow diagram below (Figure 40).

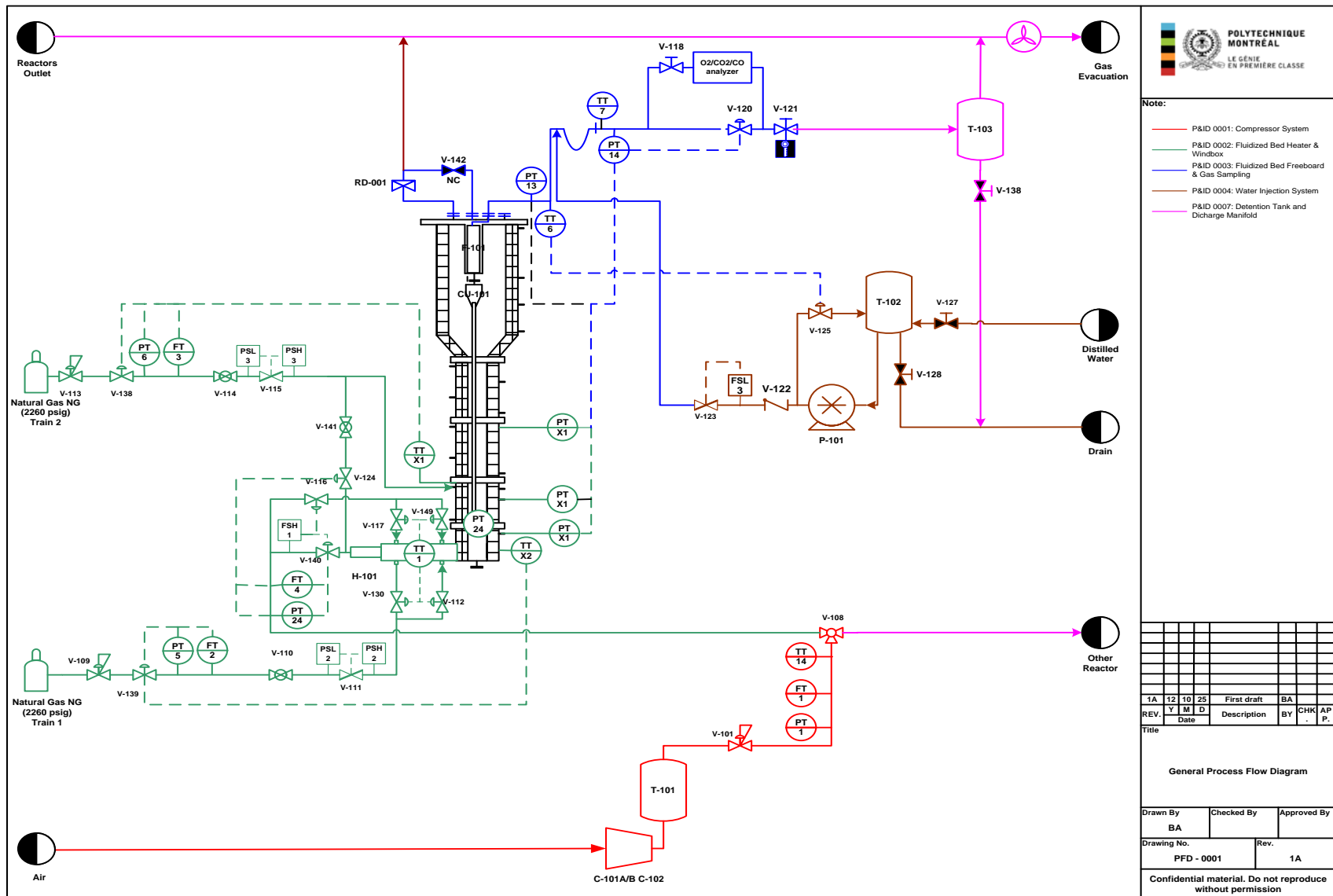


Figure 40- Process Flow Diagram

CHAPTER 5 FINAL REACTOR DESIGN AND PROCESS DESCRIPTION

In section 5.1, the final reactor design results will be presented and discussed. A detailed description of the process introduced in chapter 4 will be presented in section 5.2, followed by the reactor operating procedure in section 5.3.

5.1 Final Reactor Dimensions

5.1.1 Windbox final dimensions

For comparison purposes, the windbox height was taken as the same as that of the existent high temperature reactor currently in operation in the lab ($H_{\text{plenum}}=0.25\text{m}$). However, due to the restrictions presented earlier, this height had to be verified using the design equation in section 4.2.1. Having that combustion conversion increases with temperature and decreases with velocity, the natural gas combustion kinetics were used in order to determine methane conversion in the chosen windbox volume at a temperature of 800C (the lowest permissible combustion temperature according to NFPA 85 [126]) , a superficial gas velocity of 2m/s and different pressures. The purpose of this simulation is to verify whether the volume obtained using the chosen height is enough to achieve complete combustion using a CSTR model at the worst conditions. A summary of these findings is presented in table 23 below.

Table 23- Methane combustion conversion with respect to pressure

P(atm)	Methane Conversion (%)
1	99.996
10	99.957
20	99.952

Judging by the results, it is clear that the combustion reaction occurs to completion in the chosen volume.

Furthermore, with the gas introduced horizontally, the equation of Litz was also used to confirm the chosen dimensions. As we recall, this equation is used to compute the minimum necessary plenum height in order to ensure gas distribution. With a gas entry diameter of 0.051m (2inches), the equation of Litz resulted in a minimum windbox height of 0.085m which is largely inferior to the chosen 0.25m. This further confirms that the final windbox height obeys the gas distribution rule and provides complete natural gas combustion.

5.1.2 Distributor final dimensions

5.1.2.1 Holes final dimensions

As we recall from chapter 3, the first and upmost important variable is the pressure drop across the distributor, ΔP_d , which is defined for bubble cap as: $\frac{\Delta P_d}{\Delta P_b} \geq K$

Where $K = 0.01 + 0.2 \left[1 - \exp \left(\frac{-0.5D}{L_{mf}} \right) \right]$ and $\Delta P_b = g \times \rho_s \times L_{mf}(1 - \epsilon_{mf})$

With a minimum bed height, L_{mf} , of 1m, and sand particles with a density of 2560kg/m^3 , K was found to equal 0.024.

Currently a bubble cap distributor with 9 risers, each containing 4 holes, is being used in the existing high temperature fluidized bed reactor in our lab. For comparison purposes, the number of caps in our high temperature and pressure reactor was also taken as 9 with 4 holes each. Therefore, with K and N known d_h could be computed using the definition of ΔP_d

$$\Delta P_d = \left[\frac{4Q}{N\pi d_h^2 C_D} \right]^2 \left(\frac{\rho_g}{2} \right)$$

A first reflex might be to calculate d_h by ensuring that the lowest pressure drop ($T=1000\text{C}$, $P=1\text{atm}$, $U=0.1\text{m/s}$) is at least equal to K . Unfortunately, with ΔP_d proportional to the pressure, the square of the velocity, and inversely proportional to the temperature, this practice will result in an extremely large maximum pressure drop at a temperature of 25C , a pressure of 20atm and a superficial gas velocity of 2m/s . With a maximum allowable pressure drop of only 6atm throughout the reactor due to the compressor restrictions, it is clear that a single distributor plate might not be able to cover all of the suggested operation range. Accordingly, a Matlab program was constructed to provide the optimal design conditions that would cover the largest operation

range while respecting the aforementioned restrictions. Since the pressure drop across the cyclone is directly related to its design (section 5.1.3), it had to be incorporated in the Matlab program as well, in order to respect the maximum the pressure drop value of 6atm across the reactor. Using this simulation, d_h was calculated as 2.9mm and D_h as 8.72mm. In Appendix 6, a series of tables are provided, where the total pressure drop across the reactor for every temperature, pressure and velocity within the operation range is presented. The operating conditions, where $\Delta P_d/\Delta P_b$ falls under K, are highlighted in yellow in these tables.

5.1.2.2 Final bubble cap spacing and dimensions

As explained in section 4.2.2.2, geometric similarity was used in order to determine the hole height, B, illustrated in Figure 34. In order to determine the necessary distance between the bubble caps and the wall, the first step was to calculate the maximal horizontal jet length using the equation of Blake et al (1990). Based on this equation, jet length is highest at a pressure of 20atm, a velocity of 2m/s and a temperature of 25C and has a value of 0.054m. Unfortunately due to physical restrictions related to the chosen diameter of the reactor, such a distance could not be fulfilled and another solution had to be determined to avoid erosion of the refractory. In order to deal with this restriction, a tilt angle could be applied to ensure that the jet would not be indirect contact with the walls. Furthermore, by doing so, it is also possible to minimize stagnant zones during fluidization [127]. With the distributor currently in use in the lab having a tilt angle of 30°, this same angle was chosen for this design as illustrated in Figure 41 below.

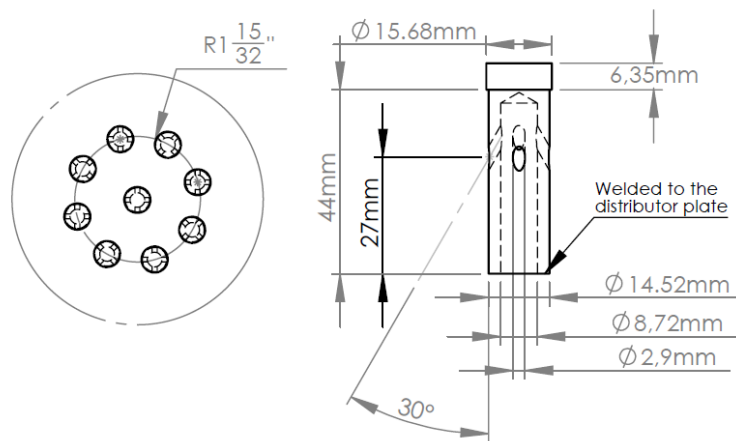


Figure 41- Final bubble cap dimensions

5.1.2.3 Final distributor thickness

As we recall in 4.2.2.2.2, the plate should be able to carry the weight of the solids, and handle the maximum pressure drop during operation. Using a minimum bed height of 1m and a maximum pressure drop of 5atm, the force due to the latter was found to be an order of magnitude higher than that due to the weight of the solids (9kN compared to 0.2kN). Using the force due to the highest pressure drop, different thicknesses were calculated and compared based on each of the methods presented in section 4.2.2.2.2 (shell and tube heat exchangers perforated plate method and the circular supported plate method). Using stainless steel as the material of construction, the values presented in table 24 were applied in both methods. Furthermore, Chen, Young and Uy (2006) [128] studied the behaviour of high strength structural steel at elevated temperatures and showed that at 900C, yield strength can be reduced by a factor of up to 91%. This factor was also incorporated in our calculations.

Table 24- Stainless steel properties

Material of construction Stainless steel	
Poissons ratio ν	0.305
Yield strength	502MPa
Yield strength at 900C	45MPa

Using the shell and tube heat exchangers perforated plate method and the circular supported plate method yielded thicknesses of 2 cm and 1cm respectively. For safety purposes, the largest value was selected. With an additional 20% safety factor, a final plate thickness of 1inch (2.54cm) was chosen. A schematic of the distributor were provided by our technician can be seen in Appendix 1.

5.1.3 Cyclone and filter final dimensions

As mentioned in section 4.2.3, a cyclone and a filter will be placed in series in order to efficiently cover the whole particle size range. After contacting several filter companies, the best option for an operating temperature of 1000C is the Fecralloy Metal Fiber filter which can provide 100% separation efficiency at 6 μ m. This filter has an outside diameter of 4.7 inch, a total length of 39 inch and a maximum pressure drop of 1psi over the superficial velocity range of 0.1 to 2m/s.

As far as the cyclone is concerned, the entrained mass flux was computed for both sand and FCC particles using the entrainment model of Choi presented in Chapter 3. As we recall, based on this correlation, entrainment was found to increase with gas velocity and pressure and decrease with temperature. Moreover, for safety purposes, the bubble size correlation of Cai et al (1994) introduced in that same chapter was used due to its application at high velocity and pressure. Accordingly, the highest and lowest mass flux values of sand and FCC are therefore presented in table 25.

With these values known, the equations in section 4.2.3.1 were used to design the cyclone. In order to achieve the highest separation efficiency, model (1) in table 20 was chosen. Furthermore, with a maximum allowable pressure drop of 6atm across the reactor, a Matlab program was constructed to provide the optimal cyclone design. However, since the pressure drop across the distributor is directly related to its design (section 5.1.2), the latter had to be incorporated in the Matlab program as well in order to respect the aforementioned pressure drop restrictions.

Finally, using the computed cyclone dimensions presented in Figure 42 below, the collection efficiency was calculated and is also presented in table 25.

As mentioned earlier, in Appendix 6, a series of tables are provided for the pressure drop across the reactor for every temperature, pressure and velocity within the operation range. Once more, the operating conditions, where $\Delta P_d/\Delta P_b$ falls under K, are highlighted in these tables.

Table 25- Cyclone simulation results

Temperature (C)	Pressure (atm)	Velocity (m/s)	Solid Type	Particle density (kg/m ³)	Average particle size (μm)	Mass flux (kg/m ² s)	Collection Efficiency (%)
25	20	2	FCC	1450	60	4.1 e-1	98.4
1000	1	0.1	FCC	1450	60	~0	95.2
25	20	2	Sand	2560	300	1.9e-1	99.73
1000	1	0.1	Sand	2560	300	~0	99.2

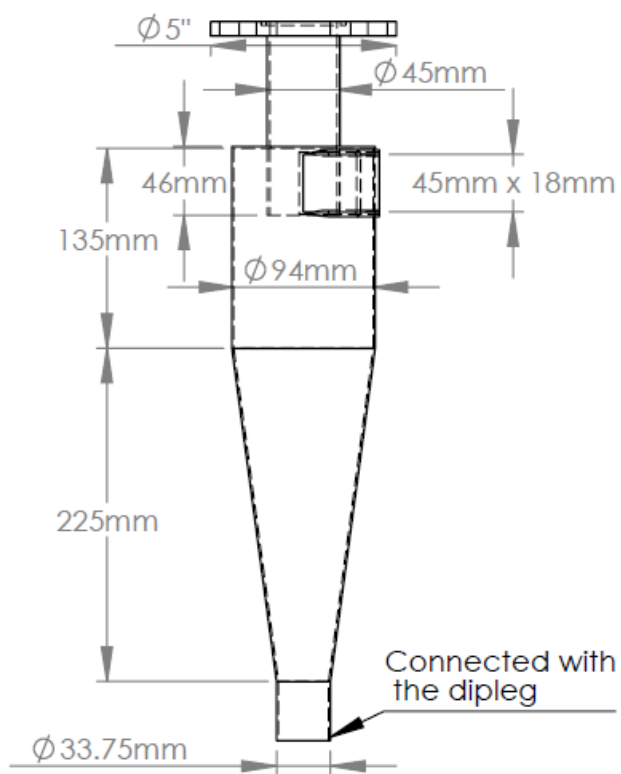


Figure 42- Final cyclone dimensions

5.1.4 Reactor shell and refractory final dimensions

Carbon steel was chosen as the reactor shell material of construction with all relevant design variables stated in table 26 below. The thickness of the reactor metal shell was computed based on the restrictions by the American Society of Mechanical Engineers (ASME) presented in table 21. For safety reasons, a design pressure of 30atm was used. Furthermore, the ASME also dictates that under elevated pressures, carbon steel temperature must not exceed 260C, and therefore the material properties were taken under this condition.

In order to ensure that this temperature is never reached at the wall, an insulation layer must be applied. With the high temperature fluidized bed currently in use in the lab being operated at up to 1000C, the same three refractory layers were chosen for this reactor due to their proven reliability. They are respectively: Kricon30, Kawool700 and Dynaguard Microporous insulation (table 27). A Matlab program was constructed to find the optimum and cheapest combination of these insulation layers to prevent the reactor wall temperature from reaching 260C. The final results are listed in table 27 below. In order to design for the worst possible case, temperature was assumed to only vary in the axial direction, and a 20% safety factor was used ($T=1200C$). Furthermore, the temperature at the inner wall was taken as the operating temperature. A full schematic of the reactor was provided by the university's technician and is presented in Appendix 1.

Table 26- Carbon steel properties

Material of construction	Stainless steel
Poissons ratio ν	0.29
Modulus of elasticity, E	202GPa
Modulus of elasticity, E at 260C	194GPa
Yield strength	207MPa
Yield strength at 260C	197MPa

Table 27- Reactor wall and refractory thickness simulation results

Layer	Thermal (W/m.K)	Conductivity	Thickness(m)	Temperature (C)
Kricon30	3.317		0.057	1170
Kawool 700	0.1		0.051	532
Dynaguard insulation	Microporous 0.027		0.011	111
Carbon Steel	33		0.02	111

5.1.5 Heating system final dimensions

The high pressure heating system comprises of an insulated pipe where an electric heater capable of withstanding low gas flowrates will be used until the auto-ignition temperature of natural gas is achieved. At this point natural gas will be fed to the pipe along with compressed air. The chosen electric heater has a diameter of 2inches and is capable of providing 900C at 30atm and 11SCFM. Similarly to the reactor shell, the outer wall temperature of the heating element must be lower than 260C. However, due to the size of the windbox on which the heater will be attached horizontally, the chosen insulation thickness must be as small as possible. Furthermore, similarly to the reactor, the shell was designed according to the ASME specification listed in table 21 and the metal properties in table 26. In order to comply with these criteria, two layers of refractory were chosen: BTU-block and Rescicast 8 (table 28). A Matlab program was constructed to find the optimum and cheapest combination of these insulation layers to prevent the reactor wall temperature from reaching 260C while limiting the total thickness to 6inch. The final results are listed in table 28. In order to account for the worst possible case, the design temperature was taken as 1200C at the inner wall and was once again assumed to only vary in the axial direction.

Table 28- Heating system wall and refractory thickness simulation results

Layer	Thermal Conductivity (W/m.K)	Thickness(m)	Temperature (C)
Rescicast 8	0.51	0.025	1063
BTU-Block	0.04	0.023	104
Carbon Steel	33	0.013	104

With the insulation chosen, the next step was to determine the length of the heating system. Since methane was proven to undergo complete combustion in the windbox (section 5.1.2.3), the main design criteria of the heating system length is the flame size.

Using the equation presented in section 4.2.5, a Matlab program was constructed to compute the maximum flame temperature while taken into consideration heat loss across the refractory layers.

The resulting maximum flame length was calculated as 0.73m at atmospheric pressure, a gas superficial velocity of 2m/s inside the reactor, and a stoichiometric air-fuel ratio of 16.8.

Finally, in order to allow flexible temperature control, several injection ports were placed along the heating pipe. The final dimensions of the heating system are presented in Appendix 2. Once again the schematics were provided by the university's technician.

5.2 Detailed Process Description

After conducting a Hazard and Operability study (HAZOP), piping and instrumentation diagrams were constructed for this reactor and are located in Appendix 3. The process description is divided into several parts, each referring to one of the P&IDs. A list of all stream lines, valves, transmitters and equipments is located in Appendix 4 along with their specifications.

For a more general process summary, please refer back to section 4.3.

5.2.1 P&ID0001: Compressor System

The first P&ID is the compressor system which will be used to achieve the required high pressure. In this system, 3 reciprocating compressors, C-101/C-102/C-103, are each equipped with a sound level silencer to reduce the noise level to 68 dB(A). Air flows out of the compressors through a high pressure filter F-101 to ensure that gas is lube and oil free before being fed to the tank T-101. To ensure that the pressure limits are respected, T-101 is equipped with a pressure switch high PSH 1 and a pressure switch low PSL 1. In case of an uncontrolled pressure increase, T-101 is also equipped with a pressure relief valve, V-102. Downstream of T-101, the pressure is regulated using the pressure regulator V-101 on stream 300 CS 001. This valve will be set to a fixed discharge pressure of 30 barg. Downstream of this valve, the pressure, temperature and flow will be monitored respectively by the transmitters TT14, PT4 and FT1. An oil water separator S-101 is located on the drain stream downstream of the compressors and the tank T-101 in order to ensure that water can be disposed of safely. Stream 300 CS 001 is divided in two streams (300 CS 003 toward the fluidized bed reactor and 300 CS 002 towards another

system) using a 3 way valve V-108. 300 CS 003 is connected to the high-pressure heating system H-101 which is attached to the windbox of the fluidized bed reactor.

5.2.2 P&ID0002: Fluidized Bed Heater and Windbox

The second P&ID comprises of the fluidized bed heater and windbox. In this diagram, two natural gas trains can be observed. Train 1 (300 CS 004) provides natural gas from a pressurized cylinder (2260 psig). The pressure downstream of this cylinder is controlled via a pressure regulator V-109 while the flow is regulated by a solenoid valve V-139.

A sequence of valves are located on stream 300 CS 004 as recommended by NFPA 85 for safety: A ball valves V-110 is placed for manual control of the natural gas flow and a safety shut-off valves (V-111), controlled by a pressure switch low and a pressure switch high, is also present in order to automatically shut-off the gas when pressure is outside the acceptable limits. A venting line (300 CS 028) is located downstream of V-109 to prevent backflow towards the natural gas cylinders. An automated valve V-146 is located on 300 CS 028 and will be switched on whenever the natural gas flow is off.

The train of natural gas (train1) is fed to the heating system H-101 along with the compressed air from the compressors (300 CS 003). This heating system comprises of an insulated pipe where a high pressure electric heater EH-101 is attached. EH-101 is only capable of withstanding low flowrates and will be used to preheat the pipe until the auto-ignition temperature of natural gas is achieved as recommended by NFPA 85. At this point, temperature transmitters (TT1, TT2, TT3) and a temperature switch (TSL1) will automatically control the flow of natural gas by adjusting the solenoid valve V-139 to achieve the desired temperature in the windbox. Furthermore, due to the existence of a maximal flowrate that EH-101 can withstand, the flow across EH-101 is fixed by a flow switch FSH1 which controls a solenoid valve V-140. When a higher flow is required, this switch will open the solenoid valve V-116 which will enable air to be introduced through ports on H-101. V-140 will also be used to regulate the flow inside the reactor. This valve will be controlled by the PLC based on the pressure drop recorded by several pressure, temperature and flow transmitters (TT14, PT4, FT1, TT3, TT2, PT7, PT8, PT9, PT10, PT11, PT12, PT13, PT14).

In order to avoid having a very high flame temperature, a temperature switch TSH1 along with the temperature transmitter TT1, turns on the solenoid valves V-117, V-149, V-130 and V-112 to

dilute the flame temperature. If the temperature inside H-101 is however still higher than 1200C (the heating system is designed to withstand up to 1400C), a temperature switch TSH2 will automatically close V-111, therefore shutting off the natural gas feed. On another hand, to avoid decreasing the temperature below the auto-ignition of natural gas, the temperature switch TSL1, will open V-139 to increase the flow of natural gas.

As mentioned in the general process description in section 4.3, in order to reach fluidized bed temperatures of 900°C to 1000°C, natural gas will be injected (non-premixed injection) and burned directly inside the reactor. This injection will only be performed when the bed temperature is equal to or above 800°C as recommended by NFPA 85. In order to be introduced inside the fluidized bed, natural gas will be fed from the second natural gas train (300 CS 006), which is provided from a second pressurized cylinder (2260 psig). The pressure downstream of the cylinder is automatically adjusted with a gas regulator V-113. Based on the desired temperature of the bed, temperature transmitters along the reactor (TT4, TT5) will control the flow of natural gas out of the solenoid valve V-138. When the bed temperature is below the threshold value of 800°C, the different temperature transmitters will send a signal to the automated valve (V-138) to stop the flow of natural gas to the bed.

Prior to reaching the reactor, a sequence of valves is located on stream 300 CS 006 to allow safe operation as recommended by NFPA 85. A ball valve V-114 is used for manual control over the natural gas flow a safety shut-off valves (V-115), controlled by a pressure switch low and a pressure switch high, is also present in order to automatically shut-off the gas when the pressure is outside the acceptable limits. A venting line (300 CS 029) is located downstream of V-113 to prevent backflow towards the natural gas cylinders, while an automated valve V-147 is located on 300 CS 029 and will be switched on whenever the natural gas flow is off.

When natural gas is not injected in the bed, a flow of compressed air (300 CS 025) will be continuously fed in order to prevent any solid particles from blocking the gas entry. The flow of compressed air will be adjusted by a pressure transmitter PT24 and a flow transmitter FT4 that will control a solenoid valve V-124. The temperature transmitters (TT2, TT3, TT4 and TT5) along the reactor will also serve as monitors in order to detect any damages that may occur to the refractory.

5.2.3 P&ID0003: Fluidized Bed Freeboard and Gas Sampling

In order to ensure that particles are not elutriated out of the reactor and into the vent, a cyclone CU-101, followed by a high pressure filter F-101 in a small chamber, are used in series inside the freeboard region.

Four lines are connected to the outlet of the fluidized bed reactor: a solid feed line and 3 outlet streams:

- a. Stream 300 CS 027.
- b. Stream 300 CS 008.
- c. Stream 300 CS 007.

Stream 300 CS 027 is the main gas exit stream where the main pressure control valve V-120 is located. This solenoid valve will be used to control the pressure inside the reactor and will be adjusted by several pressure transmitters (PT7, PT8, PT9, PT10, PT11, PT12 across the reactor, PT13 on 300 CS 027 prior to water injection and PT14 after water injection).

When the reactor is operated at high temperature and pressure, distilled water will be pumped out of pressurized tank and fed to a water atomizing nozzles in stream 300 CS 027. With V-120 able to withstand a maximum of 300C, injection of water will be done in order to reduce the gas temperature. In order to avoid blocking the lines in case of gas saturation, water injection will be performed in a U-shaped steam trap.

In order to control the hot gas temperature, a valve, V-148, is located on the water injection line 300 CS 011. If the temperature is however still high after water injection, a temperature switch high will automatically shut off the natural gas flow by closing V-139 on train1 and V-138 on train2.

A gas analyzer will be placed prior to V-120 to allow gas sampling, gas analysis and control of natural gas injection in the fluidized bed.

Stream 300 CS 007 contains a rupture disk RD-101 which will open in case of an uncontrolled pressure increase above a specific threshold. In this case, the opening of RD-101 will produce a complete decompression of the system and a complete and safe disposal to the atmosphere. In case of a mal function with the auto decompression, a panic button can be manually activated. Valve V-142 located on 300 CS 008 will then open automatically to decompress the reactor.

Finally, in order to allow safe operation of the reactor, a manual valve V-121 equipped with a lock is located on line 300 CS 010 downstream of the reactor to ensure that only one reactor in the laboratory is operational at a time.

5.2.4 P&ID0004: Water Injection System

As mentioned in the previous section, in order to reduce the temperature prior to reaching V-120 (P&ID0003) water will be directly injected into the gas stream. Aiming to achieve a temperature of 250C, the required amount of cooling water was plotted versus pressure in Figure 43 in order to determine the necessary pump flowrate.

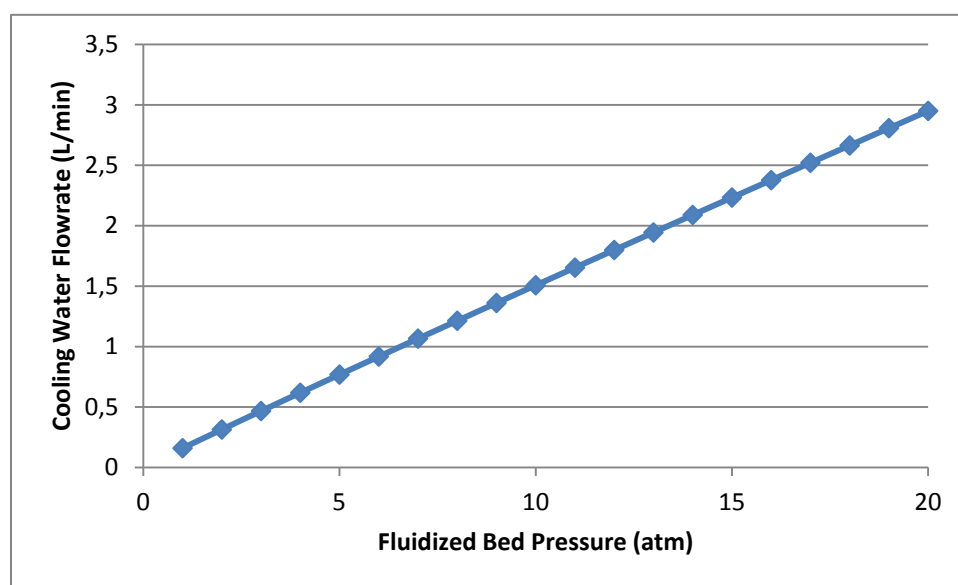


Figure 43- System pressure as a function of the required Amount of Cooling Water to reduce the gas temperature from 1000 to 250C

With a maximum required flow of 3.5L/min, a pump, P-101, with a capacity of 10L/min, will be used to inject distilled water at the reactor gas discharge form a pressurized Tank T-102. This tank will be manually filled prior to operation.

The water flow into the atomizing nozzles will be controlled by an automated 3-way valve V-126 on line 300 CS 012. This valve separates 300 CS 012 to 300 CS 011 toward the fluidized bed reactor discharge and 300 CS 015 toward another system. This valve can be turned on or off by the temperature transmitter TT6 at the fluidized bed outlet (300 CS 027, P&ID 0003).

In order to control the amount of pumped water into the fluidized bed outlet, TT6 also acts on a solenoid valve V-125 which controls a recycle stream 300 CS 013 back to T-102. The lower the temperature of the gas at the reactor outlet, the higher the water recycle will be.

In order to prevent pressurized hot gas from flowing towards the pump P-101 in case of a malfunction, a check valve (V-122) is located on stream 300 CS 012 downstream of the pump.

A solenoid valve V-123 is also located on stream 300 CS 012 and will be controlled by a flow switch low FSL1 in case of a malfunction with the pump or in case the tank is empty. FSL1 will also prevent the return of hot gas toward the pump.

5.2.5 P&ID0005: Detention Tank and Discharge Manifold

Due to the high exhaust gas temperatures and injection of water, steam will be present in the fluidized bed reactor exhaust gas. To separate this steam from the air prior to disposal in the gas manifold, stream 300 CS 010 is connected to a detention tank (flash tank) (T-103). At this tank the gas pressure is lowered to atmospheric and water condenses. T-103 has a drain with a manual valve V-138.

Downstream of T-103, the gas line 150 CS 023 will be connected to the existing manifold 150 SS 024 that discharges to the atmosphere via a fan. Gas temperature will quickly drop to acceptable levels prior to reaching the fan.

5.3 Operating Procedure

The following is a procedure that will be followed when operating the fluidized bed reactor under high temperature and pressure.

5.3.1 Operating Procedure

- 1- Perform an inspection of the fluidized bed reactor:
 - a. Check that the fluidized bed reactor system is OFF:
 - i. The compressors are OFF.
 - ii. The natural gas lines are closed.
 - iii. The water injection line is closed.
 - b. Install all probes and diagnostic systems for the experiments.

- c. Start the computer and acquisition systems.
 - d. Make sure that the temperature and pressure readings are realistic.
 - e. Inspect the fluidized bed reactor and make sure there are no open ports, flanges or connection.
 - f. Close all open ports, flanges and connections.
- 2- Manually backwash the filter using Ecole Polytechnique's sharp air through the designated backwash port on the top flange. Disconnect the ports from Ecole Polytechnique's sharp air.
 - 3- Open the drain valve at the bottom of the windbox to empty the windbox of solids. Close the drain valve.
 - 4- Start the compressors.
 - 5- Inject a small flow of air inside the fluidized bed reactor ($U_g = 0.4 \text{ m/s}$) at ambient temperature and ambient pressure (over the fluidized bed region). Note that the gas velocity and pressure are controlled by pressure regulator V-101 and valves V-140 and V-120.
 - 6- Wait for 7 minutes to make sure that the reactor is completely purged of natural gas.
 - 7- Check that the temperature and pressure readings are acceptable.
 - 8- Use SNOOP to check for leaks on the ports, flanges and connections.
 - 9- Inject the solid particles inside the reactor through the port on the top flange.
 - 10- Verify from the pressure readings that the bed is fluidized.
 - 11- Specify in the control computer the target operating conditions:
 - a. Superficial gas velocity (U_g)
 - b. Fluidized bed temperature (T_{BED})
 - c. Fluidized bed pressure (P_{BED})
 - 12- The control system adjusts the superficial gas velocity to the target value and to a maximum of 11 SCFM ($U_g = 0.3 \text{ m/s}$ @ 20°C & 1 atm).
 - 13- If the target fluidized bed temperature is $\leq 800^\circ\text{C}$, go to step 14
- If the target fluidized bed temperature is $> 800^\circ\text{C}$, go to step 19

5.3.2 Reactor heating at ambient pressure ($T_{BED} \leq 800^{\circ}\text{C}$)

- 14- If the desired bed temperature is above ambient values, the electrical heater (H-101) connected to the hybrid heating system will be initiated. This heater can increase the air temperature up to 900°C for a flowrate of up to 11 SCFM ($U_g = 0.3 \text{ m/s}$ @ 20°C & 1 atm). The system will await the fluidized bed reactor to reach steady state.
- 15- If the bed temperature is not sufficiently high, natural gas is injected in the hybrid heating system. The temperature at the outlet of H-101 and the first natural gas injection location must be above 800°C (an interlock on the thermocouples prevents natural gas injection if this condition is not satisfied). Note that a maximum natural gas flow rate is set by the control system based on two criteria:
- (1) the local temperature in the hybrid heating system must remain below 1200°C (if this criterion is reached, the control system will open V-117 and V-149).
 - (2) the mass flow rate of air and natural gas (10% excess air minimum).

The system will await the fluidized bed reactor to reach steady state.

- 16- If the bed temperature has been reached, go to step 21.
- 17- If the bed temperature has not been reached and the target U_g is higher than 11 SCFM, the control system will open valve V-117 and V-149 to inject more air inside the hybrid heating system in order to reach the desired U_g . With additional air, additional natural gas can be injected through valve V-112. The system will await the fluidized bed reactor to reach steady state.
- 18- If the bed temperature has been reached, go to step 21.

5.3.3 REACTOR HEATING AT AMBIENT PRESSURE ($800^{\circ}\text{C} < T_{BED} \leq 1000^{\circ}\text{C}$)

- 19- Follow steps 14 to 17.
- 20- Once the fluidized bed temperature has reached 800°C (or higher), the control system will initiate natural gas injection in the fluidized bed. The flow of natural gas to the hybrid burner is turned off and the flow of natural gas to the fluidized bed is adjusted to obtain the target temperature. The system will await the fluidized bed reactor to reach steady state.

5.3.4 INCREASING THE PRESSURE

- 21- Once the target fluidized bed temperature and superficial gas temperature have been reached, the control system gradually (in increment) increases the pressure. Valves V-140 and V-120 are used to increase the pressure while maintaining the superficial gas velocity constant. The flow rate of natural is adjusted to keep the temperature constant. The system will await the fluidized bed reactor to reach steady state.
- 22- Once the target pressure, temperature and superficial gas velocity have been reached, experiments can start.

5.3.5 REACTOR SHUTDOWN

- 23- The control system is set to “reactor shutdown”. Natural gas injection is stopped. The pressure over the fluidized bed is slowly decreased to ambient and the gas velocity is lowered ($U_g = 0.1$ m/s at operating temperature) to limit the decrease in temperature and maximize the life of the refractory. The system will await the fluidized bed reactor to reach steady state.
- 24- Once the reactor has reached ambient temperature (it should already be at ambient pressure), shutdown the compressors.
- 25- Perform an inspection of the fluidized bed reactor:
- a. Check that the fluidized bed reactor system is OFF:
 - i. The compressors are OFF.
 - ii. The natural gas lines are closed.
 - iii. The water injection line is closed.
 - b. Uninstall all probes and diagnostic systems for the experiments.
- 26- Clean the lab space.

CHAPTER 6 CONCLUSION AND RECOMMENDATIONS

6.1 Conclusion

This study provided important information and data to better understand the importance of developing a high pressure and temperature fluidized bed reactor. The attainments and conclusions of this thesis were compliant with the objectives described in Chapter 1 and are as follows.

Objective 1: Study and Conduct a background study on fluidized bed technology and its application in industry as well as the different fluidization regimes.

Conclusion 1: In Chapter 2, some of the most important fluidization properties and definitions were introduced. By presenting the different fluidization regimes and the effects of particle size and density, a better understanding of the chosen operating conditions for our reactor was generated. Furthermore, the section on solid mixing and entrainment helped build the necessary background information for the design of the cyclone in Chapter 4 and the impact of temperature and pressure in Chapter 3. Finally, in Chapter 2, some of the applications of high temperature and pressure in fluidization were introduced in order to highlight the relevance and importance of this work to the industrial sector.

Objective 2: Study and Conduct a full literature review on fluidization in order to illustrate the fundamental design variables, their respective correlations at extreme conditions and their limitations.

Conclusion 2: This objective was completed throughout Chapter 2 and 3. In Chapter 2, a full literature review on fluidization was provided. In Chapter 3, the effect of using extreme operating conditions (high temperature, pressure and velocity) on fluidization and more specifically bubble size was demonstrated. In this section, three bubble size correlations were chosen: the first for being respectively modeled at high pressure and velocity, the second for being modeled at high temperature and the third for being one of the most commonly used correlations in design books. Subsequently, the impact of bubble size on mass transfer, reaction conversion, entrainment and the transport disengaging height (TDH) were studied through the application of each of the aforementioned models. By doing so, the limitations of these correlations along with others were

highlighted, and the need of developing new models and a better understanding of fluidization under high temperature, pressure and velocity was demonstrated.

Objective 3: Design the fluidized bed reactor and its utilities, for flexible operation from ambient conditions up to high temperature and high pressure based on design books and papers.

Conclusion 3: In Chapter 4, the complete and detailed design procedure of a fluidized bed reactor at high temperature and pressure was presented. In this chapter, the different reactor parts were introduced along with their respective design correlations. The design procedure of several utilities such as the gas distributor, the cyclone and the heating system were also treated in this Chapter. Furthermore, the design of the high pressure heating system has lead to remarkable reductions in costs and can prove to be beneficial for future purposes. In Chapter 5, the results of were presented and discussed. This Chapter dealt with multiple limitations and restrictions such as the distributor pressure drop and the metal surface temperature.

Objective 4: Design a complete control process and operating procedure that would allow safe operation of this reactor.

Conclusion 4: After conducting a Hazard and Operability study (HAZOP), a complete control process was designed in Chapter 5 along with its respective procedure piping and instrumentation diagrams in Appendix 3. A safe operating procedure was also developed for the reactor and is explained in this Chapter. Furthermore, multiple safety procedures from pressure relief valves to water pumps to cool down the gas are presented and discussed in the detailed process description section of this same Chapter. A second HAZOP was performed to ensure that all relevant changes have been made.

6.2 Recommendations

In this work, the need of developing new fluidization models under extreme condition was demonstrated in Chapter 3, along with the design procedure and results of a fluidized bed reactor and its operating process in Chapters 4 and 5 respectively. Despite achieving the objective of this thesis, several difficulties and constraints were encountered and multiple recommendations have been reported throughout.

In Chapter 3, due to the limited scope of this work, the impact of several variables such as reactor diameter and bed height were not considered in the simulations and should be studied under high temperature and pressure. Moreover, due to the limited available experimental data, this Chapter only dealt with the effects of pressure or temperature and never both at the same time. With this reactor in place, a more detailed study on the combined effects of pressure and temperature would be greatly beneficial and is therefore recommended. In addition, several key correlations were studied in this section with their limitations highlighted. Due to the different observed trends in mass transfer, reaction conversion and bubble diameter, developing a bubble size correlation that would cover larger operation ranges is fundamental for future applications. Furthermore, with none of the existing TDH models in design books providing acceptable results and suggesting very large freeboard sections at high velocities despite a very small change in entrainment, more suitable correlations must be developed. Another recommendation can be made when studying the conversion of methane under pressure where curious trends were observed. These results suggest that more work needs to be done under these conditions in addition to the development of new hydrodynamic models where more acceptable values could be obtained.

Finally, in Chapter 4, when designing the gas distributor, the model of Quershi and Creasy[105] was used to estimate the minimum required pressure drop necessary to sustain even fluidization in the bed. Since this correlation was developed under ambient conditions, verification of its results will be important when operating this reactor. In case a higher value is obtained, another distributor must be designed to ensure more flexibility and freedom of operation.

REFERENCES

- [1] D. Kunii and O. Levenspiel, *Fluidization Engineering*: Butterworth-Heinemann, 1991.
- [2] G. X. Yue, H. R. Yang, J. F. Lu, and H. Zhang, "Latest Development of CFB Boilers in China Proceedings of the 20th International Conference on Fluidized Bed Combustion," G. Yue, Zhang Hai Zhao, Changsui Luo, Zhongyang, Ed., ed: Springer Berlin Heidelberg, 2010, pp. 3-12.
- [3] J. Yates, "Effect of Temperature and Pressure," in *Handbook of Fluidization and Fluid-Particle Systems*, ed: CRC Press, 2003.
- [4] J. Li and J. A. M. Kuipers, "Effect of pressure on gas–solid flow behavior in dense gas-fluidized beds: a discrete particle simulation study," *Powder Technology*, vol. 127, pp. 173-184, 2002.
- [5] M. Pell, "GAS FLUIDIZATION HANDBOOK OF POWDER TECHNOLOGY, VOL. 8," *Drying Technology*, vol. 10, pp. 805-805, 1992/06/01 1992.
- [6] H. Ernst-Ulrich and W. Joachim, "Elutriation and Entrainment," in *Handbook of Fluidization and Fluid-Particle Systems*, ed: CRC Press, 2003.
- [7] K. Tannous, M. W. Donida, and L. A. Obata, "Entrainment of Heterogeneous Particles from Gas-Fluidized Bed," *Particulate Science and Technology*, vol. 26, pp. 222-234.
- [8] T. Baron, C. L. Briens, and M. A. Bergounou, "Study of the transport disengaging height," *The Canadian Journal of Chemical Engineering*, vol. 66, pp. 749-760, 1988.
- [9] D. Geldart, *Gas Fluidization Technology*: U.M.I.
- [10] H.-P. Wan and C.-S. Chyang, "Transport Disengaging Height and Elutriation Rate of a Vortexing Fluidized Bed," *Journal of Chemical Engineering of Japan*, vol. 31, pp. 977-986, 1998.
- [11] E. K. Levy, H. S. Caram, J. C. Dille, and S. Edelstein, "Mechanisms for solids ejection from gas-fluidized beds," *AIChE Journal*, vol. 29, pp. 383-388, 1983.
- [12] M. Y. Large JF, Bergounou MA., "Interpretative model for entrainment in a large gas fluidized bed," presented at the International Powder Bulk Solids Handling and Processing Conference, Chicago, 1976.
- [13] C. T. Crowe, *Multiphase Flow Handbook*: CRC PressINC, 2006.
- [14] S. E. Charles Churchman, "The Effects of Increased Pressure on the Reaction Kinetics of Biomass Pyrolysis And Combustion," presented at the TAPPI Conference, Marietta, Georgia, 2009.
- [15] F. C. Brown, H. G. Hargreaves, and F. Society, *Coal Gasification - Routes to Ammonia and Methanol*: Alembic House, 1979.

- [16] S. T. Sie and R. Krishna, "Fundamentals and selection of advanced Fischer–Tropsch reactors," *Applied Catalysis A: General*, vol. 186, pp. 55-70, 1999.
- [17] C. H. Bartholomew and R. J. Farrauto, *Fundamentals of Industrial Catalytic Processes*: Wiley, 2011.
- [18] A. Pinto, "Ammonia Production Process," England Patent, 1978.
- [19] P. J. A. Tijm, F. J. Waller, and D. M. Brown, "Methanol technology developments for the new millennium," *Applied Catalysis A: General*, vol. 221, pp. 275-282, 2001.
- [20] K. J. Wolf, W. Willenborg, C. Fricke, A. Prikhodovsky, K. Hilpert, and L. Singheiser, *Studies of Alkali Sorption Kinetics for Pressurized Fluidized Bed Combustion by High Pressure Mass Spectrometry*, 2002.
- [21] A. L. ORTIZ, D. P. HARRISON, F. R. GROVES, J. D. WHITE, S. ZHANG, W.-N. HUANG, and Y. ZENG, "ADVANCED SULFUR CONTROL CONCEPTS FOR HOT-GAS DESULFURIZATION TECHNOLOGY," DE-AC21-94MC30012--18; Other: ON: DE00007129 United States10.2172/7129Other: ON: DE00007129Mon Feb 04 15:13:40 EST 2008NETL; PA: EDB-99:077222English, 1998.
- [22] D. E. Rosner, "High-Temperature Gas-Solid Reactions," *Annual Review of Materials Science*, vol. 2, pp. 573-606, 1972/08/01 1972.
- [23] I. H. Chan, C. Sishla, and T. M. Knowlton, "The effect of pressure on bubble parameters in gas-fluidized beds," *Powder Technology*, vol. 53, pp. 217-235, 1987.
- [24] K. S. Lim, J. X. Zhu, and J. R. Grace, "Hydrodynamics of gas-solid fluidization," *International Journal of Multiphase Flow*, vol. 21, Supplement, pp. 141-193, 1995.
- [25] J. S. M. Botterill and M. Desai, "Limiting factors in gas-fluidized bed heat transfer," *Powder Technology*, vol. 6, pp. 231-238, 1972.
- [26] H. W. Piepers, E. J. E. Cottaar, A. H. M. Verkooijen, and K. Rietema, "Effects of pressure and type of gas on particle-particle interaction and the consequences for gas—solid fluidization behaviour," *Powder Technology*, vol. 37, pp. 55-70, 1984.
- [27] D. F. King, F. R. G. Mitchell, and D. Harrison, "Dense phase viscosities of fluidised beds at elevated pressures," *Powder Technology*, vol. 28, pp. 55-58, 1981.
- [28] S. Alavi, N. Joffin, M. Vérelst, and B. Caussat, "Crystallization of microscopic Y2O3 powders by different techniques of fluidization at high temperature," *Chemical Engineering Journal*, vol. 125, pp. 25-33, 2006.
- [29] H. Cui, P. Sauriol, and J. Chaouki, "High temperature fluidized bed reactor: measurements, hydrodynamics and simulation," *Chemical Engineering Science*, vol. 58, pp. 1071-1077, 2003.
- [30] B. Formisani, R. Girimonte, and L. Mancuso, "Analysis of the fluidization process of particle beds at high temperature," *Chemical Engineering Science*, vol. 53, pp. 951-961, 1998.

- [31] P. Lettieri, J. G. Yates, and D. Newton, "The influence of interparticle forces on the fluidization behaviour of some industrial materials at high temperature," *Powder Technology*, vol. 110, pp. 117-127, 2000.
- [32] S. Sanaei, N. Mostoufi, R. Radmanesh, R. Sotudeh-Gharebagh, C. Guy, and J. Chaouki, "Hydrodynamic characteristics of gas–solid fluidization at high temperature," *The Canadian Journal of Chemical Engineering*, vol. 88, pp. 1-11, 2010.
- [33] M. Horio and A. Nonaka, "A generalized bubble diameter correlation for gas-solid fluidized beds," *AIChE Journal*, vol. 33, pp. 1865-1872, 1987.
- [34] C. R. Subzwari MP, Pyle DL., "Bubbling behaviour of fluidized beds at elevated pressures," *Fluidization (JF Davidson, DL Kearns, eds.)*. Cambridge University Press, pp. 50–54, 1978.
- [35] V. T. a. G. I. R., *Fluidization (Edited by Davidson J. F. and Keairns D. L.)*, Cambridge University Press, Cambridge, p. 55, 1978.
- [36] P. U. F. P.N. Rowe, A.C. Hoffman and J.G. Yates, in *D. Kunii and R. Toei (eds.)*, *Fluidization Engineering Foundation*, Tokyo, pp. 53-60, 1984.
- [37] C. S. Cai P, Jin Y, Yu ZQ, Wang ZW, "Effect of operating temperature and pressure on the transition from bubbling to turbulent fluidization.," *AIChE Symp Ser*, vol. 85, pp. 37–43, 1989.
- [38] P. N. R. a. H. J. MacGillivray, *Inst. Energy Symp. Ser.*, vol. 4, p. 1, 1980.
- [39] A. W. Weimer and G. J. Quarderer, "On dense phase voidage and bubble size in high pressure fluidized beds of fine powders," *AIChE Journal*, vol. 31, pp. 1019-1028, 1985.
- [40] K. M. Sellakumar and V. Zakkay, "Bubble Characterization in Pressurized Fluidized-Bed Combustors with Bed Internals," *Combustion Science and Technology*, vol. 60, pp. 359-374, 1988/08/01 1988.
- [41] S. Tone, H. Seko, H. Maruyama, and T. Otake, "CATALYTIC CRACKING OF METHYLCYCLOHEXANE OVER SILICA ALUMINA CATALYST IN GAS FLUIDIZED BED," *Journal of Chemical Engineering of Japan*, vol. 7, pp. 44-51, 1974.
- [42] D. Geldart and D. S. Kapoor, "Bubble sizes in a fluidized bed at elevated temperatures," *Chemical Engineering Science*, vol. 31, pp. 842-843, 1976.
- [43] M. C. Zhang, Walsh, P.M., Beer, J.M, " Proc. 7th Int. Conference on Fluidized Bed Combustion," Philadelphia, 1982, p. 75/75.
- [44] M. N. SANAEI SHABNAM, RADMANESH RAMIN,SOTUDEH GHAREBAGH RAHMAT,CHAOUKI JAMAL, "HYDRODYNAMICS OF A GAS-SOLID FLUIDIZED BED AT ELEVATED TEMPERATURES USING THE RADIOACTIVE PARTICLE TRACKING TECHNIQUE," *IRANIAN JOURNAL OF CHEMISTRY AND CHEMICAL ENGINEERING (IJCCE)*, vol. 31, pp. 65-70, 2012.

- [45] P. Cai, M. Schiavetti, G. De Michele, G. C. Grazzini, and M. Miccio, "Quantitative estimation of bubble size in PFBC," *Powder Technology*, vol. 80, pp. 99-109, 1994.
- [46] P. E. G. Gogolek and J. R. Grace, "Fundamental hydrodynamics related to pressurized fluidized bed combustion," *Progress in Energy and Combustion Science*, vol. 21, pp. 419-451, 1995.
- [47] S. Mori and C. Y. Wen, "Estimation of bubble diameter in gaseous fluidized beds," *AIChE Journal*, vol. 21, pp. 109-115, 1975.
- [48] Y. Wen-Ching, "Bubbling Fluidized Beds," in *Handbook of Fluidization and Fluid-Particle Systems*, ed: CRC Press, 2003.
- [49] C. Y. Wen and Y. H. Yu, "A generalized method for predicting the minimum fluidization velocity," *AIChE Journal*, vol. 12, pp. 610-612, 1966.
- [50] R. Yamazaki, Asai, M., Nakajima, M., & Jimbo, G., "Characteristics of transition regime in a turbulent fluidized bed," in *Proceedings of the fourth China-Japan fluidization conference*, Beijing, 1991, pp. 720-725.
- [51] A. C. Hoffmann and J. G. Yates, "EXPERIMENTAL OBSERVATIONS OF FLUIDIZED BEDS AT ELEVATED PRESSURES," *Chemical Engineering Communications*, vol. 41, pp. 133-149, 1986/04/01 1986.
- [52] A. C. Rowe. BA Partridge, "The mechanisms of solid mixing in fluidized beds," *Trans. Inst. Chem. Eng.*, vol. 9, pp. 271-283, 1965.
- [53] J.-H. Choi, H.-J. Ryu, D.-W. Shun, J.-E. Son, and S.-D. Kim, "Temperature Effect on the Particle Entrainment Rate in a Gas Fluidized Bed," *Industrial & Engineering Chemistry Research*, vol. 37, pp. 1130-1135, 1998/03/01 1998.
- [54] G. D. Wouters IM., " Entrainment at high temperatures," *Fan L-S, Knowlton TM, eds. Fluidization IX. New York: Engineering Foundation*, pp. 341-348, 1998.
- [55] K. T. Chan IH, "The effect of system pressure on the transport disengaging height above bubbling fluidized beds," *AIChE Symp. Ser.*, vol. 80, pp. 24-33, 1984.
- [56] S. T. Pemberton and J. F. Davidson, "Turbulence in the freeboard of a gas-fluidised bed: The significance of ghost bubbles," *Chemical Engineering Science*, vol. 39, pp. 829-840, 1984.
- [57] J. G. Yates, "Effects of temperature and pressure on gas-solid fluidization," *Chemical Engineering Science*, vol. 51, pp. 167-205, 1996.
- [58] F. A. Zenz and N. A. Weil, "A theoretical-empirical approach to the mechanism of particle entrainment from fluidized beds," *AIChE Journal*, vol. 4, pp. 472-479, 1958.
- [59] J.-H. Choi, I.-Y. Chang, D.-W. Shun, C.-K. Yi, J.-E. Son, and S.-D. Kim, "Correlation on the Particle Entrainment Rate in Gas Fluidized Beds," *Industrial & Engineering Chemistry Research*, vol. 38, pp. 2491-2496, 1999/06/01 1999.

- [60] M. J. Rhodes and D. Geldart, "A model for the circulating fluidized bed," *Powder Technology*, vol. 53, pp. 155-162, 1987.
- [61] C. Y. Wen and L. H. Chen, "Fluidized bed freeboard phenomena: Entrainment and elutriation," *AIChE Journal*, vol. 28, pp. 117-128, 1982.
- [62] F. A. Zenz and D. F. Othmer, *Fluidization and fluid-particle systems*: Reinhold, 1960.
- [63] I. M. F. G. Wouters, D., "Entrainment at High Temperatures," in *Fluidization IX: proceedings of the Ninth Engineering Foundation Conference on Fluidization*, Durango, Colorado, 1998, p. p 341.
- [64] J.-H. Choi, S. D. Kim, and J. R. Grace, "Entrainment Rate of Coarse Particles at Different Temperatures in Gas Fluidized Beds," *The Canadian Journal of Chemical Engineering*, vol. 85, pp. 151-157, 2007.
- [65] A. B. Fournol, M. A. Bergougnou, and C. G. J. Baker, "Solids entrainment in a large gas fluidized bed," *The Canadian Journal of Chemical Engineering*, vol. 51, pp. 401-404, 1973.
- [66] M. Ściążko, J. Bandrowski, and J. Raczek, "On the entrainment of solid particles from a fluidized bed," *Powder Technology*, vol. 66, pp. 33-39, 1991.
- [67] M. T. Horio, A.; Hsieh, Y.S. and Muchi, I., *Fluidization*, 1980.
- [68] A. S. Fung and F. Hamdullahpur, "Effect of bubble coalescence on entrainment in gas fluidized beds," *Powder Technology*, vol. 77, pp. 251-265, 1993.
- [69] K. Smolders and J. Baeyens, "Elutriation of fines from gas fluidized beds: mechanisms of elutriation and effect of freeboard geometry," *Powder Technology*, vol. 92, pp. 35-46, 1997.
- [70] W. Wu and P. K. Agarwal, "The Effect of Bed Temperature on Mass Transfer between the Bubble and Emulsion Phases in a Fluidized Bed," *The Canadian Journal of Chemical Engineering*, vol. 81, pp. 940-948, 2003.
- [71] L. D. a. J. F. Richardson, " Gas interchange between bubbles and the continuous phase in a fluidized bed," *Trans. Inst. Chem. Eng*, vol. 44, pp. 1293-1305, 1966.
- [72] S. P. Sit and J. R. Grace, "Interphase mass transfer in an aggregative fluidized bed," *Chemical Engineering Science*, vol. 33, pp. 1115-1122, 1978.
- [73] S. P. Sit and J. R. Grace, "Effect of bubble interaction on interphase mass transfer in gas fluidized beds," *Chemical Engineering Science*, vol. 36, pp. 327-335, 1981.
- [74] E. R. Gilliland, "Fluidised particles, J. F. Davidson and D. Harrison, Cambridge University Press, New York (1963). 155 pages. \$6.50," *AIChE Journal*, vol. 10, pp. 783-785, 1964.
- [75] R. a. J. R. G. Clift, " Continuous Bubbling and Slugging," in *Fluidization*, R. C. a. D. H. J.F. Davidson, Ed., Second Edition ed London, UK: Academic Press, 1985, pp. 73–132.

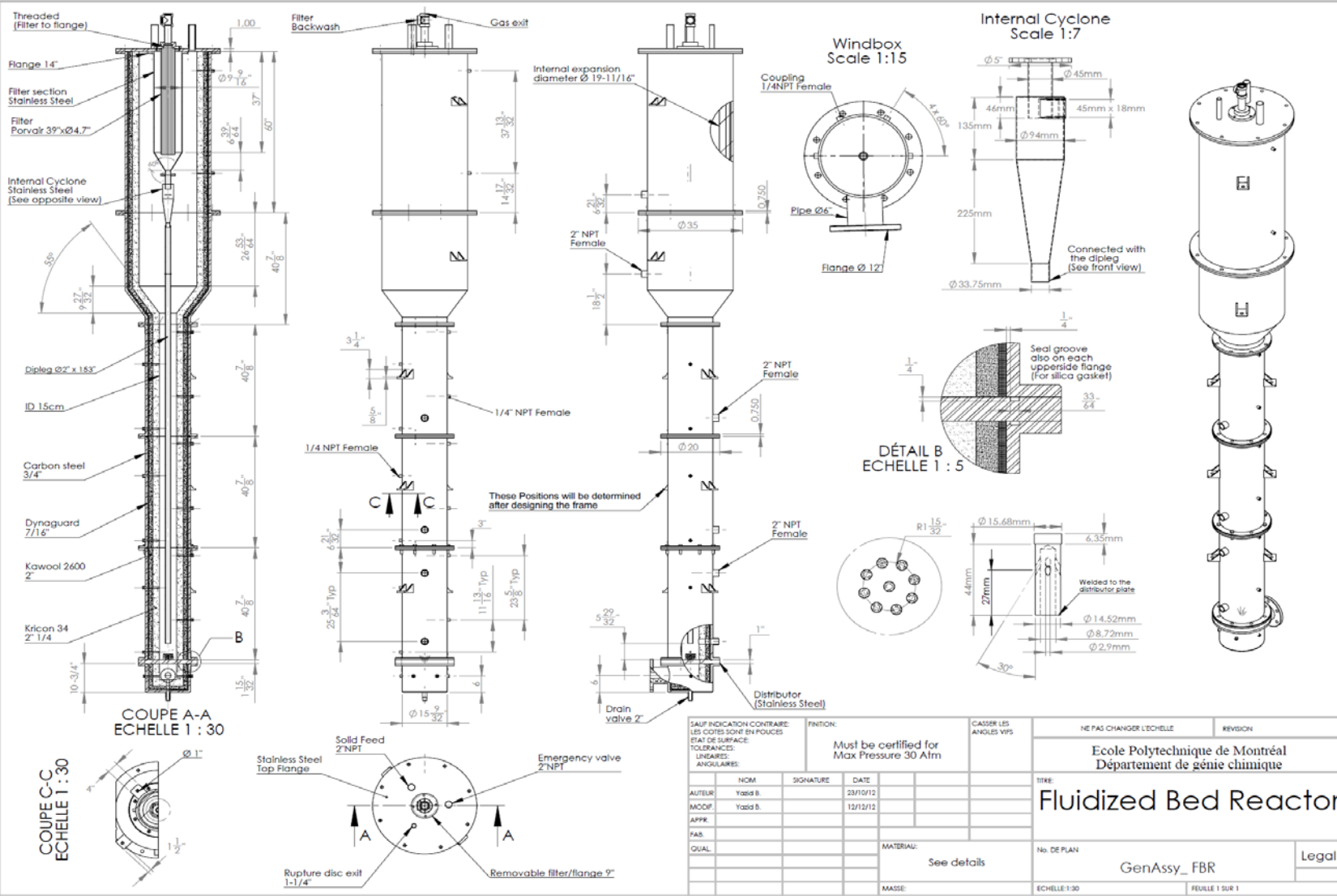
- [76] S. Furusaki, Y. Nozaki, and K. Nakagiri, "Mass transfer coefficients and amounts of direct-contact-catalyst in fluidized catalyst beds," *The Canadian Journal of Chemical Engineering*, vol. 62, pp. 610-616, 1984.
- [77] H. I. Farag, A. Grislingås, P. E. Ege, and H. I. De Lasa, "Flow patterns in a pilot plant-scale turbulent fluidized bed reactor: Concurrent application of tracers and fiber optic sensors," *The Canadian Journal of Chemical Engineering*, vol. 75, pp. 851-860, 1997.
- [78] T. Kai, T. Imamura, and T. Takahashi, "Hydrodynamic influences on mass transfer between bubble and emulsion phases in a fine particle fluidized bed," *Powder Technology*, vol. 83, pp. 105-110, 1995.
- [79] Y. Nozaki, Furusaki, S., & Miyauchi, T., "Determination of the parameters of a fluidized bed of fine catalyst particles by gas absorption," *International Chemical Engineering*, vol. 25, pp. 499-506, 1985.
- [80] H. T. Bi, N. Ellis, I. A. Abba, and J. R. Grace, "A state-of-the-art review of gas-solid turbulent fluidization," *Chemical Engineering Science*, vol. 55, pp. 4789-4825, 2000.
- [81] J. A. M. Kuipers, "Gas Dispersion and Bubble-to-Emulsion Phase Mass Exchange in a Gas-Solid Bubbling Fluidized Bed: A Computational and Experimental Study," *International Journal of Chemical Reactor Engineering*, vol. 1, 2003.
- [82] G. P. Sechenov, L. B. Rabinovich, and V. S. Al'tshuler, "Effect of pressure on mass transfer in heterogeneous chemical processes in a fluidized bed," *Journal of Engineering Physics and Thermophysics*, vol. 11, pp. 339-343, 1966.
- [83] J. Zhang, Z. Feng, X. Jia, S. Xu, W. Li, and M. Du, "Characteristics of a Pressurized Gas-Solid Magnetically Fluidized Bed," *Chemical Engineering & Technology*, vol. 36, pp. 241-250, 2013.
- [84] E. L. Cussler, *Diffusion: Mass Transfer in Fluid Systems*: Cambridge University Press, 1997.
- [85] Z. Zhiping, N. Yongjie, and L. Qinggang, "Effect of pressure on minimum fluidization velocity," *Journal of Thermal Science*, vol. 16, pp. 264-269, 2007/08/01 2007.
- [86] Z. T. A. Al-Sharify, "MATHEMATICAL MODELING OF MASS TRANSFER FROM AN IMMERSED BODY TO A FLUIDIZED GAS BED," *Al-Qadisiya Journal for Engineering Sciences*, vol. 3, pp. 192-212, 2010.
- [87] Jack. (2010, 2nd February). *The Coming World Oil Crisis*.
- [88] J. A. Liu, "Kinetics, catalysis and mechanism of methane steam reforming," Master of Science in Chemical Engineering, Chemical Engineering, WORCESTER POLYTECHNIC INSTITUTE, 2006.
- [89] G. C. a. F. Wheeler, " Hydrogen Production via Steam Reforming with CO2 Capture," *Chemical Engineering Transactions*, vol. 19, p. 37, 2010.
- [90] M. S. D. George W. Crabtree, and Michelle V. Buchanan, "The Hydrogen Economy," *Physics Today*, vol. 57, p. 39, 2004.

- [91] K. Hou and R. Hughes, "The kinetics of methane steam reforming over a Ni/ α -Al₂O₃ catalyst," *Chemical Engineering Journal*, vol. 82, pp. 311-328, 2001.
- [92] S. Roy, B. B. Pruden, A. M. Adris, J. R. Grace, and C. J. Lim, "Fluidized-bed steam methane reforming with oxygen input," *Chemical Engineering Science*, vol. 54, pp. 2095-2102, 1999.
- [93] A. M. Adris, C. J. Lim, and J. R. Grace, "The fluidized-bed membrane reactor for steam methane reforming: model verification and parametric study," *Chemical Engineering Science*, vol. 52, pp. 1609-1622, 1997.
- [94] T. Wurzel, S. Malcus, and L. Mleczko, "Reaction engineering investigations of CO₂ reforming in a fluidized-bed reactor," *Chemical Engineering Science*, vol. 55, pp. 3955-3966, 2000.
- [95] A. Yermakova, V. I. Anikeev, and A. S. Bobrin, "Kinetic model for the reaction of sulphur dioxide catalytic reduction to hydrogen sulphide," *Applied Catalysis A: General*, vol. 101, pp. 25-39, 1993.
- [96] N. Mostoufi, H. Cui, and J. Chaouki, "A Comparison of Two- and Single-Phase Models for Fluidized-Bed Reactors," *Industrial & Engineering Chemistry Research*, vol. 40, pp. 5526-5532, 2001/11/01 2001.
- [97] H. Cui, N. Mostoufi, and J. Chaouki, "Characterization of dynamic gas-solid distribution in fluidized beds," *Chemical Engineering Journal*, vol. 79, pp. 133-143, 2000.
- [98] "Fluid Bed Design Aspects," in *Fluid Bed Technology in Materials Processing*, ed: CRC Press, 1998.
- [99] W. C. Yang, "Fluidization, Solids Handling, and Processing - Industrial Applications," ed: William Andrew Publishing/Noyes, 1998.
- [100] Litz, "Design of gas distributors," *Chemical engineering*, vol. November 13, pp. 162-166, 1972.
- [101] H. Kage, N. Iwasaki, H. Yamaguchi, and Y. Matsuno, "Frequency Analysis of Pressure Fluctuation in Fluidized Bed Plenum," *Journal of Chemical Engineering of Japan*, vol. 24, pp. 76-81, 1991.
- [102] F. L. a. G. Dryer, I., "Proceedings of the 14th International Symposium on Combustion," Pennsylvania State University, 1981, p. 987.
- [103] S. R. Karri and W. Joachim, "Gas Distributor and Plenum Design in Fluidized Beds," in *Handbook of Fluidization and Fluid-Particle Systems*, ed: CRC Press, 2003.
- [104] "Air Distribution Grate," in *Combustion and Gasification in Fluidized Beds*. vol. null, ed: CRC Press, 2006, pp. 359-380.
- [105] A. E. Qureshi and D. E. Creasy, "Fluidised bed gas distributors," *Powder Technology*, vol. 22, pp. 113-119, 1979.

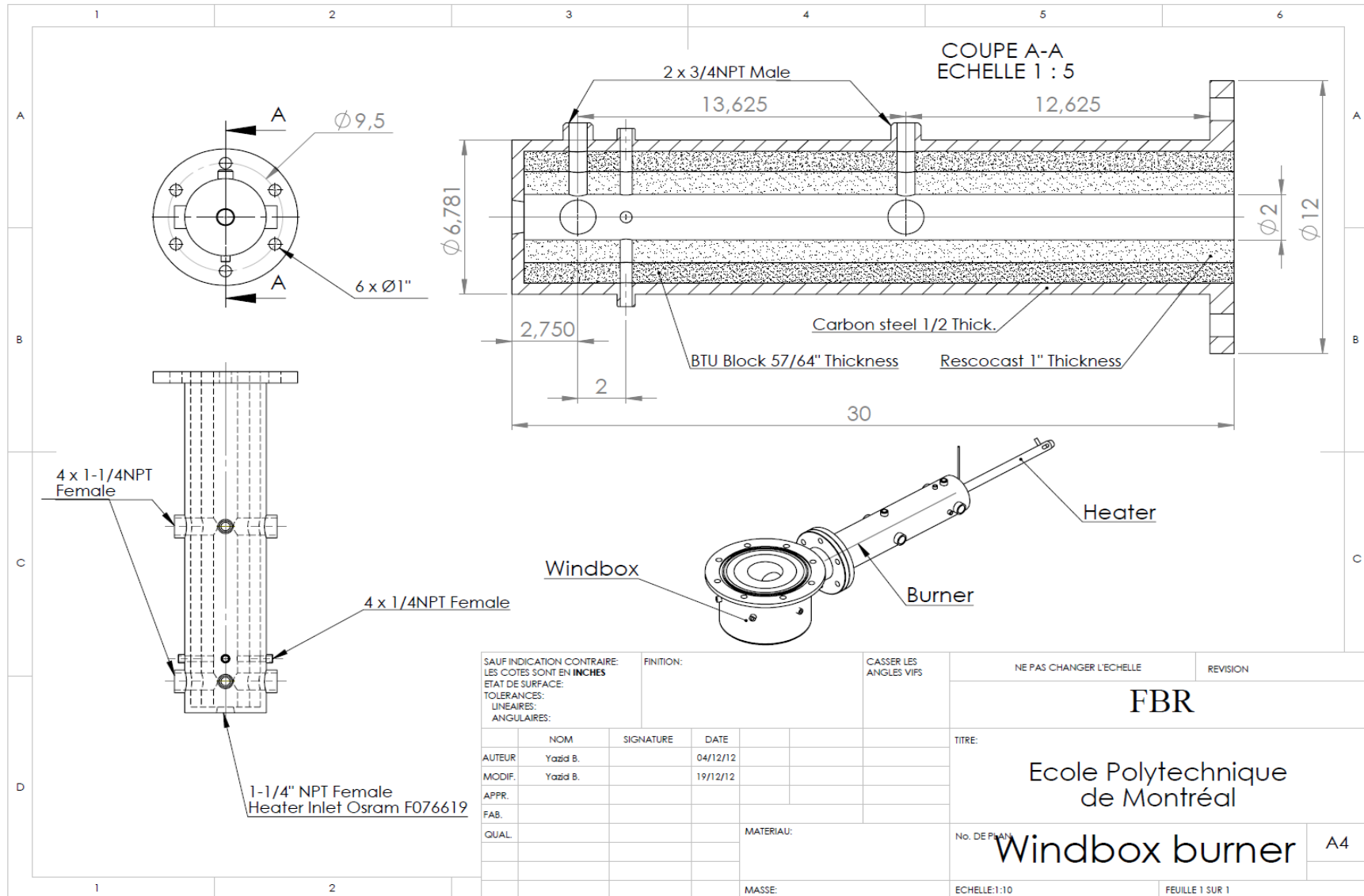
- [106] P. J. Sanderson, "Experimental verification of the simplest scaling laws for bubbling beds at large scales," Doctorate of Philosophy, Department of Chemical Engineering, Monash University, 2002.
- [107] K. SBR, *Grid Design Chapter*, 1991.
- [108] P. Sauriol, "Hydrodynamique des jets de gaz orientes vers le haut et vers le bas dans les lits fluidises gaz-solide," Doctor of Philosophy, Chemical Engineering, Ecole Polytechnique de Montreal,, 2011.
- [109] T. R. Blake, H. Webb, and P. B. Sunderland, "The nondimensionalization of equations describing fluidization with application to the correlation of jet penetration height," *Chemical Engineering Science*, vol. 45, pp. 365-371, 1990.
- [110] R. K. Sinnott, "Coulson and Richardson's Chemical Engineering Volume 6 - Chemical Engineering Design (4th Edition)," ed: Elsevier.
- [111] I. Tosun and M. S. Willis, "Drag stress—pressure drop relationship in filtration," *Chemical Engineering Science*, vol. 38, pp. 485-487, 1983.
- [112] T. Knowlton, "Cyclone Separators," in *Handbook of Fluidization and Fluid-Particle Systems*. vol. null, ed: CRC Press, 2003.
- [113] J. Chen and M. Shi, "A universal model to calculate cyclone pressure drop," *Powder Technology*, vol. 171, pp. 184-191, 2007.
- [114] X. Wang, "Biomass fast pyrolysis in fluidized bed : product cleaning by in-situ filtration," Doctor of Philosophy, Twente University, Enschede, Netherlands, 2006.
- [115] C. L. Briens, M. A. Bergougnou, and T. Baron, "Reduction of particle entrainment from gas-fluidized beds. Prediction of the effect of disengagement zones," *Powder Technology*, vol. 62, pp. 135-138, 1990.
- [116] S. M. Tasirin and D. Geldart, "ENTRAINMENT OF FINES FROM FLUIDIZED BEDS WITH AN EXPANDED FREEBOARD," *Chemical Engineering Communications*, vol. 166, pp. 217-230, 1998/01/01 1998.
- [117] C. D. Cooper and F. C. Alley, *Air pollution control: a design approach*: Waveland Press, 2002.
- [118] R. H. Perry and D. W. Green, "Perry's Chemical Engineers' Handbook (7th Edition)," ed: McGraw-Hill, 1997.
- [119] D. Leith and D. Mehta, "Cyclone performance and design," *Atmospheric Environment (1967)*, vol. 7, pp. 527-549, 1973.
- [120] C. B. Shepherd and C. E. Lapple, "Flow Pattern and Pressure Drop in Cyclone Dust Collectors Cyclone without Intel Vane," *Industrial & Engineering Chemistry*, vol. 32, pp. 1246-1248, 1940/09/01 1940.
- [121] R. L. M. e. al, "Improving hot gas filtration behaviour in PFBC power plants," in *The 15th International conference on fluidised bed combustion*, Savannah, Georgia, USA, 1999.

- [122] A. P. Baskakov, V. N. Dolgov, and Y. M. Goldobin, "Aerodynamics and heat transfer in cyclones with particle-laden gas flow," *Experimental Thermal and Fluid Science*, vol. 3, pp. 597-602, 1990.
- [123] *Section VIII-Division 1: Rules for Construction of Pressure Vessels Companion Guide to the ASME Boiler and Pressure Vessel Code, Volume 2, Third Edition*: ASME Press, 2009.
- [124] M. R. J. Charest, J. E. D. Gauthier, and X. Huang, "Design of a Lean Premixed Prevaporized Can Combustor," *ASME Conference Proceedings*, vol. 2006, pp. 781-791, 2006.
- [125] T. R. Blake and J. B. Coté, "Mass entrainment, momentum flux, and length of buoyant turbulent gas diffusion flames," *Combustion and Flame*, vol. 117, pp. 589-599, 1999.
- [126] N. F. P. Association, *NFPA 85: Boiler and Combustion Systems Hazards Code, 2007 Edition*: NationalFireProtectionAssoc.
- [127] P. C. Josephkunju, "Influence of Angle of Air Injection and Particles in Bed Hydrodynamics of Swirling Fluidized Bed," Doctor of Philosophy, Mechanical Engineering, Cochin University of Science & Technology, Kochi, Kerala, India, 2008.
- [128] J. Chen, B. Young, and B. Uy, "Behavior of High Strength Structural Steel at Elevated Temperatures," *Journal of Structural Engineering*, vol. 132, pp. 1948-1954, 2006/12/01 2006.

Appendix1: Reactor, Cyclone and Distributor Schematics



Appendix2: Heating System Schematic



C-101/A

Piston Compressor

Pressure rating: 435 Psi
Power/Voltage: 20HP/575V
Inductance/Frequency: 3PH/50HZ
Capacity: 1020 l/min
Soundproof cabinet: 68 dB(A)
Anti-vibration pads: UPH-9700

C-101/B

Piston Compressor

Pressure rating: 435 Psi
Power/Voltage: 20HP/575V
Inductance/Frequency: 3PH/50HZ
Capacity: 1020 l/min
Soundproof cabinet: 68 dB(A)
Anti-vibration pads: UPH-9700

C-102

Piston Compressor

Pressure rating: 435 Psi
Power/Voltage: 7.5HP/575V
Inductance/Frequency: 3PH/50HZ
Capacity: 384.6 l/min
Soundproof cabinet: 68 dB(A)
Anti-vibration pads: UPH-9700

F-101

High Pressure Filter

Pressure rating: 725 Psi
Filter rating: 0.01Micron
Housing Material: Aluminum

S-101

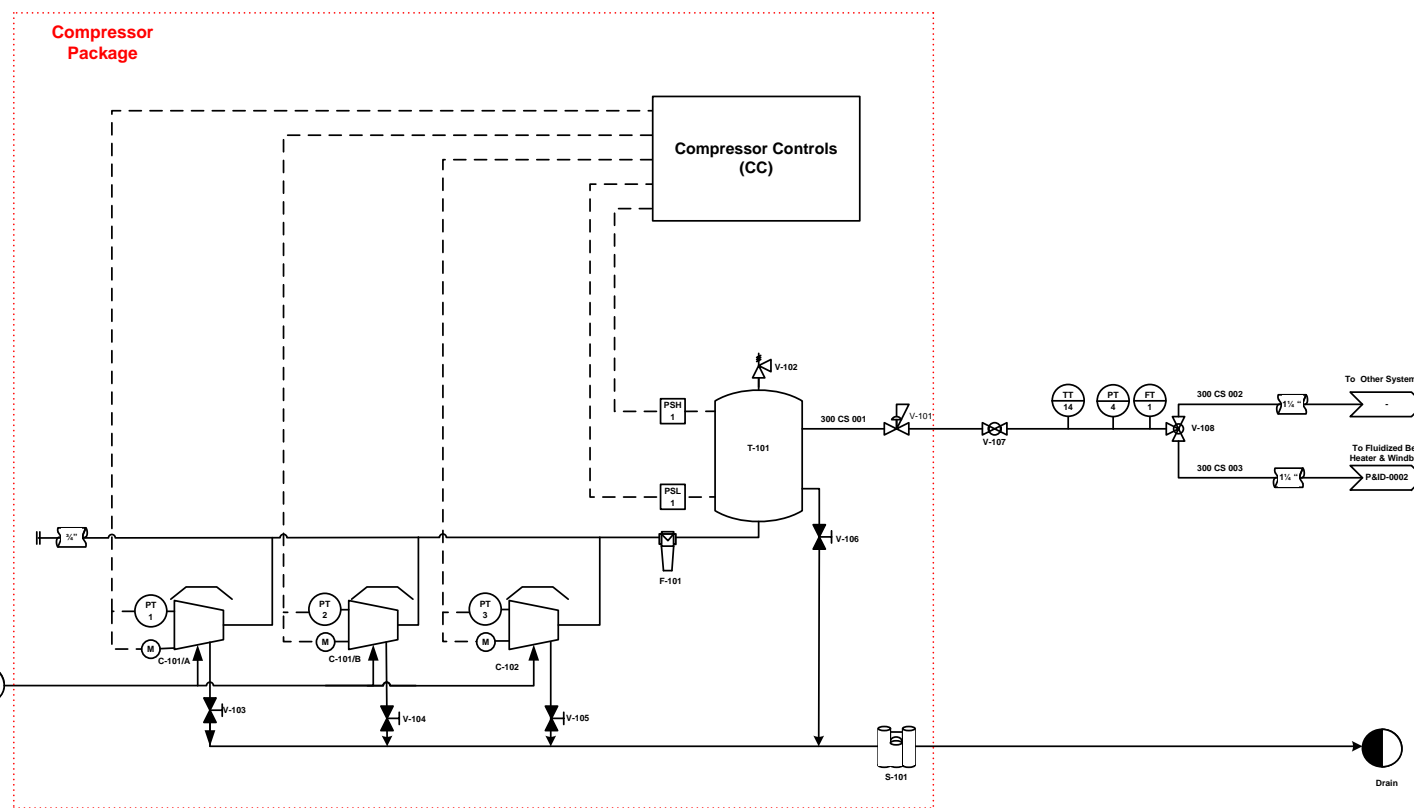
Oil Water Separator

Capacity: 65l/s (at cold)
Oil Conten: <15mg/l

T-101

High Pressure Tank

Volume: 400 gallons
Pressure rating: 500 Psi
Material: SA455



Note:

[illegible]

Compressor System

Drawn By BA	Checked By	Approved By
-----------------------	------------	-------------

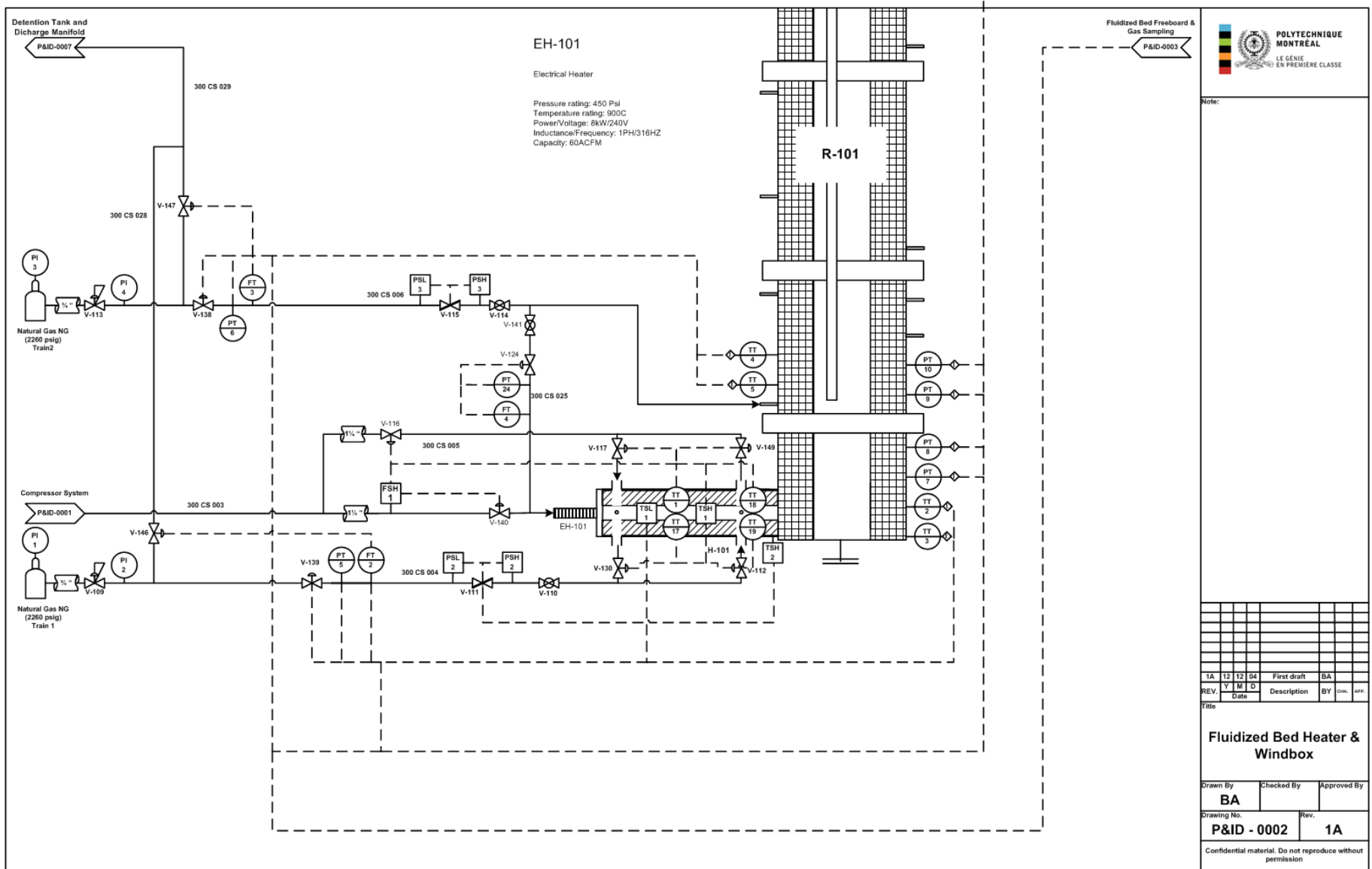
Drawing No.

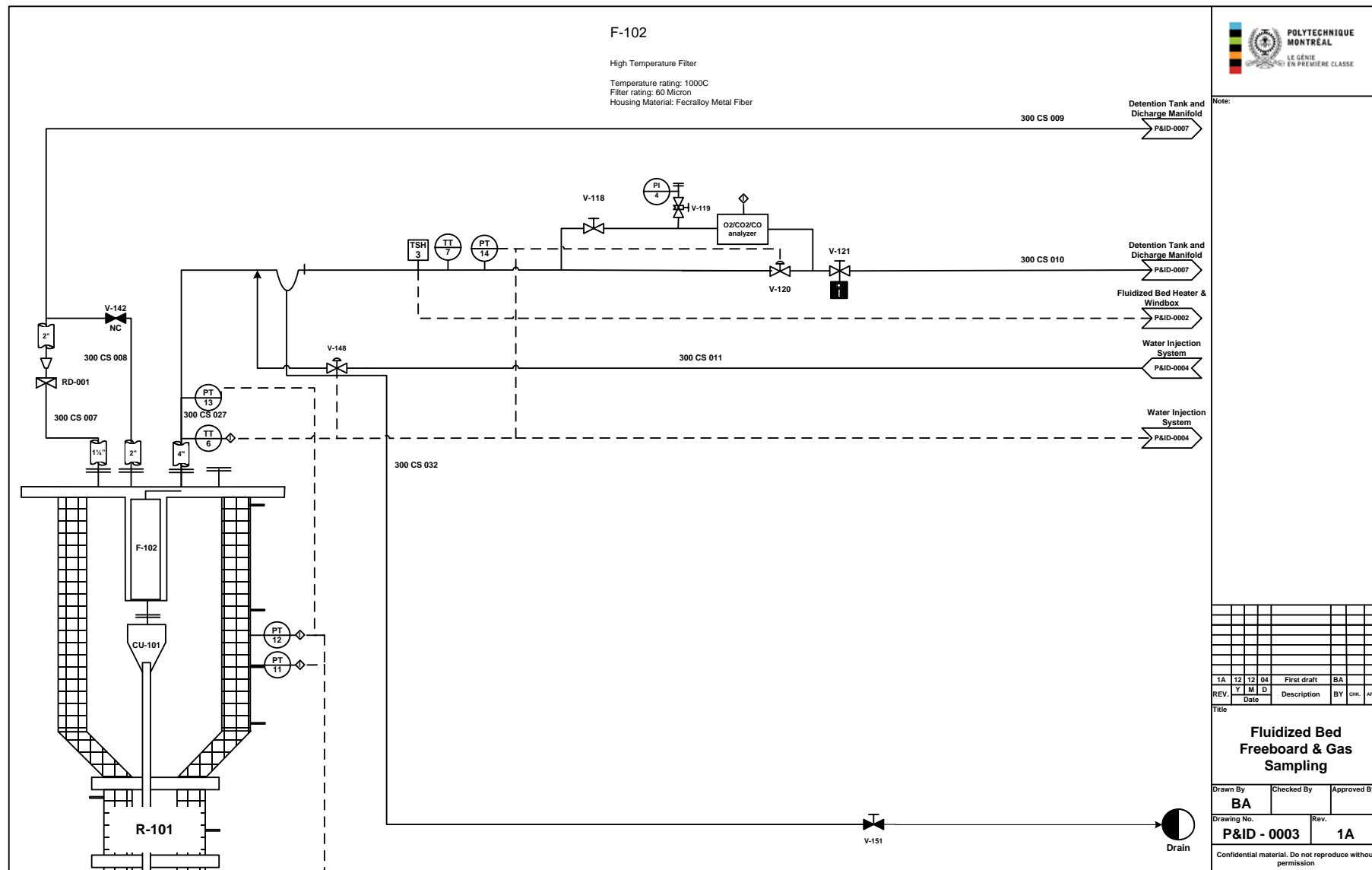
P&ID - 0001

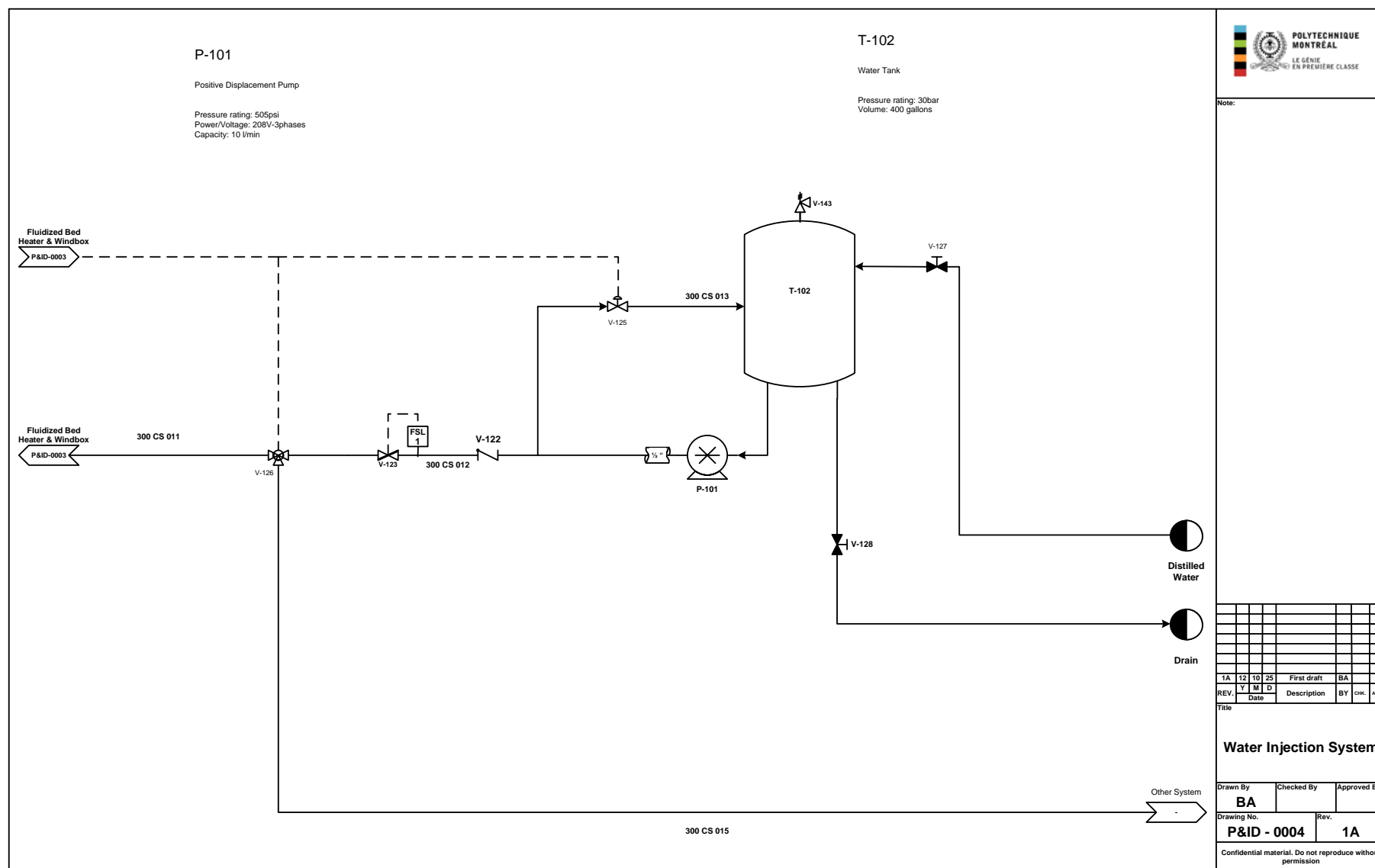
Rev.

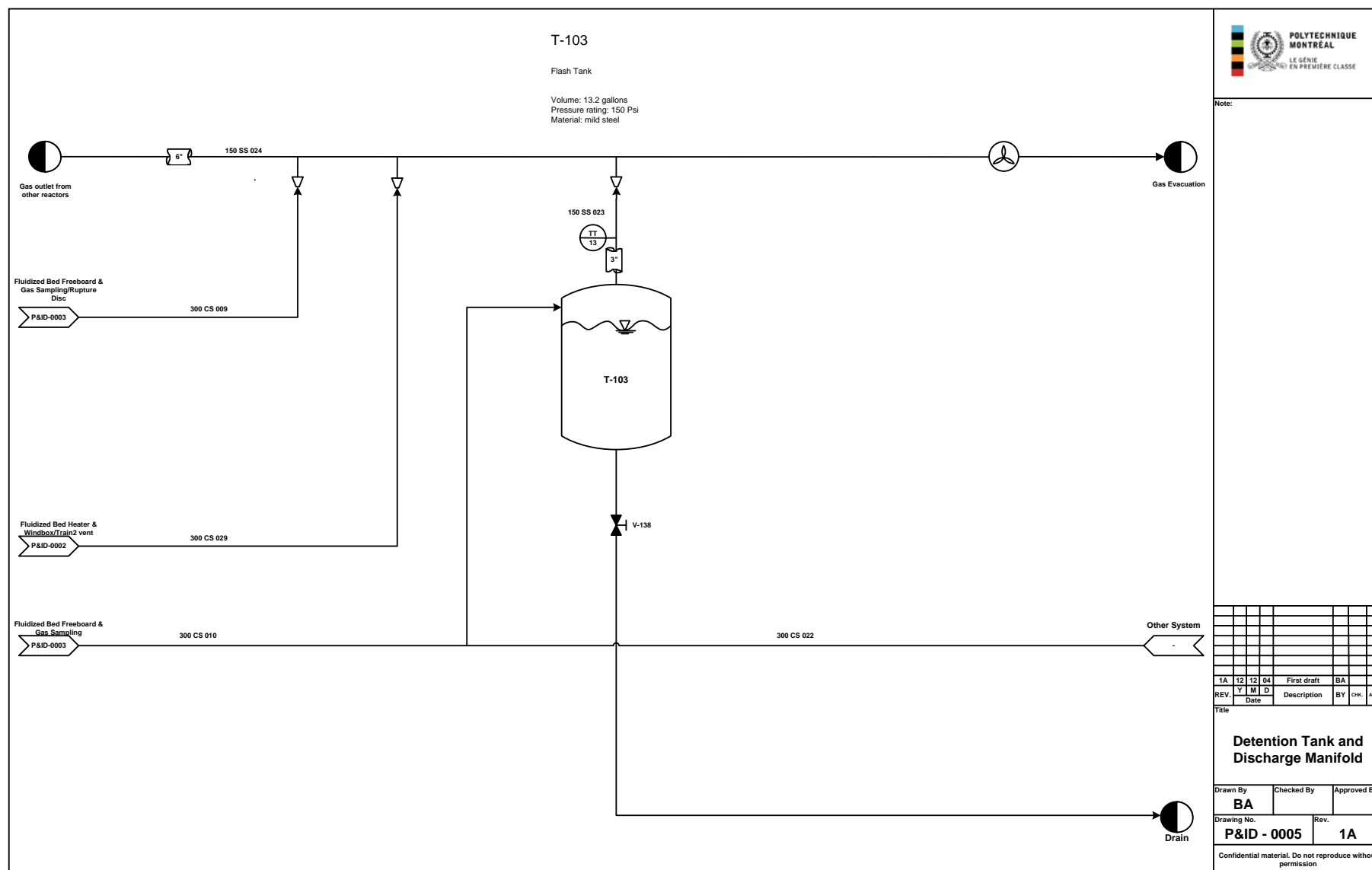
1A


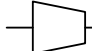



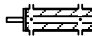






Confidential material. Do not reproduce without permission









LINES		CONTROL NOMENCLATURE				EQUIPMENT		<div><div>POLYTECHNIQUE MONTREAL LE GÉNIE EN PREMIÈRE CLASSE</div></div> <div>Note:</div>																						
<div><div><div></div><div></div><div></div></div><div>Flow</div></div> <div><div><div></div><div></div><div></div></div><div>Electrical Signal</div></div> <div><div><div></div><div></div><div></div></div><div>Flange Joint Or Connection</div></div>		<div>Letter</div>	<div>1st position</div>	<div>2nd position</div>	<div>3rd position</div>	<div></div> <div>Compressor</div>	<div></div> <div>Oil Water Separator</div>																							
PIPING		<div><div><div></div><div></div><div></div></div><div>Reducer</div></div> <div><div><div></div><div></div><div></div></div><div>Blind Flange</div></div>		<div>P</div> <div>T</div> <div>F</div> <div>I</div> <div>S</div> <div>L</div> <div>H</div> <div>A</div>	<div>Pressure</div> <div>Temperature</div> <div>Flow</div> <div>Indicator</div> <div></div> <div>Level</div> <div></div> <div></div>	<div></div> <div>Transmitter</div> <div></div> <div></div> <div>Switch</div> <div></div> <div></div> <div>Alarm</div>	<div></div> <div></div> <div></div> <div></div> <div></div> <div></div> <div></div> <div></div>	<div></div> <div>High Pressure Filter</div>																						
VALVES AND RUPTURE DISK		<div><div><div></div><div></div><div></div></div><div>Check Valve</div></div> <div><div><div></div><div></div><div></div></div><div>Solenoid Valve</div></div> <div><div><div></div><div></div><div></div></div><div>Rotary Valve</div></div> <div><div><div></div><div></div><div></div></div><div>Ball Valve</div></div> <div><div><div></div><div></div><div></div></div><div>3-Way Valve</div></div> <div><div><div></div><div></div><div></div></div><div>4-Way Valve</div></div> <div><div><div></div><div></div><div></div></div><div>Rupture Disc</div></div> <div><div><div></div><div></div><div></div></div><div>Butterfly Valve</div></div> <div><div><div></div><div></div><div></div></div><div>Sampling Valve</div></div> <div><div><div></div><div></div><div></div></div><div>Pressure Regulation Valve</div></div> <div><div><div></div><div></div><div></div></div><div>Pressure Release Valve</div></div>		<div>PROCESS NOMENCLATURE</div> <table><thead><tr><th>Letter</th><th>Process Equipment</th></tr></thead><tbody><tr><td>R</td><td>Reactor</td></tr><tr><td>B</td><td>Burner</td></tr><tr><td>C</td><td>Compressor</td></tr><tr><td>T</td><td>Tank</td></tr><tr><td>V</td><td>Valve</td></tr><tr><td>RD</td><td>Rupture Disc</td></tr><tr><td>F</td><td>Filter</td></tr><tr><td>CU</td><td>Cyclone</td></tr><tr><td>P</td><td>Pump</td></tr><tr><td>S</td><td>Separator</td></tr><tr><td>EH</td><td>Electrical Heater</td></tr></tbody></table>		Letter	Process Equipment	R	Reactor	B	Burner	C	Compressor	T	Tank	V	Valve	RD	Rupture Disc	F	Filter	CU	Cyclone	P	Pump	S	Separator	EH	Electrical Heater	<div></div> <div>Natural Gas Cylinder</div> <div></div> <div>Fluidized Bed Heater</div> <div></div> <div>Cyclone</div> <div></div> <div>High Temperature Filter</div> <div></div> <div>Pump</div> <div></div> <div>High Pressure Tank</div> <div></div> <div>Atmospheric Tank</div> <div></div> <div>Electrical Heater</div>
Letter	Process Equipment																													
R	Reactor																													
B	Burner																													
C	Compressor																													
T	Tank																													
V	Valve																													
RD	Rupture Disc																													
F	Filter																													
CU	Cyclone																													
P	Pump																													
S	Separator																													
EH	Electrical Heater																													
LINE NUMBER NOMENCLATURE		<div><div><div></div><div></div><div></div></div><div>Class Of Material</div></div> <div><div><div></div><div></div><div></div></div><div>Material Of Construction</div></div> <div><div><div></div><div></div><div></div></div><div>Line Number</div></div> <div><div><div></div><div></div><div></div></div><div>Pipe Diameter (inches)</div></div> <div>300 CS 015</div>		<div>MISCELLANEOUS SYMBOLS</div> <div><div><div></div><div></div><div></div></div><div>Fan</div></div> <div><div><div></div><div></div><div></div></div><div>Interlock</div></div> <div><div><div></div><div></div><div></div></div><div>Indicator/ Transmitter</div></div> <div><div><div></div><div></div><div></div></div><div>Switch</div></div> <div><div><div></div><div></div><div></div></div><div>Refractory</div></div> <div><div><div></div><div></div><div></div></div><div>Compressor Motor</div></div> <div><div><div></div><div></div><div></div></div><div>Sound Proof Cabinet</div></div> <div><div><div></div><div></div><div></div></div><div>Steam Trap</div></div> <div><div><div></div><div></div><div></div></div><div>Valve Lock</div></div> <div><div><div></div><div></div><div></div></div><div>Process Start</div></div> <div><div><div></div><div></div><div></div></div><div>Process End</div></div>																										
OFF SHEET NUMBER NOMENCLATURE		<div><div><div></div><div></div><div></div></div><div>P&ID Title</div></div> <div><div><div></div><div></div><div></div></div><div>P&ID Number</div></div> <div>Title</div> <div>P&ID-0001</div>		<div>MISCELLANEOUS NOMENCLATURE</div> <table><thead><tr><th>Letter</th><th>Signification</th></tr></thead><tbody><tr><td>NC</td><td>Normally Closed</td></tr><tr><td>TBA</td><td>To Be Announced</td></tr></tbody></table>		Letter	Signification	NC	Normally Closed	TBA	To Be Announced																			
Letter	Signification																													
NC	Normally Closed																													
TBA	To Be Announced																													

1A

12

12

05

First draft

BA

REV.

Y

M

D

Date

Description

BY

CHK.

Title

Legend

Drawn By

BA

Checked By

Approved By

Drawing No.

P&ID - 0006

Rev.

1A

Confidential material. Do not reproduce without permission



Note:

REV.	Y	M	D	Date	Description	BY	CHK	APP.
1A	12	12	05		First draft	BA		

Title

Legend

 Drawn By **BA** Checked By Approved By

 Drawing No. **P&ID - 0006** Rev. **1A**

Confidential material. Do not reproduce without permission

Appendix 4: Process Tables

P&ID 0001: Compressor System

Lines

Line number	Line location	Fluid Nature	Function
300 CS 001	Downstream of T-101	Compressed air	Compressed air from compressors
300 CS 002	Downstream of V-108	Compressed air	Compressed air to other system
300 CS 003	Downstream of V-108	Compressed air	Compressed air to fluidized bed heater P&ID 0002

Valves

Valve number	Valve location	Valve type	Function	Temperature range
V-101	300 CS 001	Pressure regulation valve	Regulates flow out of T-101	Ambient
V-102	T-101	Pressure relief valve	Releases gas if pressure increases critical value	Ambient
V-103	C-101/A	Drain Valve	Drains C-101/A	Ambient
V-104	C-101/B	Drain Valve	Drains C-101/B	Ambient

V-105	C-102	Drain Valve	Drains C-102	Ambient
V-106	T-101	Drain Valve	Drains T-101	Ambient
V-107	300 CS 001	Manual Valve	Manually controls the flow out of T-101	Ambient
V-108	300 CS 001	3-way valve	Separates 300 CS 001 to 300 CS 002 (toward other system) and 300 CS 003 (towards fluidized bed)	Ambient

Transmitters

Transmitter	Location	Function
PT1	C-101/A	Controls the pressure out of C-101/A
PT2	C-101/B	Controls the pressure out of C-101/B
PT3	C-102	Controls the pressure out of C-102
PT4	300 CS 001	Monitors the pressure out of T-101
FT1	300 CS 001	Monitors the flow out of T-101
PSH1	T-101	Switches off the compressor in case of an excess pressure in T-101
PSL1	T-101	Switches on the compressor in case the pressure in the Tank falls below the required value
TT14	300 CS 001	Monitors the temperature out of T-101

P&ID 0002: Fluidized Bed Heater & Windbox

Lines

Line number	Line location	Fluid Nature	Function
300 CS 003	Upstream of H-101	Compressed air	Air feed to H-101
300 CS 004	Natural gas train 1	Natural gas	Natural gas feed to H-101
300 CS 005	Upstream of H-101	Compressed air	Air dilution stream to H-101
300 CS 006	Natural gas train 2	Natural gas	Natural gas feed inside the bed
300 CS 025	Upstream of V-141	Compressed air	Air stream to V-141
300 CS 026	Downstream of V-141	Compressed air	Air to gas manifold
300 CS 014	Downstream of V-141	Natural gas	Natural gas feed to the bed
300 CS 028	Downstream of V-146	Hot Air	Venting line
300 CS 029	Downstream of V-147	Hot Air	Venting line

Valves

Valve number	Valve location	Valve type	Function	Temperature range
V-109	300 CS 004	Pressure regulation valve	Regulates pressure downstream of gas cylinder on Train1	Ambient

V-110	300 CS 004	Manual valve	Manually controls the flow downstream of gas cylinder on Train1	Ambient
V-111	300 CS 004	Emergency shutdown valve	Shuts down in case the pressure exceeds or drop the critical values	Ambient
V-112	300 CS 004	Solenoid valve	Controls the natural gas injection flow to make sure that the temperature inside the heater does not exceed the design temperature or drop below the auto ignition temperature	Ambient
V-113	300 CS 006	Pressure regulation valve	Regulates pressure downstream of gas cylinder on Train2	Ambient
V-114	300 CS 006	Manual valve	Manually controls the flow downstream of gas cylinder on Train2	Ambient
V-115	300 CS 006	Emergency shutdown valve	Shuts down in case the pressure exceeds or drop the critical values	Ambient
V-116	300 CS 005	Solenoid valve	Opens when the flow in 300 CS 003 exceed the flow design value of the Sylvania electric heater	Ambient
V-117	300 CS 005	Solenoid valve	Controls the dilution air flow to make sure that the temperature inside the heater does not exceed the design temperature or drop below the auto ignition temperature	Ambient

V-124	300 CS 025	Solenoid valve	Controls the continuous air flow that will prevent solids from blocking the entrance if natural gas is not injected in the bed	Ambient
V-138	300 CS 006	Solenoid valve	Controls the flow of natural gas to achieve the desired temperature in the bed Gas train 2	Ambient
V-139	300 CS 004	Solenoid valve	Controls the flow of natural gas to achieve the desired temperature in the windbox Gas train 1	Ambient
V-140	300 CS 003	Solenoid valve	Ensure that the flow through the Sylvania electric heater will not exceed the allowed design value. Controls the flowrate inside the reactor	Ambient
V-141	300 CS 025	Ball valve	Ensure that if natural gas is not injected in the bed, a continuous air flow will prevent solids from blocking the entrance	Ambient
V-146	300 CS 028	Solenoid valve	Opens when natural gas is off to prevent backflow from the reactor towards the cylinders	Ambient-1000C
V-147	300 CS 029	Solenoid valve	Opens when natural gas is off to prevent backflow from the reactor towards the cylinders	Ambient-1000C
V-149	300 CS 005	Solenoid valve	Controls the dilution air flow to make sure that the temperature inside the	Ambient

heater does not exceed the design temperature or drop below the auto ignition temperature

Transmitters

Transmitter	Location		Function
PT5	300 CS 004		Regulates the pressure out of V-139
PSH2	300 CS 004		Turns off V-111 in case of the pressure coming out of the cylinder exceeds the reactor design pressure
PSL2	300 CS 004		Turns off V-111 in case the cylinder is empty to prevent a low flow and therefore the possibility of a back flow.
TSL1	H-101		Turns on Natural gas (V-139) if temperature inside the heater is low (almost lower than auto ignition temperature)
TSH1	H-101		Turns on V-117 and V-112 to dilute the flame temperature
TT1	H-101		Controls the amount of dilution required by adjusting V-112 and V-117
TSH2	H-101		Turns off Natural gas (V-139) if the temperature out of the heater is still above the reactor design temperature
PI1	Gas Train1	Cylinder	Monitors the gas pressure inside the cylinder
PI2	Gas Train1	Cylinder	Monitors the gas pressure after the pressure regulation valve V-109
PI3	Gas Train2	Cylinder	Monitors the gas pressure inside the cylinder

PI4	Gas Train2	Cylinder	Monitors the gas pressure after the pressure regulation valve V-113
PT6	300 CS 006		Regulates the pressure out of V-138
PSH3	300 CS 006		Turns off V-115 in case of the pressure coming out of the cylinder exceeds the reactor design pressure
PSL3	300 CS 006		Turns off V-115 in case the cylinder is empty to prevent a low flow and therefore the possibility of a back flow.
FT2	300 CS 004		Regulates the flow out of V-139
FT3	300 CS 006		Regulates the flow out of V-138
FT4	300 CS 025		Regulates the flow out of V-124
FSH1	300 CS 003		Turn on V-116 to allow air to flow through 300 CS 005 due to the flow restrictions of the Sylvania heater. This switch will also limit the flow through V-140 by adjusting its opening
TT2	Windbox		Controls the amount of natural gas from train 1 to reach the desired temperature inside the windbox
TT3	Windbox		Controls the amount of natural gas from train 1 to reach the desired temperature inside the windbox
TT4	Bed		Controls the amount of natural gas from train 2 to reach the desired temperature inside the windbox
TT5	Bed		Controls the amount of natural gas from train 2 to reach the desired temperature inside the windbox
TT17	H-101		Controls the amount of dilution required by adjusting V-112 and V-

		117
TT18	H-101	Controls the amount of dilution required by adjusting V-112 and V-117
TT19	H-101	Controls the amount of dilution required by adjusting V-112 and V-117
PT7	Windbox	Used to control the pressure out of the compressor, natural gas cylinders, flow rate inside the reactor, etc
PT8	Windbox	Used to control the pressure out of the compressor, natural gas cylinders, flow rate inside the reactor, etc
PT9	Bed	Used to control the pressure out of the compressor, natural gas cylinders, flow rate inside the reactor, etc
PT10	Bed	Used to control the pressure out of the compressor, natural gas cylinders, flow rate inside the reactor, etc
PT24	300 CS 025	Regulates the pressure out of V-124

P&ID 0003: Fluidized Bed Freeboard & Gas Sampling

Lines

Line number	Line location	Fluid Nature	Function
300 CS 007	Upstream of rupture disk	Hot compressed air	Gas safety stream in case of reactor overpressure
300 CS 008	Upstream of safety valve	Hot compressed air	Gas safety stream in case of failure of rupture disk

300 CS 009	Downstream of rupture disk	Ambient air	Gas disposal to manifold P&ID 0007
300 CS 010	Main gas line fluidized bed after water injection	Compressed air and water vapour	Gas outlet of reactor to detention tank P&ID 0007
300 CS 011	Prior to analyzer	Water	Cools down the temperature of the air out of the reactor
300 CS 027	Prior to water injection point	Hot compressed air	Gas outlet of reactor
300 CS 030	On water injection line	Hot compressed air	Venting line
300 CS 032	On steam trap	Water	Drain

Valves

Valve number	Valve location	Valve type	Function	Temperature range
V-118	300 CS 010	Manual valve	Used to manually allow gas flow through the analyzer	Ambient-300C
V-119	300 CS 010	Sampling valve	Allows sampling	Ambient-300C
V-120	300 CS 010	Solenoid valve	Controls the pressure inside the reactor	Ambient-300C
V-121	300 CS 010	Manual valve	Valve with lock to ensure isolation of reactor during operation	Ambient
RD-101	300 CS 007	Rupture	Rupture if pressure exceeds critical pressure	Ambient-300C

		disk		
V-142	300 CS 008	Safety valve	Will be open by using a panic button if the rupture disk fails to open	Ambient-300C
V-148	300 CS 011	Solenoid valve	Will open to reduce hot gas temperature	Ambient
V-151	300 CS 032	Manual Valve	Will be opened manually after experiment is over to remove all condensed vapour	Ambient

Transmitters

Transmitter	Location	Function
PT11	Freeboard	Used to control the pressure out of the compressor, natural gas cylinders, flow rate inside the reactor, etc
PT12	Freeboard	Used to control the pressure out of the compressor, natural gas cylinders, flow rate inside the reactor, etc
PT13	300 CS 027	Used to control the pressure out of the compressor, natural gas cylinders, flow rate inside the reactor, etc
PT14	300 CS 010	Used to control the pressure out of the compressor, natural gas cylinders, flow rate inside the reactor, etc
TT6	300 CS 027	Controls the amount of injected water by adjusting V-125 in P&ID 0004 to achieve a temperature below 300C in 300 CS 010. Also used to turn on or off V-126
TT7	300 CS 010	Monitors the temperature of air after water injection
PI4	analyzer	Monitors the pressure at the sampling valve V-119

TSH3	300 CS 010	Turns off both natural gas valves if temperature is still above 300C
-------------	------------	--

P&ID 0004: Water Injection System

Lines

Line number	Line location	Fluid Nature	Function
300 CS 011	Downstream of V-126	Water	Cools down the temperature of the air out of the fluidized bed P&ID 0003
300 CS 012	Downstream of pump P-101	Water	Water from reservoir
300 CS 013	Upstream of T-102	Water	Water recycle stream
300 CS 015	Downstream of V-126	Water	Towards other system

Valves

Valve number	Valve location	Valve type	Function	Temperature range
V-122	300 CS 012	Check valve	Prevents back flow toward the tank	Ambient
V-123	300 CS 012	Emergency shutdown valve	Shuts down if insufficient flow is detected to prevent backflow toward the tank	Ambient
V-125	300 CS 013	Solenoid valve	Adjust the amount of recycle water to regulate the temperature at the outlet of the fluidized bed	Ambient
V-126	300 CS 012	3-way valve	Separates 300 CS 012 into 300 CS 011 which is used to cool down the gas coming out of the fluidized bed	Ambient

V-127	T-102	Manual Valve	Manually fills the tank with water	Ambient
V-128	T-102	Drain valve	Drains T-102	Ambient
V-143	T-102	Pressure relief valve	Releases gas if pressure increases critical value	Ambient

Transmitters

Transmitter	Location	Function
FSL1	300 CS 012	Prevents the return of hot gas at high pressure to the pump and the water tank by adjusting V-123

P&ID 0005: Detention Tank & Discharge Manifold

Lines

Line number	Line location	Fluid Nature	Function
300 CS 009	Downstream of fluidized bed rupture disk	Ambient air	Gas disposal to manifold
300 CS 010	Main gas line fluidized bed after water injection	Compressed air and water vapour	Gas outlet of fluidized bed to detention tank
150 SS 023	Downstream of T-103	Ambient air	Ambient air to Gas manifold
150 SS 024	Downstream of T-103	Ambient air	Gas manifold

Valves

Valve number	Valve location	Valve type	Function	Temperature range
--------------	----------------	------------	----------	-------------------

V-138	T-103	Drain valve	Drains T-103	Ambient
--------------	-------	-------------	--------------	---------

Transmitters

Transmitter	Location	Function
TT13	150 SS 023	Monitors the temperature out of the detention tank T-103

Appendix 5: Equipment List

Number	Equipment	Location	Dimension (mm)
C-101/A	Lubricated Piston Compressor	P&ID 0001	LxWxH(1268x682x815)
C-101/B	Lubricated Piston Compressor	P&ID 0001	LxWxH(1268x682x815)
C-102	Lubricated Piston Compressor	P&ID 0001	LxWxH(1016x619x699)
F-101	High Pressure Filter ACS 0285G	P&ID 0001	LxWxH(122x116x423)
T-101	High Pressure Tank	P&ID 0001	(D=914, L=2362)
S-101	Oil/Water Separator	P&ID 0001	LxWxH(470x165x600)
EH-101	Electrical Heater	P&ID 0002	(D=43.18, L=559)
H-101	Burner/Heater Hybrid for Fluidized Bed	P&ID 0002	(D=172, L=762)
CU-101	Internal Cyclone	P&ID 0003	(Dcylinder=94, Lcylinder=135, Lcone=225)
F-102	Internal High Temperature Filter	P&ID 0003	(D=120, L=991)
P-101	Water Pump	P&ID 0004	LxWxH(462x241x216)
T-102	Pressurized Water Reservoir	P&ID 0004	(D=914, L=2362)
T-103	Detention Tank/Flash Tank	P&ID 0005	(D=219, L=1391)

Appendix 6: Distributor Pressure Drop

All pressure drop values are in atm

Yellow Highlighted Section: Pressure drop across the distributor falls below $K\Delta P_b$

U(m/s)	0.1										
P(atm)/T(C)	25	122.5	220	317.5	415	512.5	610	707.5	805	902.5	1000
1	0.132	0.135	0.138	0.141	0.143	0.145	0.147	0.149	0.150	0.152	0.153
2	0.133	0.136	0.139	0.142	0.144	0.146	0.148	0.149	0.151	0.152	0.154
3	0.135	0.137	0.140	0.142	0.145	0.146	0.148	0.150	0.151	0.153	0.154
4	0.136	0.138	0.141	0.143	0.145	0.147	0.149	0.150	0.152	0.153	0.154
5	0.137	0.139	0.142	0.144	0.146	0.147	0.149	0.151	0.152	0.153	0.155
6	0.139	0.141	0.143	0.145	0.146	0.148	0.150	0.151	0.152	0.154	0.155
7	0.140	0.142	0.143	0.145	0.147	0.148	0.150	0.151	0.153	0.154	0.155
8	0.141	0.143	0.144	0.146	0.147	0.149	0.150	0.152	0.153	0.154	0.156
9	0.143	0.144	0.145	0.147	0.148	0.150	0.151	0.152	0.153	0.155	0.156
10	0.144	0.145	0.146	0.147	0.149	0.150	0.151	0.153	0.154	0.155	0.156
11	0.145	0.146	0.147	0.148	0.149	0.151	0.152	0.153	0.154	0.155	0.157
12	0.147	0.147	0.148	0.149	0.150	0.151	0.152	0.153	0.155	0.156	0.157
13	0.148	0.148	0.148	0.149	0.150	0.152	0.153	0.154	0.155	0.156	0.157
14	0.150	0.149	0.149	0.150	0.151	0.152	0.153	0.154	0.155	0.156	0.157
15	0.151	0.150	0.150	0.151	0.152	0.153	0.154	0.155	0.156	0.157	0.158
16	0.152	0.151	0.151	0.151	0.152	0.153	0.154	0.155	0.156	0.157	0.158
17	0.154	0.152	0.152	0.152	0.153	0.154	0.155	0.156	0.156	0.157	0.158
18	0.155	0.153	0.153	0.153	0.153	0.154	0.155	0.156	0.157	0.158	0.159
19	0.156	0.154	0.153	0.153	0.154	0.155	0.156	0.156	0.157	0.158	0.159
20	0.158	0.155	0.154	0.154	0.155	0.155	0.156	0.157	0.158	0.159	0.159

U(m/s)	0.2										
P(atm)/T(C)	25	122.5	220	317.5	415	512.5	610	707.5	805	902.5	1000
1	0.135	0.142	0.148	0.153	0.157	0.161	0.165	0.168	0.171	0.174	0.177
2	0.138	0.144	0.150	0.155	0.159	0.163	0.166	0.169	0.172	0.175	0.178
3	0.142	0.147	0.152	0.156	0.160	0.164	0.167	0.170	0.173	0.176	0.179
4	0.145	0.149	0.154	0.158	0.162	0.165	0.168	0.171	0.174	0.177	0.179
5	0.148	0.152	0.156	0.160	0.163	0.167	0.170	0.172	0.175	0.178	0.180
6	0.152	0.155	0.158	0.161	0.165	0.168	0.171	0.174	0.176	0.179	0.181
7	0.155	0.157	0.160	0.163	0.166	0.169	0.172	0.175	0.177	0.180	0.182
8	0.159	0.160	0.162	0.165	0.168	0.170	0.173	0.176	0.178	0.180	0.183
9	0.162	0.162	0.164	0.167	0.169	0.172	0.174	0.177	0.179	0.181	0.184
10	0.166	0.165	0.166	0.168	0.171	0.173	0.175	0.178	0.180	0.182	0.184
11	0.169	0.168	0.169	0.170	0.172	0.174	0.177	0.179	0.181	0.183	0.185
12	0.173	0.170	0.171	0.172	0.174	0.176	0.178	0.180	0.182	0.184	0.186
13	0.176	0.173	0.173	0.174	0.175	0.177	0.179	0.181	0.183	0.185	0.187
14	0.180	0.175	0.175	0.175	0.177	0.178	0.180	0.182	0.184	0.186	0.188
15	0.183	0.178	0.177	0.177	0.178	0.180	0.181	0.183	0.185	0.187	0.188
16	0.186	0.181	0.179	0.179	0.180	0.181	0.182	0.184	0.186	0.187	0.189
17	0.190	0.183	0.181	0.181	0.181	0.182	0.184	0.185	0.187	0.188	0.190
18	0.193	0.186	0.183	0.182	0.183	0.184	0.185	0.186	0.188	0.189	0.191
19	0.197	0.188	0.185	0.184	0.184	0.185	0.186	0.187	0.189	0.190	0.192
20	0.200	0.191	0.187	0.186	0.186	0.186	0.187	0.188	0.190	0.191	0.192

U(m/s)	0.3										
P(atm)/T(C)	25	122.5	220	317.5	415	512.5	610	707.5	805	902.5	1000
1	0.139	0.149	0.158	0.165	0.172	0.178	0.183	0.188	0.193	0.197	0.201
2	0.146	0.154	0.162	0.169	0.175	0.180	0.185	0.190	0.195	0.199	0.203
3	0.153	0.159	0.166	0.172	0.178	0.183	0.188	0.192	0.196	0.201	0.204
4	0.160	0.164	0.170	0.176	0.181	0.186	0.190	0.194	0.198	0.202	0.206
5	0.167	0.170	0.174	0.179	0.184	0.188	0.192	0.196	0.200	0.204	0.208
6	0.173	0.175	0.179	0.183	0.187	0.191	0.195	0.199	0.202	0.206	0.209
7	0.180	0.180	0.183	0.186	0.190	0.193	0.197	0.201	0.204	0.208	0.211
8	0.187	0.185	0.187	0.190	0.193	0.196	0.199	0.203	0.206	0.209	0.212
9	0.194	0.191	0.191	0.193	0.196	0.199	0.202	0.205	0.208	0.211	0.214
10	0.201	0.196	0.195	0.197	0.199	0.201	0.204	0.207	0.210	0.213	0.216
11	0.208	0.201	0.200	0.200	0.202	0.204	0.206	0.209	0.212	0.215	0.217
12	0.215	0.206	0.204	0.204	0.205	0.207	0.209	0.211	0.214	0.216	0.219
13	0.222	0.211	0.208	0.207	0.208	0.209	0.211	0.213	0.216	0.218	0.221
14	0.229	0.217	0.212	0.211	0.211	0.212	0.213	0.215	0.218	0.220	0.222
15	0.236	0.222	0.216	0.214	0.214	0.215	0.216	0.218	0.219	0.222	0.224
16	0.243	0.227	0.221	0.218	0.217	0.217	0.218	0.220	0.221	0.223	0.225
17	0.250	0.232	0.225	0.221	0.220	0.220	0.221	0.222	0.223	0.225	0.227
18	0.257	0.238	0.229	0.225	0.223	0.222	0.223	0.224	0.225	0.227	0.229
19	0.264	0.243	0.233	0.228	0.226	0.225	0.225	0.226	0.227	0.229	0.230
20	0.271	0.248	0.237	0.232	0.229	0.228	0.228	0.228	0.229	0.230	0.232

U(m/s)	0.4										
P(atm)/T(C)	25	122.5	220	317.5	415	512.5	610	707.5	805	902.5	1000
1	0.144	0.157	0.168	0.178	0.187	0.195	0.202	0.208	0.214	0.220	0.226
2	0.156	0.166	0.176	0.184	0.192	0.199	0.206	0.212	0.218	0.223	0.228
3	0.168	0.175	0.183	0.190	0.197	0.204	0.210	0.215	0.221	0.226	0.231
4	0.180	0.184	0.190	0.196	0.202	0.208	0.214	0.219	0.224	0.229	0.234
5	0.192	0.193	0.197	0.202	0.207	0.213	0.218	0.223	0.227	0.232	0.237
6	0.203	0.202	0.204	0.208	0.212	0.217	0.222	0.226	0.231	0.235	0.239
7	0.215	0.210	0.211	0.214	0.218	0.222	0.226	0.230	0.234	0.238	0.242
8	0.227	0.219	0.218	0.220	0.223	0.226	0.230	0.233	0.237	0.241	0.245
9	0.239	0.228	0.226	0.226	0.228	0.230	0.234	0.237	0.240	0.244	0.248
10	0.251	0.237	0.233	0.232	0.233	0.235	0.238	0.241	0.244	0.247	0.250
11	0.262	0.246	0.240	0.238	0.238	0.239	0.242	0.244	0.247	0.250	0.253
12	0.274	0.255	0.247	0.244	0.243	0.244	0.246	0.248	0.250	0.253	0.256
13	0.286	0.264	0.254	0.250	0.248	0.248	0.250	0.251	0.253	0.256	0.259
14	0.298	0.273	0.261	0.256	0.253	0.253	0.253	0.255	0.257	0.259	0.261
15	0.310	0.282	0.268	0.262	0.258	0.257	0.257	0.258	0.260	0.262	0.264
16	0.321	0.290	0.276	0.268	0.264	0.262	0.261	0.262	0.263	0.265	0.267
17	0.333	0.299	0.283	0.274	0.269	0.266	0.265	0.266	0.267	0.268	0.270
18	0.345	0.308	0.290	0.280	0.274	0.271	0.269	0.269	0.270	0.271	0.272
19	0.357	0.317	0.297	0.285	0.279	0.275	0.273	0.273	0.273	0.274	0.275
20	0.369	0.326	0.304	0.291	0.284	0.280	0.277	0.276	0.276	0.277	0.278

U(m/s)	0.5										
P(atm)/T(C)	25	122.5	220	317.5	415	512.5	610	707.5	805	902.5	1000
1	0.151	0.166	0.180	0.192	0.203	0.212	0.221	0.229	0.236	0.244	0.250
2	0.169	0.180	0.191	0.201	0.210	0.219	0.227	0.234	0.241	0.248	0.254
3	0.187	0.194	0.202	0.210	0.218	0.226	0.233	0.240	0.246	0.253	0.259
4	0.206	0.207	0.213	0.219	0.226	0.233	0.239	0.245	0.251	0.257	0.263
5	0.224	0.221	0.224	0.229	0.234	0.240	0.245	0.251	0.256	0.262	0.267
6	0.242	0.234	0.235	0.238	0.242	0.246	0.251	0.256	0.261	0.266	0.271
7	0.260	0.248	0.246	0.247	0.250	0.253	0.257	0.262	0.266	0.271	0.276
8	0.278	0.262	0.257	0.256	0.257	0.260	0.263	0.267	0.271	0.276	0.280
9	0.296	0.275	0.268	0.265	0.265	0.267	0.270	0.273	0.276	0.280	0.284
10	0.314	0.289	0.278	0.274	0.273	0.274	0.276	0.278	0.281	0.285	0.288
11	0.332	0.302	0.289	0.283	0.281	0.281	0.282	0.284	0.286	0.289	0.292
12	0.350	0.316	0.300	0.292	0.289	0.287	0.288	0.289	0.291	0.294	0.297
13	0.368	0.330	0.311	0.301	0.296	0.294	0.294	0.295	0.296	0.298	0.301
14	0.386	0.343	0.322	0.311	0.304	0.301	0.300	0.300	0.301	0.303	0.305
15	0.404	0.357	0.333	0.320	0.312	0.308	0.306	0.306	0.306	0.308	0.309
16	0.422	0.371	0.344	0.329	0.320	0.315	0.312	0.311	0.311	0.312	0.314
17	0.440	0.384	0.355	0.338	0.328	0.322	0.318	0.317	0.316	0.317	0.318
18	0.459	0.398	0.366	0.347	0.336	0.329	0.324	0.322	0.321	0.321	0.322
19	0.477	0.411	0.377	0.356	0.343	0.335	0.330	0.328	0.326	0.326	0.326
20	0.495	0.425	0.388	0.365	0.351	0.342	0.337	0.333	0.331	0.330	0.330

U(m/s)	0.6										
P(atm)/T(C)	25	122.5	220	317.5	415	512.5	610	707.5	805	902.5	1000
1	0.160	0.177	0.193	0.207	0.219	0.230	0.240	0.250	0.259	0.267	0.275
2	0.185	0.196	0.208	0.220	0.230	0.240	0.249	0.258	0.266	0.274	0.281
3	0.211	0.216	0.224	0.233	0.241	0.250	0.258	0.266	0.273	0.280	0.287
4	0.237	0.235	0.239	0.246	0.252	0.259	0.266	0.273	0.280	0.287	0.293
5	0.263	0.254	0.255	0.259	0.263	0.269	0.275	0.281	0.287	0.293	0.299
6	0.288	0.274	0.270	0.271	0.275	0.279	0.284	0.289	0.294	0.300	0.305
7	0.314	0.293	0.286	0.284	0.286	0.289	0.292	0.297	0.301	0.306	0.311
8	0.340	0.312	0.301	0.297	0.297	0.298	0.301	0.305	0.309	0.313	0.317
9	0.366	0.332	0.317	0.310	0.308	0.308	0.310	0.312	0.316	0.319	0.323
10	0.391	0.351	0.333	0.323	0.319	0.318	0.318	0.320	0.323	0.326	0.329
11	0.417	0.370	0.348	0.336	0.330	0.328	0.327	0.328	0.330	0.332	0.335
12	0.443	0.390	0.364	0.349	0.341	0.337	0.336	0.336	0.337	0.339	0.341
13	0.468	0.409	0.379	0.362	0.353	0.347	0.344	0.344	0.344	0.345	0.347
14	0.494	0.429	0.395	0.375	0.364	0.357	0.353	0.351	0.351	0.352	0.353
15	0.520	0.448	0.410	0.388	0.375	0.367	0.362	0.359	0.358	0.358	0.359
16	0.546	0.467	0.426	0.401	0.386	0.376	0.370	0.367	0.365	0.365	0.365
17	0.571	0.487	0.441	0.414	0.397	0.386	0.379	0.375	0.372	0.371	0.371
18	0.597	0.506	0.457	0.427	0.408	0.396	0.388	0.383	0.380	0.378	0.377
19	0.623	0.525	0.472	0.440	0.419	0.406	0.396	0.390	0.387	0.385	0.384
20	0.648	0.545	0.488	0.453	0.430	0.415	0.405	0.398	0.394	0.391	0.390

U(m/s)	0.7										
P(atm)/T(C)	25	122.5	220	317.5	415	512.5	610	707.5	805	902.5	1000
1	0.169	0.188	0.206	0.222	0.236	0.249	0.260	0.271	0.282	0.291	0.301
2	0.204	0.214	0.227	0.239	0.251	0.262	0.272	0.282	0.291	0.300	0.309
3	0.239	0.241	0.248	0.257	0.266	0.275	0.284	0.292	0.301	0.309	0.317
4	0.274	0.267	0.269	0.274	0.281	0.288	0.296	0.303	0.310	0.318	0.325
5	0.309	0.293	0.290	0.292	0.296	0.301	0.307	0.314	0.320	0.327	0.333
6	0.343	0.319	0.311	0.309	0.311	0.315	0.319	0.324	0.330	0.335	0.341
7	0.378	0.345	0.332	0.327	0.326	0.328	0.331	0.335	0.339	0.344	0.349
8	0.413	0.371	0.353	0.345	0.341	0.341	0.342	0.345	0.349	0.353	0.358
9	0.448	0.398	0.374	0.362	0.356	0.354	0.354	0.356	0.358	0.362	0.366
10	0.482	0.424	0.395	0.380	0.371	0.367	0.366	0.366	0.368	0.371	0.374
11	0.517	0.450	0.416	0.397	0.386	0.380	0.378	0.377	0.378	0.379	0.382
12	0.552	0.476	0.437	0.415	0.401	0.394	0.389	0.387	0.387	0.388	0.390
13	0.587	0.502	0.458	0.432	0.416	0.407	0.401	0.398	0.397	0.397	0.398
14	0.621	0.528	0.479	0.450	0.431	0.420	0.413	0.409	0.406	0.406	0.406
15	0.656	0.555	0.500	0.467	0.446	0.433	0.424	0.419	0.416	0.415	0.414
16	0.691	0.581	0.521	0.485	0.461	0.446	0.436	0.430	0.426	0.423	0.423
17	0.726	0.607	0.542	0.502	0.477	0.459	0.448	0.440	0.435	0.432	0.431
18	0.760	0.633	0.563	0.520	0.492	0.473	0.460	0.451	0.445	0.441	0.439
19	0.795	0.659	0.584	0.537	0.507	0.486	0.471	0.461	0.454	0.450	0.447
20	0.830	0.685	0.605	0.555	0.522	0.499	0.483	0.472	0.464	0.459	0.455

U(m/s)	0.8										
P(atm)/T(C)	25	122.5	220	317.5	415	512.5	610	707.5	805	902.5	1000
1	0.181	0.201	0.220	0.238	0.253	0.268	0.281	0.293	0.305	0.316	0.326
2	0.226	0.235	0.248	0.261	0.273	0.285	0.296	0.307	0.317	0.327	0.337
3	0.271	0.269	0.275	0.283	0.293	0.302	0.311	0.321	0.330	0.339	0.347
4	0.316	0.303	0.302	0.306	0.312	0.319	0.327	0.334	0.342	0.350	0.358
5	0.361	0.337	0.329	0.329	0.332	0.336	0.342	0.348	0.355	0.362	0.369
6	0.407	0.371	0.357	0.352	0.351	0.353	0.357	0.362	0.367	0.373	0.379
7	0.452	0.405	0.384	0.374	0.371	0.371	0.372	0.376	0.380	0.385	0.390
8	0.497	0.439	0.411	0.397	0.390	0.388	0.388	0.389	0.392	0.396	0.400
9	0.542	0.473	0.439	0.420	0.410	0.405	0.403	0.403	0.405	0.407	0.411
10	0.587	0.507	0.466	0.443	0.429	0.422	0.418	0.417	0.417	0.419	0.421
11	0.633	0.541	0.493	0.466	0.449	0.439	0.433	0.430	0.430	0.430	0.432
12	0.678	0.575	0.520	0.488	0.468	0.456	0.449	0.444	0.442	0.442	0.443
13	0.723	0.609	0.548	0.511	0.488	0.473	0.464	0.458	0.455	0.453	0.453
14	0.768	0.643	0.575	0.534	0.508	0.490	0.479	0.472	0.467	0.465	0.464
15	0.813	0.677	0.602	0.557	0.527	0.507	0.494	0.485	0.480	0.476	0.474
16	0.859	0.711	0.630	0.579	0.547	0.525	0.509	0.499	0.492	0.488	0.485
17	0.904	0.745	0.657	0.602	0.566	0.542	0.525	0.513	0.505	0.499	0.495
18	0.949	0.779	0.684	0.625	0.586	0.559	0.540	0.526	0.517	0.510	0.506
19	0.994	0.813	0.711	0.648	0.605	0.576	0.555	0.540	0.529	0.522	0.517
20	1.039	0.847	0.739	0.671	0.625	0.593	0.570	0.554	0.542	0.533	0.527

U(m/s)	0.9										
P(atm)/T(C)	25	122.5	220	317.5	415	512.5	610	707.5	805	902.5	1000
1	0.193	0.214	0.235	0.254	0.272	0.287	0.302	0.316	0.329	0.341	0.352
2	0.250	0.257	0.270	0.283	0.296	0.309	0.321	0.333	0.344	0.355	0.366
3	0.307	0.300	0.304	0.312	0.321	0.331	0.340	0.350	0.360	0.370	0.379
4	0.364	0.343	0.339	0.341	0.346	0.352	0.360	0.368	0.376	0.384	0.392
5	0.421	0.386	0.373	0.369	0.370	0.374	0.379	0.385	0.391	0.398	0.406
6	0.478	0.429	0.408	0.398	0.395	0.395	0.398	0.402	0.407	0.413	0.419
7	0.535	0.472	0.442	0.427	0.420	0.417	0.417	0.419	0.423	0.427	0.432
8	0.592	0.515	0.476	0.456	0.444	0.439	0.436	0.437	0.439	0.442	0.446
9	0.649	0.558	0.511	0.484	0.469	0.460	0.456	0.454	0.454	0.456	0.459
10	0.706	0.600	0.545	0.513	0.494	0.482	0.475	0.471	0.470	0.471	0.472
11	0.763	0.643	0.580	0.542	0.518	0.503	0.494	0.489	0.486	0.485	0.486
12	0.820	0.686	0.614	0.570	0.543	0.525	0.513	0.506	0.502	0.499	0.499
13	0.877	0.729	0.648	0.599	0.568	0.547	0.533	0.523	0.517	0.514	0.512
14	0.934	0.772	0.683	0.628	0.592	0.568	0.552	0.541	0.533	0.528	0.526
15	0.991	0.815	0.717	0.657	0.617	0.590	0.571	0.558	0.549	0.543	0.539
16	1.048	0.858	0.752	0.685	0.641	0.611	0.590	0.575	0.565	0.557	0.552
17	1.105	0.901	0.786	0.714	0.666	0.633	0.609	0.592	0.580	0.572	0.566
18	1.162	0.944	0.821	0.743	0.691	0.655	0.629	0.610	0.596	0.586	0.579
19	1.219	0.987	0.855	0.772	0.715	0.676	0.648	0.627	0.612	0.601	0.592
20	1.276	1.030	0.889	0.800	0.740	0.698	0.667	0.644	0.628	0.615	0.606

U(m/s)	1										
P(atm)/T(C)	25	122.5	220	317.5	415	512.5	610	707.5	805	902.5	1000
1	0.207	0.229	0.251	0.272	0.290	0.307	0.323	0.338	0.352	0.366	0.379
2	0.277	0.282	0.294	0.307	0.321	0.334	0.347	0.360	0.372	0.384	0.395
3	0.348	0.335	0.336	0.342	0.351	0.361	0.371	0.381	0.391	0.401	0.412
4	0.418	0.387	0.378	0.378	0.381	0.387	0.394	0.402	0.411	0.419	0.428
5	0.488	0.440	0.421	0.413	0.412	0.414	0.418	0.424	0.430	0.437	0.444
6	0.558	0.493	0.463	0.449	0.442	0.440	0.442	0.445	0.449	0.455	0.461
7	0.629	0.546	0.506	0.484	0.473	0.467	0.465	0.466	0.469	0.473	0.477
8	0.699	0.599	0.548	0.519	0.503	0.494	0.489	0.488	0.488	0.490	0.494
9	0.769	0.652	0.590	0.555	0.533	0.520	0.513	0.509	0.508	0.508	0.510
10	0.839	0.705	0.633	0.590	0.564	0.547	0.536	0.530	0.527	0.526	0.526
11	0.910	0.757	0.675	0.626	0.594	0.574	0.560	0.552	0.546	0.544	0.543
12	0.980	0.810	0.718	0.661	0.624	0.600	0.584	0.573	0.566	0.561	0.559
13	1.050	0.863	0.760	0.696	0.655	0.627	0.607	0.594	0.585	0.579	0.576
14	1.120	0.916	0.802	0.732	0.685	0.653	0.631	0.615	0.605	0.597	0.592
15	1.190	0.969	0.845	0.767	0.716	0.680	0.655	0.637	0.624	0.615	0.609
16	1.260	1.022	0.887	0.803	0.746	0.707	0.678	0.658	0.643	0.633	0.625
17	1.330	1.074	0.930	0.838	0.776	0.733	0.702	0.679	0.663	0.650	0.641
18	1.401	1.127	0.972	0.873	0.807	0.760	0.726	0.701	0.682	0.668	0.658
19	1.471	1.180	1.014	0.909	0.837	0.786	0.749	0.722	0.701	0.686	0.674
20	1.541	1.233	1.057	0.944	0.867	0.813	0.773	0.743	0.721	0.704	0.691

U(m/s)	1.1										
P(atm)/T(C)	25	122.5	220	317.5	415	512.5	610	707.5	805	902.5	1000
1	0.222	0.244	0.268	0.290	0.310	0.328	0.345	0.362	0.377	0.391	0.405
2	0.307	0.308	0.319	0.332	0.346	0.360	0.374	0.387	0.400	0.413	0.425
3	0.392	0.372	0.370	0.375	0.383	0.392	0.402	0.413	0.424	0.434	0.445
4	0.477	0.436	0.422	0.418	0.420	0.424	0.431	0.439	0.447	0.456	0.465
5	0.562	0.500	0.473	0.461	0.456	0.457	0.460	0.465	0.471	0.477	0.485
6	0.647	0.564	0.524	0.503	0.493	0.489	0.488	0.490	0.494	0.499	0.505
7	0.732	0.627	0.575	0.546	0.530	0.521	0.517	0.516	0.517	0.520	0.524
8	0.816	0.691	0.626	0.589	0.566	0.553	0.545	0.542	0.541	0.542	0.544
9	0.901	0.755	0.678	0.632	0.603	0.585	0.574	0.568	0.564	0.563	0.564
10	0.986	0.819	0.729	0.674	0.640	0.617	0.603	0.593	0.588	0.585	0.584
11	1.071	0.883	0.780	0.717	0.677	0.649	0.631	0.619	0.611	0.606	0.604
12	1.156	0.947	0.831	0.760	0.713	0.682	0.660	0.645	0.634	0.628	0.624
13	1.240	1.011	0.883	0.803	0.750	0.714	0.688	0.670	0.658	0.649	0.643
14	1.325	1.074	0.934	0.845	0.787	0.746	0.717	0.696	0.681	0.671	0.663
15	1.410	1.138	0.985	0.888	0.823	0.778	0.746	0.722	0.705	0.692	0.683
16	1.494	1.202	1.036	0.931	0.860	0.810	0.774	0.748	0.728	0.714	0.703
17	1.579	1.266	1.087	0.974	0.897	0.842	0.803	0.773	0.752	0.735	0.723
18	1.664	1.330	1.139	1.016	0.933	0.874	0.831	0.799	0.775	0.757	0.742
19	1.749	1.394	1.190	1.059	0.970	0.907	0.860	0.825	0.798	0.778	0.762
20	1.833	1.457	1.241	1.102	1.007	0.939	0.889	0.851	0.822	0.799	0.782

U(m/s)	1.2										
P(atm)/T(C)	25	122.5	220	317.5	415	512.5	610	707.5	805	902.5	1000
1	0.239	0.261	0.285	0.308	0.330	0.349	0.368	0.385	0.402	0.417	0.432
2	0.340	0.337	0.346	0.359	0.373	0.387	0.402	0.416	0.429	0.443	0.456
3	0.441	0.413	0.407	0.410	0.417	0.426	0.436	0.446	0.457	0.468	0.480
4	0.542	0.489	0.468	0.461	0.460	0.464	0.470	0.477	0.485	0.494	0.503
5	0.643	0.565	0.529	0.512	0.504	0.502	0.504	0.508	0.513	0.519	0.527
6	0.743	0.640	0.590	0.562	0.548	0.540	0.538	0.538	0.541	0.545	0.550
7	0.844	0.716	0.651	0.613	0.591	0.578	0.572	0.569	0.569	0.570	0.574
8	0.945	0.792	0.712	0.664	0.635	0.617	0.606	0.599	0.596	0.596	0.597
9	1.046	0.868	0.772	0.715	0.678	0.655	0.640	0.630	0.624	0.622	0.621
10	1.147	0.944	0.833	0.766	0.722	0.693	0.674	0.661	0.652	0.647	0.644
11	1.247	1.020	0.894	0.817	0.766	0.731	0.708	0.691	0.680	0.673	0.668
12	1.348	1.096	0.955	0.867	0.809	0.769	0.741	0.722	0.708	0.698	0.692
13	1.449	1.172	1.016	0.918	0.853	0.808	0.775	0.752	0.736	0.724	0.715
14	1.549	1.247	1.077	0.969	0.897	0.846	0.809	0.783	0.763	0.749	0.739
15	1.650	1.323	1.138	1.020	0.940	0.884	0.843	0.814	0.791	0.775	0.762
16	1.751	1.399	1.199	1.071	0.984	0.922	0.877	0.844	0.819	0.800	0.786
17	1.851	1.475	1.259	1.121	1.027	0.960	0.911	0.875	0.847	0.826	0.809
18	1.952	1.551	1.320	1.172	1.071	0.999	0.945	0.905	0.875	0.851	0.833
19	2.053	1.627	1.381	1.223	1.115	1.037	0.979	0.936	0.903	0.877	0.857
20	2.153	1.703	1.442	1.274	1.158	1.075	1.013	0.967	0.930	0.902	0.880

U(m/s)	1.3										
P(atm)/T(C)	25	122.5	220	317.5	415	512.5	610	707.5	805	902.5	1000
1	0.257	0.279	0.304	0.328	0.350	0.371	0.391	0.409	0.427	0.444	0.460
2	0.376	0.368	0.375	0.387	0.401	0.416	0.430	0.445	0.459	0.474	0.487
3	0.494	0.457	0.447	0.447	0.452	0.460	0.470	0.481	0.492	0.503	0.515
4	0.612	0.546	0.518	0.507	0.503	0.505	0.510	0.517	0.525	0.533	0.543
5	0.730	0.635	0.589	0.566	0.555	0.550	0.550	0.553	0.557	0.563	0.570
6	0.848	0.724	0.661	0.626	0.606	0.595	0.590	0.589	0.590	0.593	0.598
7	0.967	0.813	0.732	0.685	0.657	0.640	0.630	0.624	0.623	0.623	0.625
8	1.085	0.901	0.803	0.745	0.708	0.684	0.669	0.660	0.655	0.653	0.653
9	1.203	0.990	0.875	0.804	0.759	0.729	0.709	0.696	0.688	0.683	0.681
10	1.321	1.079	0.946	0.864	0.810	0.774	0.749	0.732	0.720	0.713	0.708
11	1.439	1.168	1.018	0.924	0.861	0.819	0.789	0.768	0.753	0.743	0.736
12	1.557	1.257	1.089	0.983	0.913	0.864	0.829	0.804	0.786	0.773	0.764
13	1.675	1.346	1.160	1.043	0.964	0.908	0.869	0.840	0.818	0.803	0.791
14	1.793	1.435	1.232	1.102	1.015	0.953	0.908	0.876	0.851	0.833	0.819
15	1.911	1.524	1.303	1.162	1.066	0.998	0.948	0.911	0.884	0.863	0.847
16	2.029	1.613	1.374	1.221	1.117	1.043	0.988	0.947	0.916	0.892	0.874
17	2.147	1.702	1.446	1.281	1.168	1.088	1.028	0.983	0.949	0.922	0.902
18	2.265	1.791	1.517	1.341	1.219	1.132	1.068	1.019	0.982	0.952	0.929
19	2.383	1.880	1.588	1.400	1.270	1.177	1.108	1.055	1.014	0.982	0.957
20	2.501	1.969	1.660	1.460	1.322	1.222	1.148	1.091	1.047	1.012	0.985

U(m/s)	1.4										
P(atm)/T(C)	25	122.5	220	317.5	415	512.5	610	707.5	805	902.5	1000
1	0.277	0.297	0.323	0.348	0.371	0.393	0.414	0.434	0.452	0.470	0.487
2	0.414	0.401	0.406	0.417	0.430	0.445	0.460	0.475	0.490	0.505	0.519
3	0.551	0.504	0.489	0.486	0.490	0.497	0.506	0.517	0.528	0.540	0.551
4	0.688	0.607	0.571	0.555	0.549	0.549	0.552	0.558	0.566	0.574	0.583
5	0.825	0.710	0.654	0.624	0.608	0.601	0.599	0.600	0.604	0.609	0.615
6	0.962	0.813	0.737	0.693	0.667	0.653	0.645	0.641	0.641	0.644	0.647
7	1.099	0.916	0.819	0.762	0.727	0.705	0.691	0.683	0.679	0.678	0.679
8	1.236	1.019	0.902	0.831	0.786	0.756	0.737	0.725	0.717	0.713	0.711
9	1.372	1.122	0.985	0.900	0.845	0.808	0.783	0.766	0.755	0.748	0.744
10	1.509	1.225	1.067	0.969	0.905	0.860	0.829	0.808	0.793	0.782	0.776
11	1.646	1.328	1.150	1.038	0.964	0.912	0.876	0.849	0.830	0.817	0.808
12	1.783	1.431	1.233	1.107	1.023	0.964	0.922	0.891	0.868	0.852	0.840
13	1.920	1.535	1.316	1.176	1.082	1.016	0.968	0.932	0.906	0.886	0.872
14	2.056	1.638	1.398	1.245	1.142	1.068	1.014	0.974	0.944	0.921	0.904
15	2.193	1.741	1.481	1.314	1.201	1.120	1.060	1.016	0.982	0.956	0.936
16	2.330	1.844	1.564	1.384	1.260	1.172	1.106	1.057	1.020	0.990	0.968
17	2.467	1.947	1.646	1.453	1.319	1.224	1.153	1.099	1.057	1.025	1.000
18	2.604	2.050	1.729	1.522	1.379	1.275	1.199	1.140	1.095	1.060	1.032
19	2.740	2.153	1.812	1.591	1.438	1.327	1.245	1.182	1.133	1.094	1.064
20	2.877	2.256	1.894	1.660	1.497	1.379	1.291	1.224	1.171	1.129	1.096

U(m/s)	1.5										
P(atm)/T(C)	25	122.5	220	317.5	415	512.5	610	707.5	805	902.5	1000
1	0.298	0.317	0.343	0.369	0.393	0.416	0.438	0.458	0.478	0.497	0.515
2	0.455	0.435	0.438	0.448	0.461	0.475	0.491	0.506	0.522	0.537	0.552
3	0.612	0.554	0.533	0.527	0.529	0.535	0.544	0.554	0.565	0.577	0.589
4	0.769	0.672	0.628	0.606	0.597	0.595	0.597	0.601	0.608	0.616	0.626
5	0.926	0.790	0.723	0.686	0.665	0.654	0.650	0.649	0.652	0.656	0.662
6	1.083	0.909	0.818	0.765	0.733	0.714	0.703	0.697	0.695	0.696	0.699
7	1.240	1.027	0.912	0.844	0.801	0.773	0.755	0.745	0.738	0.736	0.736
8	1.397	1.145	1.007	0.923	0.869	0.833	0.808	0.792	0.782	0.776	0.772
9	1.554	1.263	1.102	1.002	0.937	0.892	0.861	0.840	0.825	0.815	0.809
10	1.711	1.382	1.197	1.082	1.005	0.952	0.914	0.888	0.869	0.855	0.846
11	1.868	1.500	1.292	1.161	1.073	1.011	0.967	0.935	0.912	0.895	0.883
12	2.025	1.618	1.387	1.240	1.141	1.071	1.020	0.983	0.955	0.935	0.919
13	2.182	1.736	1.482	1.319	1.209	1.130	1.073	1.031	0.999	0.975	0.956
14	2.339	1.855	1.577	1.398	1.277	1.190	1.126	1.078	1.042	1.014	0.993
15	2.496	1.973	1.671	1.478	1.345	1.249	1.179	1.126	1.086	1.054	1.030
16	2.653	2.091	1.766	1.557	1.413	1.309	1.232	1.174	1.129	1.094	1.066
17	2.810	2.210	1.861	1.636	1.481	1.369	1.285	1.222	1.172	1.134	1.103
18	2.967	2.328	1.956	1.715	1.549	1.428	1.338	1.269	1.216	1.173	1.140
19	3.124	2.446	2.051	1.794	1.617	1.488	1.391	1.317	1.259	1.213	1.177
20	3.281	2.564	2.146	1.874	1.685	1.547	1.444	1.365	1.302	1.253	1.213

U(m/s)	1.6										
P(atm)/T(C)	122.5	220	317.5	415	512.5	610	707.5	805	902.5	1000	25
1	0.338	0.364	0.390	0.415	0.439	0.462	0.484	0.504	0.524	0.544	0.344
2	0.473	0.472	0.480	0.493	0.507	0.522	0.538	0.554	0.570	0.585	0.545
3	0.607	0.580	0.570	0.570	0.575	0.582	0.592	0.603	0.615	0.627	0.747
4	0.742	0.688	0.660	0.647	0.642	0.643	0.646	0.652	0.660	0.669	0.949
5	0.876	0.796	0.751	0.725	0.710	0.703	0.701	0.702	0.705	0.711	1.150
6	1.011	0.904	0.841	0.802	0.778	0.763	0.755	0.751	0.751	0.752	1.352
7	1.145	1.011	0.931	0.879	0.845	0.823	0.809	0.800	0.796	0.794	1.553
8	1.279	1.119	1.021	0.956	0.913	0.884	0.863	0.850	0.841	0.836	1.754
9	1.414	1.227	1.111	1.034	0.981	0.944	0.918	0.899	0.886	0.878	1.956
10	1.548	1.335	1.201	1.111	1.049	1.004	0.972	0.948	0.932	0.920	2.157
11	1.683	1.443	1.291	1.188	1.116	1.064	1.026	0.998	0.977	0.961	2.359
12	1.817	1.551	1.381	1.266	1.184	1.124	1.080	1.047	1.022	1.003	2.560
13	1.952	1.659	1.471	1.343	1.252	1.185	1.135	1.096	1.067	1.045	2.761
14	2.086	1.767	1.561	1.420	1.319	1.245	1.189	1.146	1.113	1.087	2.963
15	2.221	1.875	1.651	1.498	1.387	1.305	1.243	1.195	1.158	1.129	3.164
16	2.356	1.982	1.741	1.575	1.455	1.365	1.297	1.245	1.203	1.170	3.366
17	2.490	2.090	1.831	1.652	1.523	1.426	1.352	1.294	1.248	1.212	3.567
18	2.625	2.198	1.921	1.729	1.590	1.486	1.406	1.343	1.294	1.254	3.768
19	2.759	2.306	2.012	1.807	1.658	1.546	1.460	1.393	1.339	1.296	3.970
20	2.894	2.414	2.102	1.884	1.726	1.606	1.514	1.442	1.384	1.337	4.171

U(m/s)	1.7										
P(atm)/T(C)	25	122.5	220	317.5	415	512.5	610	707.5	805	902.5	1000
1	0.344	0.360	0.386	0.412	0.438	0.463	0.487	0.509	0.531	0.552	0.572
2	0.545	0.512	0.508	0.514	0.525	0.539	0.555	0.571	0.587	0.603	0.619
3	0.747	0.663	0.629	0.616	0.613	0.616	0.623	0.632	0.642	0.654	0.667
4	0.949	0.815	0.751	0.717	0.700	0.692	0.691	0.693	0.698	0.705	0.714
5	1.150	0.967	0.873	0.819	0.787	0.769	0.759	0.754	0.754	0.756	0.761
6	1.352	1.119	0.995	0.921	0.874	0.845	0.827	0.815	0.809	0.807	0.808
7	1.553	1.270	1.116	1.022	0.962	0.921	0.894	0.877	0.865	0.858	0.855
8	1.754	1.422	1.238	1.124	1.049	0.998	0.962	0.938	0.921	0.909	0.902
9	1.956	1.574	1.360	1.226	1.136	1.074	1.030	0.999	0.977	0.960	0.949
10	2.157	1.726	1.482	1.327	1.223	1.151	1.098	1.060	1.032	1.012	0.997
11	2.359	1.878	1.603	1.429	1.311	1.227	1.166	1.121	1.088	1.063	1.044
12	2.560	2.029	1.725	1.530	1.398	1.303	1.234	1.183	1.144	1.114	1.091
13	2.761	2.181	1.847	1.632	1.485	1.380	1.302	1.244	1.199	1.165	1.138
14	2.963	2.333	1.969	1.734	1.572	1.456	1.370	1.305	1.255	1.216	1.185
15	3.164	2.485	2.090	1.835	1.659	1.533	1.438	1.366	1.311	1.267	1.232
16	3.366	2.636	2.212	1.937	1.747	1.609	1.506	1.427	1.366	1.318	1.279
17	3.567	2.788	2.334	2.039	1.834	1.685	1.574	1.489	1.422	1.369	1.327
18	3.768	2.940	2.456	2.140	1.921	1.762	1.642	1.550	1.478	1.420	1.374
19	3.970	3.092	2.577	2.242	2.008	1.838	1.710	1.611	1.533	1.471	1.421
20	4.171	3.244	2.699	2.344	2.096	1.915	1.778	1.672	1.589	1.522	1.468

U(m/s)	1.8										
P(atm)/T(C)	25	122.5	220	317.5	415	512.5	610	707.5	805	902.5	1000
1	0.369	0.383	0.408	0.435	0.462	0.487	0.512	0.535	0.558	0.580	0.601
2	0.595	0.553	0.545	0.549	0.560	0.573	0.588	0.604	0.621	0.637	0.654
3	0.821	0.723	0.681	0.663	0.657	0.659	0.664	0.673	0.683	0.695	0.707
4	1.047	0.893	0.818	0.777	0.755	0.744	0.740	0.741	0.745	0.752	0.760
5	1.272	1.063	0.954	0.891	0.853	0.830	0.817	0.810	0.808	0.809	0.813
6	1.498	1.233	1.091	1.005	0.951	0.915	0.893	0.878	0.870	0.866	0.865
7	1.724	1.403	1.227	1.119	1.048	1.001	0.969	0.947	0.933	0.923	0.918
8	1.950	1.573	1.364	1.233	1.146	1.087	1.045	1.016	0.995	0.981	0.971
9	2.175	1.743	1.500	1.347	1.244	1.172	1.121	1.084	1.057	1.038	1.024
10	2.401	1.914	1.636	1.460	1.342	1.258	1.197	1.153	1.120	1.095	1.077
11	2.627	2.084	1.773	1.574	1.439	1.344	1.274	1.221	1.182	1.152	1.130
12	2.852	2.254	1.909	1.688	1.537	1.429	1.350	1.290	1.245	1.209	1.182
13	3.078	2.424	2.046	1.802	1.635	1.515	1.426	1.359	1.307	1.267	1.235
14	3.304	2.594	2.182	1.916	1.733	1.600	1.502	1.427	1.369	1.324	1.288
15	3.530	2.764	2.319	2.030	1.830	1.686	1.578	1.496	1.432	1.381	1.341
16	3.755	2.934	2.455	2.144	1.928	1.772	1.654	1.564	1.494	1.438	1.394
17	3.981	3.104	2.592	2.258	2.026	1.857	1.731	1.633	1.556	1.496	1.447
18	4.207	3.274	2.728	2.372	2.124	1.943	1.807	1.702	1.619	1.553	1.499
19	4.432	3.444	2.864	2.486	2.222	2.029	1.883	1.770	1.681	1.610	1.552
20	4.658	3.615	3.001	2.600	2.319	2.114	1.959	1.839	1.744	1.667	1.605

U(m/s)	1.9										
P(atm)/T(C)	25	122.5	220	317.5	415	512.5	610	707.5	805	902.5	1000
1	0.395	0.407	0.432	0.459	0.486	0.512	0.538	0.562	0.586	0.608	0.630
2	0.647	0.596	0.584	0.586	0.595	0.608	0.622	0.638	0.655	0.672	0.689
3	0.898	0.786	0.736	0.713	0.704	0.703	0.707	0.715	0.725	0.736	0.748
4	1.150	0.975	0.888	0.840	0.813	0.798	0.792	0.791	0.794	0.800	0.807
5	1.402	1.165	1.040	0.966	0.921	0.894	0.877	0.868	0.864	0.863	0.866
6	1.653	1.354	1.192	1.093	1.030	0.989	0.962	0.944	0.933	0.927	0.925
7	1.905	1.543	1.344	1.220	1.139	1.084	1.047	1.020	1.003	0.991	0.984
8	2.156	1.733	1.496	1.347	1.248	1.180	1.131	1.097	1.072	1.055	1.042
9	2.407	1.922	1.648	1.474	1.357	1.275	1.216	1.173	1.142	1.118	1.101
10	2.659	2.112	1.800	1.601	1.466	1.371	1.301	1.250	1.211	1.182	1.160
11	2.910	2.301	1.952	1.728	1.575	1.466	1.386	1.326	1.281	1.246	1.219
12	3.162	2.491	2.104	1.855	1.684	1.561	1.471	1.402	1.350	1.309	1.278
13	3.413	2.680	2.256	1.981	1.793	1.657	1.556	1.479	1.420	1.373	1.337
14	3.664	2.870	2.408	2.108	1.902	1.752	1.641	1.555	1.489	1.437	1.395
15	3.916	3.059	2.560	2.235	2.010	1.847	1.725	1.632	1.559	1.501	1.454
16	4.167	3.249	2.712	2.362	2.119	1.943	1.810	1.708	1.628	1.564	1.513
17	4.419	3.438	2.864	2.489	2.228	2.038	1.895	1.785	1.698	1.628	1.572
18	4.670	3.628	3.016	2.616	2.337	2.134	1.980	1.861	1.767	1.692	1.631
19	4.921	3.817	3.167	2.743	2.446	2.229	2.065	1.937	1.837	1.756	1.690
20	5.173	4.006	3.319	2.870	2.555	2.324	2.150	2.014	1.906	1.819	1.749

U(m/s)	2										
P(atm)/T(C)	25	122.5	220	317.5	415	512.5	610	707.5	805	902.5	1000
1	0.423	0.432	0.456	0.483	0.511	0.538	0.564	0.589	0.613	0.637	0.660
2	0.702	0.642	0.625	0.624	0.631	0.643	0.658	0.674	0.690	0.708	0.725
3	0.981	0.851	0.793	0.764	0.752	0.749	0.752	0.758	0.767	0.778	0.790
4	1.259	1.061	0.961	0.905	0.873	0.854	0.846	0.843	0.844	0.849	0.856
5	1.538	1.271	1.130	1.045	0.993	0.960	0.940	0.928	0.921	0.920	0.921
6	1.816	1.481	1.298	1.186	1.114	1.066	1.034	1.012	0.998	0.990	0.986
7	2.095	1.691	1.466	1.327	1.234	1.171	1.128	1.097	1.075	1.061	1.051
8	2.373	1.901	1.635	1.467	1.355	1.277	1.222	1.181	1.152	1.131	1.116
9	2.652	2.111	1.803	1.608	1.476	1.383	1.316	1.266	1.229	1.202	1.182
10	2.930	2.321	1.971	1.748	1.596	1.488	1.410	1.351	1.306	1.273	1.247
11	3.209	2.530	2.140	1.889	1.717	1.594	1.504	1.435	1.383	1.343	1.312
12	3.487	2.740	2.308	2.029	1.838	1.700	1.598	1.520	1.460	1.414	1.377
13	3.766	2.950	2.476	2.170	1.958	1.805	1.692	1.605	1.537	1.484	1.442
14	4.044	3.160	2.645	2.310	2.079	1.911	1.785	1.689	1.614	1.555	1.508
15	4.323	3.370	2.813	2.451	2.199	2.017	1.879	1.774	1.691	1.626	1.573
16	4.601	3.580	2.981	2.591	2.320	2.122	1.973	1.859	1.768	1.696	1.638
17	4.880	3.790	3.150	2.732	2.441	2.228	2.067	1.943	1.845	1.767	1.703
18	5.158	4.000	3.318	2.873	2.561	2.334	2.161	2.028	1.922	1.837	1.768
19	5.437	4.209	3.487	3.013	2.682	2.439	2.255	2.113	1.999	1.908	1.833
20	5.715	4.419	3.655	3.154	2.803	2.545	2.349	2.197	2.076	1.979	1.899